

**2012 Volume 4**

**The Journal on Advanced Studies in Theoretical and Experimental Physics,  
including Related Themes from Mathematics**

# **PROGRESS IN PHYSICS**

**“All scientists shall have the right to present their scientific research results, in whole or in part, at relevant scientific conferences, and to publish the same in printed scientific journals, electronic archives, and any other media.”  
— Declaration of Academic Freedom, Article 8**

**ISSN 1555-5534**

# PROGRESS IN PHYSICS

A quarterly issue scientific journal, registered with the Library of Congress (DC, USA). This journal is peer reviewed and included in the abstracting and indexing coverage of: Mathematical Reviews and MathSciNet (AMS, USA), DOAJ of Lund University (Sweden), Zentralblatt MATH (Germany), Scientific Commons of the University of St. Gallen (Switzerland), Open-J-Gate (India), Referativnyi Zhurnal VINITI (Russia), etc.

Electronic version of this journal:  
<http://www.ptep-online.com>

## Editorial Board

Dmitri Rabounski, Editor-in-Chief  
rabounski@ptep-online.com  
Florentin Smarandache, Assoc. Editor  
smarand@unm.edu  
Larissa Borissova, Assoc. Editor  
borissova@ptep-online.com

## Editorial Team

Gunn Quznetsov  
quznetsov@ptep-online.com  
Andreas Ries  
ries@ptep-online.com  
Chifu Ebenezer Ndikilar  
ndikilar@ptep-online.com  
Felix Scholkmann  
scholkmann@ptep-online.com

## Postal Address

Department of Mathematics and Science,  
University of New Mexico,  
705 Gurley Ave., Gallup, NM 87301, USA

Copyright © *Progress in Physics*, 2012

All rights reserved. The authors of the articles do hereby grant *Progress in Physics* non-exclusive, worldwide, royalty-free license to publish and distribute the articles in accordance with the Budapest Open Initiative: this means that electronic copying, distribution and printing of both full-size version of the journal and the individual papers published therein for non-commercial, academic or individual use can be made by any user without permission or charge. The authors of the articles published in *Progress in Physics* retain their rights to use this journal as a whole or any part of it in any other publications and in any way they see fit. Any part of *Progress in Physics* howsoever used in other publications must include an appropriate citation of this journal.

This journal is powered by  $\text{\LaTeX}$

A variety of books can be downloaded free from the Digital Library of Science:  
<http://www.gallup.unm.edu/~smarandache>

ISSN: 1555-5534 (print)

ISSN: 1555-5615 (online)

Standard Address Number: 297-5092

Printed in the United States of America

OCTOBER 2012

VOLUME 4

## CONTENTS

<b>Potter F.</b> Pluto Moons Exhibit Orbital Angular Momentum Quantization per Mass . . . . .	3
<b>Millette P. A.</b> On the Decomposition of the Spacetime Metric Tensor and of Tensor Fields in Strained Spacetime . . . . .	5
<b>Comay E.</b> Quantum Constraints on a Charged Particle Structure . . . . .	9
<b>Drezet A.</b> Should the Wave-Function be a Part of the Quantum Ontological State? . . . . .	14
<b>Ndikilar C. E. and Lumbi L. W.</b> Relativistic Dynamics in the Vicinity of a Uniformly Charged Sphere . . . . .	18
<b>Ries A.</b> A Bipolar Model of Oscillations in a Chain System for Elementary Particle Masses . . . . .	20
<b>Potter F.</b> Galaxy S-Stars Exhibit Orbital Angular Momentum Quantization per Unit Mass . . . . .	29
<b>Lebed A. G.</b> Does the Equivalence between Gravitational Mass and Energy Survive for a Quantum Body? . . . . .	31
<b>Tank H. K.</b> Genesis of the “Critical-Acceleration of MOND” and Its Role in “Formation of Structures” . . . . .	36
<b>Khalaf A. M., Taha M. M., Kotb M.</b> Identical Bands and $\Delta I = 2$ Staggering in Superdeformed Nuclei in $A \sim 150$ Mass Region Using Three Parameters Rotational Model . . . . .	39
<b>Müller H.</b> Emergence of Particle Masses in Fractal Scaling Models of Matter . . . . .	44
<b>Panchelyuga V. A. and Panchelyuga M. S.</b> Resonance and Fractals on the Real Numbers Set . . . . .	48
<b>LETTERS</b>	
<b>Khazan A.</b> Atomic Masses of the Synthesed Elements (No.104–118) being Compared to Albert Khazan’s Data . . . . .	L1

## Information for Authors and Subscribers

*Progress in Physics* has been created for publications on advanced studies in theoretical and experimental physics, including related themes from mathematics and astronomy. All submitted papers should be professional, in good English, containing a brief review of a problem and obtained results.

All submissions should be designed in  $\text{\LaTeX}$  format using *Progress in Physics* template. This template can be downloaded from *Progress in Physics* home page <http://www.ptep-online.com>. Abstract and the necessary information about author(s) should be included into the papers. To submit a paper, mail the file(s) to the Editor-in-Chief.

All submitted papers should be as brief as possible. We accept brief papers, no larger than 8 typeset journal pages. Short articles are preferable. Large papers can be considered in exceptional cases to the section *Special Reports* intended for such publications in the journal. Letters related to the publications in the journal or to the events among the science community can be applied to the section *Letters to Progress in Physics*.

All that has been accepted for the online issue of *Progress in Physics* is printed in the paper version of the journal. To order printed issues, contact the Editors.

This journal is non-commercial, academic edition. It is printed from private donations. (Look for the current author fee in the online version of the journal.)

---

# Pluto Moons exhibit Orbital Angular Momentum Quantization per Mass

Franklin Potter

Sciencegems.com, 8642 Marvale Drive, Huntington Beach, CA, 92646, USA. E-mail: frank11hb@yahoo.com

The Pluto satellite system of the planet plus five moons is shown to obey the quantum celestial mechanics (QCM) angular momentum *per mass* quantization condition predicted for any gravitationally bound system.

The Pluto satellite system has at least five moons, Charon, P5, Nix, P4, and Hydra, and they are nearly in a 1:3:4:5:6 resonance condition! Before the recent detection of P5, Youdin et al. [1] (2012) analyzed the orbital behavior of the other four moons via standard Newtonian gravitation and found regions of orbital stability using distances from the Pluto-Charon barycenter.

I report here that these five moons each exhibit angular momentum quantization *per mass* in amazing agreement with the prediction of the quantum celestial mechanics (QCM) proposed by H. G. Preston and F. Potter [2, 3] in 2003. QCM predicts that bodies orbiting a central massive object in gravitationally bound systems obey the angular momentum  $L$  per mass  $\mu$  quantization condition

$$\frac{L}{\mu} = mcH, \tag{1}$$

with  $m$  an integer and  $c$  the speed of light. For most systems studied,  $m$  is an integer less than 20. The Preston gravitational distance  $H$  defined by the system total angular momentum divided by its total mass

$$H = \frac{L_T}{M_T c} \tag{2}$$

provides a characteristic QCM distance scale for the system.

At the QCM equilibrium orbital radius, the  $L$  of the orbiting body agrees with its Newtonian value  $\mu \sqrt{GM_T r}$ . One assumes that after tens of millions of years that the orbiting body is at or near its QCM equilibrium orbital radius  $r$  and that the orbital eccentricity is low so that our nearly circular orbit approximation leading to these particular equations holds true. For the Pluto system, Hydra has the largest eccentricity of 0.0051 and an  $m$  value of 12.

Details about the derivation of QCM from the general relativistic Hamilton-Jacobi equation and its applications to orbiting bodies in the Schwarzschild metric approximation and to the Universe in the the interior metric can be found in our original 2003 paper [2] titled “Exploring Large-scale Gravitational Quantization without  $\hbar$  in Planetary Systems, Galaxies, and the Universe”. Further applications to gravitational lensing [4], clusters of galaxies [5], the cosmological redshift as a gravitational redshift [6], exoplanetary systems and the Kepler-16 circumbinary system [7] all support this QCM approach.

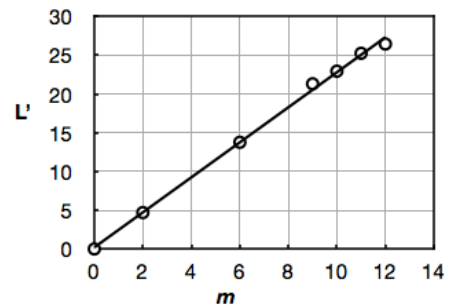


Fig. 1: The Pluto System fit to QCM

Table 1: Pluto system orbital parameters

	$r \times 10^6$ m	period (d)	$\epsilon$	$m$	$P_2/P_1$
Pluto	2.035	6.387230	0.0022	2	
Charon	17.536	6.387230	0.0022	6	1
P5	42.	20.2	$\sim 0$	9	2.915
Nix	48.708	24.856	0.0030	10	3.880
P4	59.	32.1	$\sim 0$	11	5.038
Hydra	64.749	38.206	0.0051	12	6.405

The important physical parameters of the Pluto system satellites from NASA, ESA, and M. Showalter (SETI Institute) et al. [8] as listed at Wikipedia are given in the table. The system total mass is essentially the combined mass of Pluto ( $13.05 \times 10^{21}$  kg) and Charon ( $1.52 \times 10^{21}$  kg). The QCM values of  $m$  in the next to last column were determined by the best linear regression fit ( $R^2 = 0.998$ ) to the angular momentum quantization per mass equation and are shown in the figure as  $L' = L/\mu c$  plotted against  $m$  with slope  $H = 2.258$  meters. Using distances from the center of Pluto instead of from the barycenter produces the same  $m$  values ( $R^2 = 0.995$ ) but a slightly different slope.

In QCM the orbital resonance condition is given by the period ratio given in the last column calculated from

$$\frac{P_2}{P_1} = \frac{(m_2 + 1)^3}{(m_1 + 1)^3}. \tag{3}$$

With Charon as the reference, this system of moons has nearly a 1:3:4:5:6 commensuration, with the last moon Hydra having

the largest discrepancy of almost 7%. If Hydra moves further out from the barycenter toward its QCM equilibrium orbital radius for  $m = 12$  in the next few million years, then its position on the plot will improve but its  $m$  value will remain the same. Note also that P5 at  $m = 9$  may move slightly closer to the barycenter. Dynamic analysis via the appropriate QCM equations will be reported later. Note that additional moons of Pluto may be found at non-occupied  $m$  values.

The QCM plot reveals that not all possible  $m$  values are occupied by moons of Pluto and at the same time predicts orbital radii where additional moons are expected to be. The present system configuration depends upon its history of formation and its subsequent evolution, both processes being dependent upon the dictates of QCM. Recall [2] that the satellite systems of the Jovian planets were shown to obey QCM, with some QCM orbital states occupied by more than one moon.

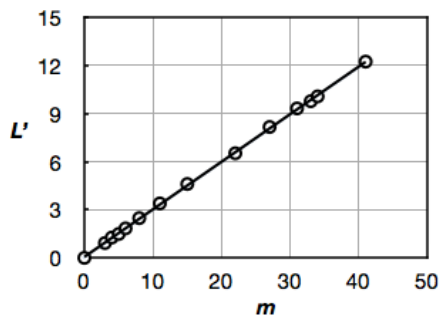


Fig. 2: The Solar System fit to QCM

I show in Fig. 2 the linear regression plot ( $r^2 = 0.999$ ) for the Solar System, this time with 8 planets plus the largest 5 additional minor planets Ceres, Pluto, Haumea, Makemake, and Eris. From the fit, the slope gives us a Solar System total angular momentum of about  $1.78 \times 10^{45}$  kg m<sup>2</sup>/s, far exceeding the angular momentum contributions of the planets by a factor of at least 50! Less than a hundred Earth masses at the 50,000–100,000 A.U. distance of the Oort Cloud therefore determines the angular momentum of the Solar System. Similar analyses have been done for numerous exoplanet systems [7] with multiple planets with the result that additional angular momentum is required, meaning that more planets and/or the equivalent of an Oort Cloud are to be expected.

The existence of angular momentum per mass quantization dictates also that the energy per mass quantization for a QCM state obeys

$$\frac{E}{\mu} = -\frac{r_g^2 c^2}{8n^2 H^2} = -\frac{G^2 M_T^4}{2n^2 L_T^2} \quad (4)$$

with  $n = m + 1$  for circular orbits and Schwarzschild radius  $r_g$ . One expects  $H \gg r_g$  for the Schwarzschild approximation to be acceptable, a condition upheld by the Pluto system, the Solar System, and all exoplanet systems. The correspond-

ing QCM state wave functions are confluent hypergeometric functions that reduce to hydrogen-like wave functions for circular orbits. Therefore, a QCM energy state exists for each  $n \geq 2$ . A body in a QCM state but not yet at the equilibrium radius for its  $m$  value will slowly drift toward this radius over significant time periods because the QCM accelerations are small.

In retrospect, the Pluto system is probably more like a binary system than a system with a single central mass, with the moons beyond Charon in circumbinary orbits around the barycenter. As such, I was surprised to find such a good fit to the QCM angular momentum restriction which was derived for the single dominant mass system. Additional moons of Pluto, should they exist, can provide some more insight into the application of QCM to this gravitationally bound system.

Meanwhile, the identification of additional exoplanets in nearby systems, particularly circumbinary planets, promises to create an interesting challenge for establishing QCM as a viable approach toward a better understanding of gravitation theory at all size scales.

#### Acknowledgements

The author acknowledges Sciencegems.com for its generous support.

Submitted on August 02, 2012 / Accepted on August 07, 2012

#### References

1. Youdin A. N., Kratter K. M., Kenyon S. J. Circumbinary Chaos: Using Pluto's Newest Moon to Constrain the Masses of Nix & Hydra. arXiv: 1205.5273v1.
2. Preston H. P., Potter F. Exploring Large-scale Gravitational Quantization without h-bar in Planetary Systems, Galaxies, and the Universe. arXiv: gr-qc/030311v1.
3. Potter F., Preston H. G. Quantum Celestial Mechanics: large-scale gravitational quantization states in galaxies and the Universe. *1st Crisis in Cosmology Conference: CCC-I*, Lerner E. J. and Almeida J. B., eds., AIP CP822, 2006, 239–252.
4. Potter F., Preston H. G. Gravitational Lensing by Galaxy Quantization States. arXiv: gr-qc/0405025v1.
5. Potter F., Preston H. G. Quantization State of Baryonic Mass in Clusters of Galaxies. *Progress in Physics*, 2007, v. 1, 61–63.
6. Potter F., Preston H. G. Cosmological Redshift Interpreted as Gravitational Redshift. *Progress in Physics*, 2007, v. 2, 31–33.
7. Potter F., Preston H. G. Kepler-16 Circumbinary System Validates Quantum Celestial Mechanics. *Progress in Physics*, 2012, v. 1, 52–53.
8. Showalter M., Weaver H. A., Stern S. A., Steffi A. J., Buie M. W. Hubble Discovers New Pluto Moon, 11 July 2012. [www.spacetelescope.org/news/heic1212](http://www.spacetelescope.org/news/heic1212)

# On the Decomposition of the Spacetime Metric Tensor and of Tensor Fields in Strained Spacetime

Pierre A. Millette

University of Ottawa (alumnus), K4A 2C3 747, Ottawa, CANADA. E-mail: PierreAMillette@alumni.uottawa.ca

We propose a natural decomposition of the spacetime metric tensor of General Relativity into a background and a dynamical part based on an analysis from first principles of the effect of a test mass on the background metric. We find that the presence of mass results in strains in the spacetime continuum. Those strains correspond to the dynamical part of the spacetime metric tensor. We then apply the stress-strain relation of Continuum Mechanics to the spacetime continuum to show that rest-mass energy density arises from the volume dilatation of the spacetime continuum. Finally we propose a natural decomposition of tensor fields in strained spacetime, in terms of dilatations and distortions. We show that dilatations correspond to rest-mass energy density, while distortions correspond to massless shear transverse waves. We note that this decomposition in a massive dilatation and a massless transverse wave distortion, where both are present in spacetime continuum deformations, is somewhat reminiscent of wave-particle duality. We note that these results are considered to be local effects in the particular reference frame of the observer. In addition, the applicability of the proposed metric to the Einstein field equations remains open.

## 1 Introduction

We first demonstrate from first principles that spacetime is strained by the presence of mass. Strained spacetime has been explored recently by Tartaglia *et al.* in the cosmological context, as an extension of the spacetime Lagrangian to obtain a generalized Einstein equation [1, 2]. Instead, in this analysis, we consider strained spacetime within the framework of Continuum Mechanics and General Relativity. This allows for the application of continuum mechanical results to the spacetime continuum. In particular, this provides a natural decomposition of the spacetime metric tensor and of spacetime tensor fields, both of which are still unresolved and are the subject of continuing investigations (see for example [3–7]).

## 2 Decomposition of the Spacetime Metric Tensor

There is no straightforward definition of local energy density of the gravitational field in General Relativity [8, see p. 84, p. 286] [6, 9, 10]. This arises because the spacetime metric tensor includes both the background spacetime metric and the local dynamical effects of the gravitational field. No natural way of decomposing the spacetime metric tensor into its background and dynamical parts is known.

In this section, we propose a natural decomposition of the spacetime metric tensor into a background and a dynamical part. This is derived from first principles by introducing a test mass in the spacetime continuum described by the background metric, and calculating the effect of this test mass on the metric.

Consider the diagram of Figure 1. Points  $A$  and  $B$  of the spacetime continuum, with coordinates  $x^\mu$  and  $x^\mu + dx^\mu$  re-

spectively, are separated by the infinitesimal line element

$$ds^2 = g_{\mu\nu} dx^\mu dx^\nu \quad (1)$$

where  $g_{\mu\nu}$  is the metric tensor describing the background state of the spacetime continuum.

We now introduce a test mass in the spacetime continuum. This results in the displacement of point  $A$  to  $\tilde{A}$ , where the displacement is written as  $u^\mu$ . Similarly, the displacement of point  $B$  to  $\tilde{B}$  is written as  $u^\mu + du^\mu$ . The infinitesimal line element between points  $\tilde{A}$  and  $\tilde{B}$  is given by  $\tilde{ds}^2$ .

By reference to Figure 1, the infinitesimal line element  $\tilde{ds}^2$  can be expressed in terms of the background metric tensor as

$$\tilde{ds}^2 = g_{\mu\nu} (dx^\mu + du^\mu)(dx^\nu + du^\nu). \quad (2)$$

Multiplying out the terms in parentheses, we get

$$\tilde{ds}^2 = g_{\mu\nu} (dx^\mu dx^\nu + dx^\mu du^\nu + du^\mu dx^\nu + du^\mu du^\nu). \quad (3)$$

Expressing the differentials  $du$  as a function of  $x$ , this equation becomes

$$\begin{aligned} \tilde{ds}^2 = & g_{\mu\nu} (dx^\mu dx^\nu + dx^\mu u^\nu{}_{;\alpha} dx^\alpha + u^\mu{}_{;\alpha} dx^\alpha dx^\nu + \\ & + u^\mu{}_{;\alpha} dx^\alpha u^\nu{}_{;\beta} dx^\beta) \end{aligned} \quad (4)$$

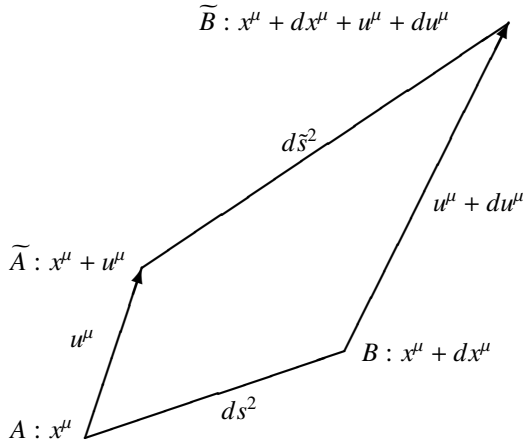
where the semicolon (;) denotes covariant differentiation. Rearranging the dummy indices, this expression can be written as

$$\tilde{ds}^2 = (g_{\mu\nu} + g_{\mu\alpha} u^\alpha{}_{;\nu} + g_{\alpha\nu} u^\alpha{}_{;\mu} + g_{\alpha\beta} u^\alpha{}_{;\mu} u^\beta{}_{;\nu}) dx^\mu dx^\nu \quad (5)$$

and lowering indices, the equation becomes

$$\tilde{ds}^2 = (g_{\mu\nu} + u_{\mu;\nu} + u_{\nu;\mu} + u^\alpha{}_{;\mu} u_{\alpha;\nu}) dx^\mu dx^\nu. \quad (6)$$

Fig. 1: Effect of a test mass on the background metric tensor



The expression  $u_{\mu;\nu} + u_{\nu;\mu} + u^{\alpha}{}_{;\mu}u_{\alpha;\nu}$  is equivalent to the definition of the strain tensor  $\varepsilon^{\mu\nu}$  of Continuum Mechanics. The strain  $\varepsilon^{\mu\nu}$  is expressed in terms of the displacements  $u^{\mu}$  of a continuum through the kinematic relation [11, see p. 149] [12, see pp. 23–28]:

$$\varepsilon^{\mu\nu} = \frac{1}{2}(u^{\mu;\nu} + u^{\nu;\mu} + u^{\alpha;\mu}u_{\alpha}{}^{;\nu}). \quad (7)$$

Substituting for  $\varepsilon^{\mu\nu}$  from Eq.(7) into Eq.(6), we get

$$\tilde{d}s^2 = (g_{\mu\nu} + 2\varepsilon_{\mu\nu})dx^{\mu}dx^{\nu}. \quad (8)$$

Setting [12, see p. 24]

$$\tilde{g}_{\mu\nu} = g_{\mu\nu} + 2\varepsilon_{\mu\nu} \quad (9)$$

then Eq.(8) becomes

$$\tilde{d}s^2 = \tilde{g}_{\mu\nu}dx^{\mu}dx^{\nu} \quad (10)$$

where  $\tilde{g}_{\mu\nu}$  is the metric tensor describing the spacetime continuum with the test mass.

Given that  $g_{\mu\nu}$  is the background metric tensor describing the background state of the continuum, and  $\tilde{g}_{\mu\nu}$  is the spacetime metric tensor describing the final state of the continuum with the test mass, then  $2\varepsilon_{\mu\nu}$  must represent the dynamical part of the spacetime metric tensor due to the test mass:

$$g_{\mu\nu}^{dyn} = 2\varepsilon_{\mu\nu}. \quad (11)$$

We are thus led to the conclusion that the presence of mass results in strains in the spacetime continuum. Those strains correspond to the dynamical part of the spacetime metric tensor. Hence the applied stresses from mass (i.e. the energy-momentum stress tensor) result in strains in the spacetime continuum, that is strained spacetime.

### 3 Rest-Mass Energy Relation

The introduction of strains in the spacetime continuum as a result of the energy-momentum stress tensor allows us to use by analogy results from Continuum Mechanics, in particular the stress-strain relation, to provide a better understanding of strained spacetime.

The stress-strain relation for an isotropic and homogeneous spacetime continuum can be written as [12, see pp. 50–53]:

$$2\mu_0\varepsilon^{\mu\nu} + \lambda_0g^{\mu\nu}\varepsilon = T^{\mu\nu} \quad (12)$$

where  $T^{\mu\nu}$  is the energy-momentum stress tensor,  $\varepsilon^{\mu\nu}$  is the resulting strain tensor, and

$$\varepsilon = \varepsilon^{\alpha}{}_{\alpha} \quad (13)$$

is the trace of the strain tensor obtained by contraction.  $\varepsilon$  is the volume dilatation defined as the change in volume per original volume [11, see p. 149–152] and is an invariant of the strain tensor.  $\lambda_0$  and  $\mu_0$  are the Lamé elastic constants of the spacetime continuum:  $\mu_0$  is the shear modulus and  $\lambda_0$  is expressed in terms of  $\kappa_0$ , the bulk modulus:

$$\lambda_0 = \kappa_0 - \mu_0/2 \quad (14)$$

in a four-dimensional continuum. The contraction of Eq.(12) yields the relation

$$2(\mu_0 + 2\lambda_0)\varepsilon = T^{\alpha}{}_{\alpha} \equiv T. \quad (15)$$

The time-time component  $T^{00}$  of the energy-momentum stress tensor represents the total energy density given by [13, see pp. 37–41]

$$T^{00}(x^k) = \int d^3\mathbf{p} E_p f(x^k, \mathbf{p}) \quad (16)$$

where  $E_p = (\rho^2 c^4 + p^2 c^2)^{1/2}$ ,  $\rho$  is the rest-mass energy density,  $c$  is the speed of light,  $\mathbf{p}$  is the momentum 3-vector and  $f(x^k, \mathbf{p})$  is the distribution function representing the number of particles in a small phase space volume  $d^3\mathbf{x}d^3\mathbf{p}$ . The space-space components  $T^{ij}$  of the energy-momentum stress tensor represent the stresses within the medium given by

$$T^{ij}(x^k) = c^2 \int d^3\mathbf{p} \frac{p^i p^j}{E_p} f(x^k, \mathbf{p}). \quad (17)$$

They are the components of the net force acting across a unit area of a surface, across the  $x^i$  planes in the case where  $i = j$ .

In the simple case of a particle, they are given by [14, see p. 117]

$$T^{ii} = \rho v^i v^i \quad (18)$$

where  $v^i$  are the spatial components of velocity. If the particles are subject to forces, these stresses must be included in the energy-momentum stress tensor.

Explicitly separating the time-time and the space-space components, the trace of the energy-momentum stress tensor is written as

$$T^\alpha_\alpha = T^0_0 + T^i_i. \quad (19)$$

Substituting from Eq.(16) and Eq.(17), using the metric  $\eta^{\mu\nu}$  of signature (+---), we obtain:

$$T^\alpha_\alpha(x^k) = \int d^3\mathbf{p} \left( E_p - \frac{p^2 c^2}{E_p} \right) f(x^k, \mathbf{p}) \quad (20)$$

which simplifies to

$$T^\alpha_\alpha(x^k) = \rho^2 c^4 \int d^3\mathbf{p} \frac{f(x^k, \mathbf{p})}{E_p}. \quad (21)$$

Using the relation [13, see p. 37]

$$\frac{1}{\bar{E}_{har}(x^k)} = \int d^3\mathbf{p} \frac{f(x^k, \mathbf{p})}{E_p} \quad (22)$$

in equation Eq.(21), we obtain the relation

$$T^\alpha_\alpha(x^k) = \frac{\rho^2 c^4}{\bar{E}_{har}(x^k)} \quad (23)$$

where  $\bar{E}_{har}(x^k)$  is the Lorentz invariant harmonic mean of the energy of the particles at  $x^k$ .

In the harmonic mean of the energy of the particles  $\bar{E}_{har}$ , the momentum contribution  $\mathbf{p}$  will tend to average out and be dominated by the mass term  $\rho c^2$ , so that we can write

$$\bar{E}_{har}(x^k) \simeq \rho c^2. \quad (24)$$

Substituting for  $\bar{E}_{har}$  in Eq.(23), we obtain the relation

$$T^\alpha_\alpha(x^k) \simeq \rho c^2. \quad (25)$$

The total rest-mass energy density of the system is obtained by integrating over all space:

$$T^\alpha_\alpha = \int d^3\mathbf{x} T^\alpha_\alpha(x^k). \quad (26)$$

The expression for the trace derived from Eq.(19) depends on the composition of the sources of the gravitational field. Considering the energy-momentum stress tensor of the electromagnetic field, we can show that  $T^\alpha_\alpha = 0$  as expected for massless photons, while

$$T^{00} = \frac{\epsilon_0}{2} (E^2 + c^2 B^2)$$

is the total energy density, where  $\epsilon_0$  is the electromagnetic permittivity of free space, and  $E$  and  $B$  have their usual significance.

Hence  $T^\alpha_\alpha$  corresponds to the invariant rest-mass energy density and we write

$$T^\alpha_\alpha = T = \rho c^2 \quad (27)$$

where  $\rho$  is the rest-mass energy density. Using Eq.(27) into Eq.(15), the relation between the invariant volume dilatation  $\varepsilon$  and the invariant rest-mass energy density becomes

$$2(\mu_0 + 2\lambda_0)\varepsilon = \rho c^2 \quad (28)$$

or, in terms of the bulk modulus  $\kappa_0$ ,

$$4\kappa_0\varepsilon = \rho c^2. \quad (29)$$

This equation demonstrates that rest-mass energy density arises from the volume dilatation of the spacetime continuum. The rest-mass energy is equivalent to the energy required to dilate the volume of the spacetime continuum, and is a measure of the energy stored in the spacetime continuum as volume dilatation.  $\kappa_0$  represents the resistance of the spacetime continuum to dilatation. The volume dilatation is an invariant, as is the rest-mass energy density.

#### 4 Decomposition of Tensor Fields in Strained Spacetime

As opposed to vector fields which can be decomposed into longitudinal (irrotational) and transverse (solenoidal) components using the Helmholtz representation theorem [11, see pp. 260–261], the decomposition of spacetime tensor fields can be done in many ways (see for example [3–5, 7]).

The application of Continuum Mechanics to a strained spacetime continuum offers a natural decomposition of tensor fields, in terms of dilatations and distortions [12, see pp. 58–60]. A *dilatation* corresponds to a change of volume of the spacetime continuum without a change of shape (as seen in Section 3) while a *distortion* corresponds to a change of shape of the spacetime continuum without a change in volume. Dilatations correspond to longitudinal displacements and distortions correspond to transverse displacements [11, see p. 260].

The strain tensor  $\varepsilon^{\mu\nu}$  can thus be decomposed into a strain deviation tensor  $e^{\mu\nu}$  (the *distortion*) and a scalar  $e$  (the *dilatation*) according to [12, see pp. 58–60]:

$$\varepsilon^{\mu\nu} = e^{\mu\nu} + e g^{\mu\nu} \quad (30)$$

where

$$e^\mu_\nu = \varepsilon^\mu_\nu - e \delta^\mu_\nu \quad (31)$$

$$e = \frac{1}{4} \varepsilon^\alpha_\alpha = \frac{1}{4} \varepsilon. \quad (32)$$

Similarly, the energy-momentum stress tensor  $T^{\mu\nu}$  is decomposed into a stress deviation tensor  $t^{\mu\nu}$  and a scalar  $t$  according to

$$T^{\mu\nu} = t^{\mu\nu} + t g^{\mu\nu} \quad (33)$$

where similarly

$$t^\mu_\nu = T^\mu_\nu - t \delta^\mu_\nu \quad (34)$$

$$t = \frac{1}{4} T^\alpha_\alpha. \quad (35)$$

Using Eq.(30) to Eq.(35) into the strain-stress relation of Eq.(12) and making use of Eq.(15) and Eq.(14), we obtain separated dilatation and distortion relations respectively:

$$\begin{aligned} \text{dilatation : } t &= 2(\mu_0 + 2\lambda_0)e = 4\kappa_0e = \kappa_0\varepsilon \\ \text{distortion : } t^{\mu\nu} &= 2\mu_0e^{\mu\nu}. \end{aligned} \quad (36)$$

The distortion-dilatation decomposition is evident in the dependence of the dilatation relation on the bulk modulus  $\kappa_0$  and of the distortion relation on the shear modulus  $\mu_0$ . As shown in Section 3, the dilatation relation of Eq.(36) corresponds to rest-mass energy, while the distortion relation is traceless and thus massless, and corresponds to shear transverse waves.

This decomposition in a massive dilatation and a massless transverse wave distortion, where both are present in space-time continuum deformations, is somewhat reminiscent of wave-particle duality. This could explain why dilatation-measuring apparatus measure the massive 'particle' properties of the deformation, while distortion-measuring apparatus measure the massless transverse 'wave' properties of the deformation.

## 5 Conclusion

In this paper, we have proposed a natural decomposition of the spacetime metric tensor into a background and a dynamical part based on an analysis from first principles, of the impact of introducing a test mass in the spacetime continuum. We have found that the presence of mass results in strains in the spacetime continuum. Those strains correspond to the dynamical part of the spacetime metric tensor.

We have applied the stress-strain relation of Continuum Mechanics to the spacetime continuum to show that rest-mass energy density arises from the volume dilatation of the spacetime continuum.

Finally we have proposed a natural decomposition of tensor fields in strained spacetime, in terms of dilatations and distortions. We have shown that dilatations correspond to rest-mass energy density, while distortions correspond to massless shear transverse waves. We have noted that this decomposition in a dilatation with rest-mass energy density and a massless transverse wave distortion, where both are simultaneously present in spacetime continuum deformations, is somewhat reminiscent of wave-particle duality.

It should be noted that these results are considered to be local effects in the particular reference frame of the observer. In addition, the applicability of the proposed metric to the Einstein field equations remains open.

Submitted on August 5, 2012 / Accepted on August 08, 2012

## References

1. Tartaglia A. A Strained Space-time to Explain the large Scale Properties of the Universe. *International Journal of Modern Physics: Conference Series*, 2011, v. 3, 303–311.
2. Tartaglia A., Radicella N., Sereno M. Lensing in an elastically strained space-time. *Journal of Physics: Conference Series*, 2011, v. 283, 012037.
3. Deser S. Covariant decomposition of symmetric tensors and the gravitational Cauchy problem. *Annales de l'Institut Henri Poincaré A*, 1967, v. 7(2), 149–188.
4. Krupka D. The Trace Decomposition Problem. *Contributions to Algebra and Geometry*, 1995, v. 36(2), 303–315.
5. Straumann N. Proof of a decomposition theorem for symmetric tensors on spaces with constant curvature. arXiv: gr-qc/0805.4500v1.
6. Chen X.-S., Zhu B.-C. Physical decomposition of the gauge and gravitational fields. arXiv: gr-qc/1006.3926v3.
7. Chen X.-S., Zhu B.-C. Tensor gauge condition and tensor field decomposition. arXiv: gr-qc/1101.2809v5.
8. Wald R.M. *General Relativity*. The University of Chicago Press, Chicago, 1984.
9. Szabados L.B. Quasi-Local Energy-Momentum and Angular Momentum in GR: A Review Article. *Living Reviews in Relativity*, 2004, v. 7, 4.
10. Jaramillo J.L.,ourgoulhon E. Mass and Angular Momentum in General Relativity. arXiv: gr-qc/1001.5429v2.
11. Segel L.A. *Mathematics Applied to Continuum Mechanics*. Dover Publications, New York, 1987.
12. Flügge W. *Tensor Analysis and Continuum Mechanics*. Springer-Verlag, New York, 1972.
13. Padmanabhan T. *Gravitation, Foundations and Frontiers*. Cambridge University Press, Cambridge, 2010.
14. Eddington A.S. *The Mathematical Theory of Relativity*. Cambridge University Press, Cambridge, 1957.

# Quantum Constraints on a Charged Particle Structure

Eliahu Comay

Charactell Ltd., PO Box 39019, Tel-Aviv, 61390, Israel. E-mail: elicomay@post.tau.ac.il

The crucial role of a Lorentz scalar Lagrangian density whose dimension is  $[L^{-4}]$  ( $\hbar = c = 1$ ) in a construction of a quantum theory is explained. It turns out that quantum functions used in this kind of Lagrangian density have a definite dimension. It is explained why quantum functions that have the dimension  $[L^{-1}]$  cannot describe particles that carry electric charge. It is shown that the 4-current of a quantum particle should satisfy further requirements. It follows that the pion and the  $W^\pm$  must be composite particles. This outcome is inconsistent with the electroweak theory. It is also argued that the 125 GeV particle found recently by two LHC collaborations is not a Higgs boson but a  $t\bar{t}$  meson.

## 1 Introduction

The fundamental role of mathematics in the structure of theoretical physics is regarded as an indisputable element of the theory [1]. This principle is utilized here. The analysis relies on special relativity and derives constraints on the structure of equations of motion of quantum particles. The discussion examines the dimensions of wave functions and explains why spin-0 and spin-1 elementary quantum particles cannot carry an electric charge. This conclusion is relevant to the validity of the electroweak theory and to the meaning of recent results concerning the existence of a particle having a mass of 125 GeV [2, 3].

Units where  $\hbar = c = 1$  are used in this work. Hence, only one dimension is required and it is the length, denoted by  $[L]$ . For example, mass, energy and momentum have the dimension  $[L^{-1}]$ , etc. Greek indices run from 0 to 3 and the diagonal metric used is  $g_{\mu\nu} = (1, -1, -1, -1)$ . The symbol  $_{,\mu}$  denotes the partial differentiation with respect to  $x^\mu$  and an upper dot denotes a differentiation with respect to time. The summation convention is used for Greek indices.

The second section shows that quantum functions have a definite dimension. This property is used in the third section where it is proved that Klein-Gordon (KG) fields and those of the  $W^\pm$  particle have no self-consistent Hamiltonian. The final section contains a discussion of the significance of the results obtained in this work.

## 2 The dimensions of quantum fields

In this section some fundamental properties of quantum theory are used for deriving the dimensions of quantum fields. A massive quantum mechanical particle is described by a wave function  $\psi(x^\mu)$ . The phase  $\varphi(\alpha)$  is an important factor of  $\psi(x^\mu)$  because it determines the form of an interference pattern. For the present discussion it is enough to demand that the phase is an analytic function which can be expanded in a power series that contains more than one term. It means that in the

following expansion of the phase,

$$\varphi(\alpha) = \sum_{i=0}^{\infty} a_i \alpha^i, \quad (1)$$

the inequality  $a_i \neq 0$  holds for two or more values of the index  $i$ .

The requirement stating that all terms of a physical expression must have the same dimension and the form of the right hand side of (1) prove that  $\alpha$  must be dimensionless. By the same token, in a relativistic quantum theory,  $\alpha$  must also be a Lorentz scalar. (The possibility of using a pseudoscalar factor is not discussed here because this work aims to examine the parity conserving electromagnetic interactions of a quantum mechanical particle.) It is shown below how these two requirements impose dramatic constraints on acceptable quantum mechanical equations of motion of a charged particle.

Evidently, a pure number satisfies the two requirements. However, a pure number is inadequate for our purpose, because the phase varies with the particle's energy and momentum. The standard method of constructing a quantum theory is to use the Planck's constant  $\hbar$  which has the dimension of the action, and to define the phase as the action divided by  $\hbar$ . In the units used here,  $\hbar = 1$  and the action is dimensionless. Thus, a relativistic quantum theory satisfies the two requirements presented above if it is derived from a Lagrangian density  $\mathcal{L}$  that is a Lorentz scalar having the dimension  $[L^{-4}]$ . Indeed, in this case, the action

$$S = \int \mathcal{L} d^4 x^\mu \quad (2)$$

is a dimensionless Lorentz scalar. It is shown below how the dimension  $[L^{-4}]$  of  $\mathcal{L}$  defines the dimension of quantum fields.

Being aware of these requirements, let us find the dimension of the quantum functions used for a description of three kinds of quantum particles. The Dirac Lagrangian density of

a free spin-1/2 particle is [4, see p. 54]

$$\mathcal{L} = \bar{\psi}[\gamma^\mu i\partial_\mu - m]\psi. \quad (3)$$

Here the operator has the dimension  $[L^{-1}]$  and the Dirac wave function  $\psi$  has the dimension  $[L^{-3/2}]$ .

The Klein-Gordon Lagrangian density of a free spin-0 particle is [4, see p. 38]

$$\mathcal{L} = \phi_{,\mu}^* \phi_{,\nu} g^{\mu\nu} - m^2 \phi^* \phi. \quad (4)$$

Here the operator has the dimension  $[L^{-2}]$  and the KG wave function  $\phi$  has the dimension  $[L^{-1}]$ .

The electrically charged spin-1  $W^\pm$  particle is described by a 4-vector function  $W_\mu$ .  $W_\mu$  and the electromagnetic 4-potential  $A_\mu$  are linear combinations of related quantities [5, see p. 518]. Evidently, they have the same dimension. Hence, like the KG field, the dimension of  $W_\mu$  is  $[L^{-1}]$ .

The dimension of each of these fields is used in the discussions presented in the rest of this work.

### 3 Consequences of the dimensions of quantum fields

Before analyzing the consequences of the dimension of quantum fields and of the associated wave functions, it is required to realize the Hamiltonian's role in quantum theories. The following lines explain why the Hamiltonian is an indispensable element of Relativistic Quantum Mechanics (RQM) and of Quantum Field Theory (QFT). This status of the Hamiltonian is required for the analysis presented below.

The significance of hierarchical relationships that hold between physical theories is discussed in the literature [6, see pp. 1-6] and [7, see pp. 85, 86]. The foundation of the argument can be described as follows. Physical theories take the form of differential equations. These equations can be examined in appropriate limits. Now RQM is a limit of QFT. The former holds for cases where the number of particles can be regarded as a constant of the motion. Therefore, if examined in this limit, QFT must agree with RQM. By the same token, the classical limit of RQM must agree with classical physics. This matter has been recognized by the founders of quantum mechanics who have proven that the classical limit of quantum mechanics agrees with classical physics. The following example illustrates the importance of this issue. Let us examine an inelastic scattering event. The chronological order of this process is as follows:

- First, two particles move in external electromagnetic fields. Relativistic classical mechanics and classical electrodynamics describe the motion.
- The two particles are very close to each other. RQM describes the process.
- The two particles collide and interact. New particles are created. The process is described by QFT.
- Particle creation ends but particles are still very close to one another. RQM describes the state.

- Finally, the outgoing particles depart. Relativistic classical mechanics and classical electrodynamics describe the motion.

Evidently, in this kind of experiment, energy and momentum of the initial and the final states are well defined quantities and their final state values abide by the law of energy-momentum conservation. It means that the specific values of the energy-momentum of the final state agree with the corresponding quantities of the initial state. Now, the initial and the final states are connected by processes that are described by RQM and QFT. In particular, the process of new particle creation is described only by QFT. Hence, RQM and QFT must "tell" the final state what are the precise initial values of the energy-momentum. It follows that RQM as well as QFT must use field functions that have a self-consistent Hamiltonian.

The Hamiltonian  $H$  and the de Broglie relations between a particle's energy-momentum and its wave properties yield the fundamental equation of quantum mechanics

$$i\frac{\partial\psi}{\partial t} = H\psi. \quad (5)$$

The Hamiltonian density  $\mathcal{H}$  is derived from the Lagrangian density by the following well known Legendre transformation

$$\mathcal{H} = \sum_i \dot{\psi}_i \frac{\partial\mathcal{L}}{\partial\dot{\psi}_i} - \mathcal{L}, \quad (6)$$

where the index  $i$  runs on all functions.

The standard form of representing the interaction of an electric charge with external fields relies on the following transformation [8, see p. 10]

$$-i\frac{\partial}{\partial x^\mu} \rightarrow -i\frac{\partial}{\partial x^\mu} - eA_\mu(x^\nu). \quad (7)$$

Now let us examine the electromagnetic interaction of the three kinds of quantum mechanical particle described in the previous section. This is done by adding an interaction term  $\mathcal{L}_{int}$  to the Lagrangian density. As explained above, this term must be a Lorentz scalar whose dimension is  $[L^{-4}]$ . The required form of the electromagnetic interaction term represents the interaction of charged particles with electromagnetic fields *and* the interaction of electromagnetic fields with charged particles. This term is written as follows [9, see p. 75]

$$\mathcal{L}_{int} = -j^\mu A_\mu. \quad (8)$$

Here  $j^\mu$  is the 4-current of the quantum particle and  $A_\mu$  is the electromagnetic 4-potential.

Charge conservation requires that  $j^\mu$  satisfies the continuity equation

$$j_{,\mu}^\mu = 0. \quad (9)$$

The 0-component of the 4-vector  $j^\mu$  represents density. It follows that its dimension is  $[L^{-3}]$  and the electromagnetic interaction (8) is a term of the Lagrangian density. For this reason, it is a Lorentz scalar whose dimension is  $[L^{-4}]$ . Hence,

a quantum particle can carry electric charge provided a self-consistent 4-current can be defined for it. Furthermore, a self-consistent definition of density is also required for a construction the Hilbert space where density is used for defining its inner product.

It is well known that a self-consistent 4-current can be defined for a Dirac particle [8, see pp. 8,9,23,24]

$$j^\mu = e\bar{\psi}\gamma^\mu\psi. \quad (10)$$

This expression has properties that are consistent with general requirements of a quantum theory. In particular, the 4-current is related to a construction of a Hilbert space. Here the density  $\psi^\dagger\psi$  is the 0-component of the 4-current (10). As required, this quantity has the dimension  $[L^{-3}]$ . Thus, electromagnetic interactions of charged spin-1/2 Dirac particles are properly described by the Dirac equation.

Let us turn to the case of a charged KG or  $W^\mu$  particle. Here the appropriate wave function has the dimension  $[L^{-1}]$ . This dimension proves that it cannot be used for constructing a self-consistent Hilbert space. Indeed, let  $\phi$  denote a function of such a Hilbert space and let  $O$  be an operator operating on this space. Then, the expectation value of  $O$  is

$$\langle O \rangle = \int \phi^* O \phi d^3x. \quad (11)$$

Now,  $\langle O \rangle$  and  $O$  have the same dimension. Therefore  $\phi$  must have the dimension  $[L^{-3/2}]$ . This requirement is not satisfied by the function  $\phi$  of a KG particle or by  $W^\mu$  because here the dimension is  $[L^{-1}]$ . Hence, there is no Hilbert space for a KG or  $W^\mu$  particle. For this reason, there is also no Hamiltonian for these functions, because a Hamiltonian is an operator operating on a Hilbert space. Analogous results are presented for the specific case of the KG equation [10].

The dimension  $[L^{-1}]$  of the KG and the  $W^\mu$  functions also yields another very serious mathematical problem. Indeed, in order to have a dimension  $[L^{-4}]$ , their Lagrangian density has terms that are *bilinear* in derivatives with respect to the space-time coordinates. Thus, the KG Lagrangian density is (4) and the  $W^\mu$  Lagrangian density takes the following form [11, see p. 307]

$$\mathcal{L}_W = -\frac{1}{4}(\partial_\mu W_\nu - \partial_\nu W_\mu + gW_\mu \times W_\nu)^2. \quad (12)$$

As is well known, an operation of the Legendre transformation (6) on a Lagrangian density that is *linear* in time derivatives yields an expression that is *independent* of time derivatives. Thus, the Dirac Lagrangian density (3) yields a Hamiltonian that is free of time derivatives. On the other hand, the Hamiltonian density of the KG and  $W^\mu$  particles depends on time derivatives. Indeed, using (5), one infers that for these particles, the Hamiltonian density depends quadratically on the Hamiltonian. Hence, there is no explicit expression for the Hamiltonian of the KG and the  $W^\mu$  particles.

Two results are directly obtained from the foregoing discussion. The Fock space, which denotes the occupation number of particles in appropriate states, is based on functions of the associated Hilbert space. Hence, in the case of KG or  $W^\mu$  function there are very serious problems with the construction of a Fock space because these functions have no Hilbert space. Therefore, one also wonders what is the meaning of the creation and the annihilation operators of QFT.

Another result refers to the 4-current. Thus, both the KG equations and the  $W^\mu$  function have a 4-current that satisfies (9) [11, see p. 12] and [12, see p. 199]. However, the contradictions derived above prove the following important principle: *The continuity relation (9) is just a necessary condition for an acceptable 4-current. This condition is not sufficient and one must also confirm that a theory that uses a 4-current candidate is contradiction free.*

The contradictions which are described above hold for the KG and the  $W^\pm$  particles provided that these particles are elementary pointlike quantum mechanical objects which are described by a function of the form  $\psi(x^\mu)$ . Hence, *in order to avoid contradictions with the existence of charged pions and  $W^\pm$ , one must demand that the pions and the  $W^\pm$  are composite particles.* Several aspects of this conclusion are discussed in the next section. It should also be noted that the results of this section are consistent with Dirac's lifelong objection to the KG equation [13].

#### 4 Discussion

An examination of textbooks provides a simple argument supporting the main conclusion of this work. Indeed, quantum mechanics is known for more than 80 years. It turns out that the Hamiltonian problem of the hydrogen atom of a Dirac particle is discussed adequately in relevant textbooks [8, 14]. By contrast, in spite of the long duration of quantum mechanics as a valid theory, an appropriate discussion of the Hamiltonian solution of a hydrogen-like atom of a relativistic electrically charged integral spin particle is not presented in textbooks. Note that the operator on the left hand side of the KG equation [14, see p. 886]

$$(\partial_\mu + ieA_\mu)g^{\mu\nu}(\partial_\nu + ieA_\nu)\phi = -m^2\phi \quad (13)$$

is *not* related to a Hamiltonian because (13) is a Lorentz scalar whereas the Hamiltonian is a 0-component of a 4-vector.

An analogous situation holds for the Hilbert and the Fock spaces that are created from functions on which the Hamiltonian operates. Thus, in the case of a Dirac particle, the density  $\psi^\dagger\psi$  is the 0-component of the conserved 4-current (10). This expression is suitable for a definition of the Hilbert space inner product of any pair of integrable functions

$$(\psi_i^\dagger, \psi_j) \equiv \int \psi_i^\dagger \psi_j d^3x. \quad (14)$$

Indeed, it is derivative free and this property enables the usage of the Heisenberg picture which is based on time-

independent functions. Integration properties prove that (14) is linear in  $\psi_i^\dagger$  and  $\psi_j$ . Thus,

$$(a\psi_i^\dagger + b\psi_k^\dagger, \psi_j) = a(\psi_i^\dagger, \psi_j) + b(\psi_k^\dagger, \psi_j).$$

Furthermore,  $(\psi_i^\dagger, \psi_i)$  is a real non-negative number that vanishes if and only if  $\psi_i \equiv 0$ . These properties are required from a Hilbert space inner product. It turns out that the construction of a Hilbert space is the cornerstone used for calculating successful solutions of the Dirac equation and of its associated Pauli and Schroedinger equations as well.

By contrast, in the case of particles having an integral spin, one cannot find in the literature an explicit construction of a Hilbert space. Indeed, the  $[L^{-1}]$  dimension of their functions proves that the simple definition of an inner product in the form  $\int \phi_i^* \phi_j d^3x$  has the dimension  $[L]$  which is unacceptable. An application of the 0-component of these particles 4-current [11, see p. 12] and [12, see p. 199] is not free of contradictions. Thus, the time derivative included in these expressions prevents the usage of the Heisenberg picture. Relation (7) proves that in the case of a charged particle the density depends on *external* quantities. These quantities may vary in time and for this reason it cannot be used in a definition of a Hilbert space inner product. In the case of the  $W^\mu$  function, the expression is inconsistent with the linearity required from a Hilbert space inner product.

The results found in this work apply to particles described by a function of the form

$$\psi(x^\mu). \quad (15)$$

Their dependence on a single set of four space-time coordinates  $x^\mu$  means that they describe an elementary pointlike particle. For example, this kind of function cannot adequately describe a pion because this particle is not an elementary particle but a quark-antiquark bound state. Thus, it consists of a quark-antiquark pair which are described by *two* functions of the form (15). For this reason, one function of the form (15) cannot describe a pion simply because a description of a pion should use a larger number of degrees of freedom. It follows that the existence of a  $\pi^+$ , which is a spin-0 charged particle, does not provide an experimental refutation of the theoretical results obtained above.

Some general aspects of this work are pointed out here. There are two kinds of objects in electrodynamics of Dirac particles: massive charged spin-1/2 particles and charge-free photons. The dimension of a Dirac function is  $[L^{-3/2}]$  and the dimension of the electromagnetic 4-potential is  $[L^{-1}]$ . Now, the spin of any interaction carrying particle must take an integral value in order that the matrix element connecting initial and final states should not vanish. The dimension of an interaction carrying particle must be  $[L^{-1}]$  so that the Lagrangian density interaction term have the dimension  $[L^{-4}]$ . These properties must be valid for particles that carry any kind of interaction between Dirac-like particles. Hence, the pions and

the  $W^\pm$  have integral spin and dimension  $[L^{-1}]$ . However, in order to have a self-consistent Hilbert and Fock spaces, a function describing an elementary massive particle must have the dimension  $[L^{-3/2}]$ . Neither a KG function nor the  $W^\mu$  function satisfies this requirement.

The conclusion stating that the continuity equation (9) is only a *necessary condition* required from a physically acceptable 4-current and that further consistency tests must be carried out, looks like a new result of this work that has a general significance.

Before discussing the state of the  $W^\pm$  charged particles, let us examine the strength of strong interactions. Each of the following arguments proves that strong interactions yield extremely relativistic bound states and that the interaction part of the Hamiltonian swallows a large portion of the quarks' mass.

- A. Antiquarks have been measured directly in the proton [15, see p. 282]. This is a clear proof of the extremely relativistic state of hadrons. Indeed, for reducing the overall mass of the proton, it is energetically "profitable" to add the mass of two quarks because the increased interaction is very strong.
- B. The mass of the  $\rho$  meson is about five times greater than the pion's mass. Now these mesons differ by the relative spin alignment of their quark constituents. Evidently, spin interaction is a relativistic effect and the significant  $\pi$ ,  $\rho$  mass difference indicates that strong interactions are very strong indeed.
- C. The pion is made of a  $u, d$  quark-antiquark pair and its mass is about  $140 \text{ MeV}$ . Measurements show that there are mesons made of the  $u, d$  flavors whose mass is greater than  $2000 \text{ MeV}$  [6]. Hence, strong interactions consume most of the original mass of quarks.
- D. Let us examine the pion and find an estimate for the intensity of its interactions. The first objective is to find an estimate for the strength of the momentum of the pion's quarks. The calculation is done in units of  $\text{fm}$ , and  $1 \text{ fm}^{-1} \approx 200 \text{ MeV}$ . The pion's spatial size is somewhat smaller than that of the proton [16]. Thus, let us assume that the pion's quark-antiquark pair are enclosed inside a box whose size is  $2.2 \text{ fm}$  and the pion's quark wave function vanishes on its boundary. For the  $x$ -component, one finds that the smallest absolute value of the momentum is obtained from a function of the form  $\sin(\pi x/2.2)$ . Hence, the absolute value of this component of the momentum is  $\pi/2.2$ . Thus, for the three spatial coordinates, one multiplies this number by  $\sqrt{3}$  and another factor of 2 accounts for the quark-antiquark pair. It follows that the absolute value of the momentum enclosed inside a pion is

$$|\mathbf{p}| \approx 1000 \text{ MeV}. \quad (16)$$

This value of the momentum is much greater than the

pion's mass. It means that the system is extremely relativistic and (16) is regarded as the quarks' kinetic energy. Thus, the interaction consumes about 6/7 of the kinetic energy *and* the entire mass of the quark-antiquark pair. In other word, the pion's kinetic energy is about 7 times greater than its final mass. It is interesting to compare these values to the corresponding quantities of the positronium, which is an electron-positron system bound by the electromagnetic force. Here the ratio of the kinetic energy to the final mass is about 7/1000000. On the basis of this evidence one concludes that strong interactions must be much stronger than the experimental mass of the pion.

Relying on these arguments and on the theoretical conclusion stating that the  $W^\pm$  must be composite objects, it is concluded that the  $W^\pm$  particles contain one top quark. Thus, the  $W^+$  is a superposition of three meson families:  $t\bar{d}$ ,  $t\bar{s}$  and  $t\bar{b}$ . Here the top quark mass is 173 GeV and the mass of the  $W$  is 80 GeV [16]. The difference indicates the amount swallowed by strong interactions. This outcome also answers the question where are the mesons of the top quark? The fact that the  $W^\pm$  is a composite particle which is a superposition of mesons is inconsistent with the electroweak theory and this fact indicates that the foundations of this theory should be examined.

Another result of this analysis pertains to recent reports concerning the existence of a new particle whose mass is about 125 GeV and its width is similar to that of the  $W^\pm$  [2,3]. Thus, since the mass of the top quark is about 173 GeV and this quantity is by far greater than the mass of any other quark, it makes sense to regard the 125 GeV particle as a  $t\bar{t}$  meson. For this reason, the  $t\bar{t}$  meson is heavier than the 80 GeV  $W^\pm$  which consists of one top quark and a lighter quark.

A  $t\bar{t}$  mesonic structure of the 125 GeV particle explains naturally its quite sharp disintegration into two photons. Indeed, the disintegration of a bound system of charged spin-1/2 particle-antiparticle pair into two photons is a well known effect of the ground state of the positronium and of the  $\pi^0$  meson. On the other hand, the results obtained in this work deny the  $W^+ W^-$  disintegration channel of the 125 GeV particle, because the  $W$ s are composite particles and a  $W^+ W^-$  system is made of two quark-antiquark pairs. For this reason, their two photon disintegration should be accompanied by other particles. Hence, a  $W^+ W^-$  two photon outcome should show a much wider energy distribution. This kind of  $W^+ W^- \rightarrow \gamma\gamma$  disintegration is inconsistent with the quite narrow width of the 125 GeV data. It turns out that for a Higgs mass of 125 GeV, Standard Model Higgs decay calculations show that the  $W^+ W^- \rightarrow \gamma\gamma$  channel is dominant [17, see section 2.3.1]. However, it is proved in this work that the  $W^+ W^-$  disintegration channel of the 125 GeV particle is incompatible with the data. Therefore, one denies the Higgs boson interpretation of the 125 GeV particle found at the LHC [2, 3]. This

outcome is consistent with the Higgs boson inherent contradictions which are discussed elsewhere [10].

Submitted on July 29, 2012 / Accepted on August 10, 2012

## References

1. Wigner E. P. The unreasonable effectiveness of mathematics in the natural sciences. *Communications in Pure and Applied Mathematics*, 1960, v. 13, 1–14.
2. The ATLAS Collaboration. Latest Results from ATLAS Higgs Search. <http://www.atlas.ch/news/2012/latest-results-from-higgs-search.html>.
3. The CMS Collaboration. Evidence for a new state decaying into two photons in the search for the standard model Higgs boson in pp collisions. <http://cdsweb.cern.ch/record/1460419/files/HIG-12-015-pas.pdf>.
4. Bjorken J. D. and Drell S. D. *Relativistic Quantum Fields*. McGraw, New York, 1965.
5. Serman G. *An Introduction to Quantum Field Theory*. Cambridge University Press, Cambridge, 1993.
6. Rohrlich F. *Classical Charged Particle*. Addison-Wesley, Reading MA, 1965.
7. Einstein A. *Albert Einstein in His Own Words*. Portland House, New York, 2000.
8. Bjorken J. D. and Drell S. D. *Relativistic Quantum Mechanics*. McGraw, New York, 1964.
9. Landau L. D., Lifshitz E. M. *The classical theory of fields*. Elsevier, Amsterdam, 2005.
10. Comay E. Physical Consequences of Mathematical Principles. *Progress in Physics*, 2009, v. 4, 91–98.
11. Weinberg S. *The Quantum Theory of Fields*. Cambridge University Press, Cambridge, 1996.
12. Pauli W., Weisskopf V. The quantization of the scalar relativistic wave equation. *Helvetica Physica Acta*, 1934, v. 7, 709–731. English translation: Miller A. I. *Early Quantum Electrodynamics*. Cambridge University Press, Cambridge, 1994. pp. 188–205. (In the text, page references apply to the English translation.)
13. Dirac P. A. M. *Mathematical Foundations of Quantum Theory*, in: Marlow A. R. (Editor), *Mathematical Foundations of Quantum Theory*. Academic, New York, 1978.
14. Messiah A. *Quantum Mechanics v.2*, North-Holland, Amsterdam, 1966.
15. Perkins D. H. *Introduction to high energy physics*. Addison-Wesley, Menlo Park (CA), 1987.
16. Amsler C. et al. Review of particle physics. *Physics Letters B*, 2008, v. 667, 1–1340.
17. Djouadi A. The anatomy of electroweak symmetry breaking Tome I: The Higgs boson in the Standard Model. *Physics Reports*, 2008 v. 457, 1–216. arXiv: hep-ph/0503172v2.

# Should the Wave-Function be a Part of the Quantum Ontological State?

Aurélien Drezet

Institut Neel, 25 rue des Martyrs 38042, Grenoble, France. E-mail: aurelien.drezet@grenoble.cnrs.fr

We analyze the recent no go theorem by Pusey, Barrett and Rudolph (PBR) concerning ontic and epistemic hidden variables. We define two fundamental requirements for the validity of the result. We finally compare the models satisfying the theorem with the historical hidden variable approach proposed by de Broglie and Bohm.

## 1 Introduction

Recently, a new no go theorem by M. Pusey, J. Barret and T. Rudolph (PBR in the following) was published [1]. The result concerns ontic versus epistemic interpretations of quantum mechanics. Epistemic means here knowledge by opposition to “ontic” or ontological and is connected with the statistical interpretation defended by Einstein. This of course stirred much debates and discussions to define the condition of validity of this fundamental theorem. Here, we discuss two fundamental requirements necessary for the demonstration of the result and also discuss the impact of the result on possible hidden variable models. In particular, we will stress the difference between the models satisfying the PBR theorem and those who apparently contradict its generality.

## 2 The axioms of the PBR theorem

In order to identify the main assumptions and conclusions of the PBR theorem we first briefly restate the original reasoning of ref. 1 in a slightly different language. In the simplest version PBR considered two non orthogonal pure quantum states  $|\Psi_1\rangle = |0\rangle$  and  $|\Psi_2\rangle = [|0\rangle + |1\rangle]/\sqrt{2}$  belonging to a 2-dimensional Hilbert space  $\mathbb{E}$  with basis vectors  $\{|0\rangle, |1\rangle\}$ . Using a specific (nonlocal) measurement  $M$  with basis  $|\xi_i\rangle$  ( $i \in [1, 2, 3, 4]$ ) in  $\mathbb{E} \otimes \mathbb{E}$  (see their equation 1 in [1]) they deduced that  $\langle \xi_1 | \Psi_1 \otimes \Psi_1 \rangle = \langle \xi_2 | \Psi_1 \otimes \Psi_2 \rangle = \langle \xi_3 | \Psi_2 \otimes \Psi_1 \rangle = \langle \xi_4 | \Psi_2 \otimes \Psi_2 \rangle = 0$ . In a second step they introduced hypothetical “Bell’s like” hidden variables  $\lambda$  and wrote implicitly the probability of occurrence  $P_M(\xi_i; j, k) = |\langle \xi_i | \Psi_j \otimes \Psi_k \rangle|^2$  in the form:

$$P_M(\xi_i; j, k) = \int P_M(\xi_i | \lambda, \lambda') \varrho_j(\lambda) \varrho_k(\lambda') d\lambda d\lambda' \quad (1)$$

where  $i \in [1, 2, 3, 4]$  and  $j, k \in [1, 2]$ . One of the fundamental axiom used by PBR (axiom 1) is an independence criterion at the preparation which reads  $\varrho_{j,k}(\lambda, \lambda') = \varrho_j(\lambda) \varrho_k(\lambda')$ . In these equations we introduced the conditional “transition” probabilities  $P_M(\xi_i | \lambda, \lambda')$  for the outcomes  $\xi_i$  supposing the hidden state  $\lambda, \lambda'$  associated with the two independent Q-bits are given. The fundamental point here is that  $P_M(\xi_i | \lambda, \lambda')$  is independent of  $\Psi_1, \Psi_2$ . This a very natural looking-like axiom (axiom 2) which was implicit in ref. 1 and was not further discussed by the authors. We will see later what are the consequence of its abandonment.

For now, from the definitions and axioms we obtain:

$$\left. \begin{aligned} \int P_M(\xi_1 | \lambda, \lambda') \varrho_1(\lambda) \varrho_1(\lambda') d\lambda d\lambda' &= 0 \\ \int P_M(\xi_2 | \lambda, \lambda') \varrho_1(\lambda) \varrho_2(\lambda') d\lambda d\lambda' &= 0 \\ \int P_M(\xi_3 | \lambda, \lambda') \varrho_2(\lambda) \varrho_1(\lambda') d\lambda d\lambda' &= 0 \\ \int P_M(\xi_4 | \lambda, \lambda') \varrho_2(\lambda) \varrho_2(\lambda') d\lambda d\lambda' &= 0 \end{aligned} \right\} \quad (2)$$

The first line implies  $P_M(\xi_1 | \lambda, \lambda') = 0$  if  $\varrho_1(\lambda) \varrho_1(\lambda') \neq 0$ . This condition is always satisfied if  $\lambda$  and  $\lambda'$  are in the support of  $\varrho_1$  in the  $\lambda$ -space and  $\lambda'$ -space. Similarly, the fourth line implies  $P_M(\xi_4 | \lambda, \lambda') = 0$  if  $\varrho_2(\lambda) \varrho_2(\lambda') \neq 0$  which is again always satisfied if  $\lambda$  and  $\lambda'$  are in the support of  $\varrho_2$  in the  $\lambda$ -space and  $\lambda'$ -space. Finally, the second and third lines imply  $P_M(\xi_2 | \lambda, \lambda') = 0$  if  $\varrho_1(\lambda) \varrho_2(\lambda') \neq 0$  and  $P_M(\xi_3 | \lambda, \lambda') = 0$  if  $\varrho_2(\lambda) \varrho_1(\lambda') \neq 0$ .

Taken separately these four conditions are not problematic. But, in order to be true simultaneously and then to have

$$P_M(\xi_i | \lambda, \lambda') = 0 \quad (3)$$

for a same pair of  $\lambda, \lambda'$  (with  $[i = 1, 2, 3, 4]$ ) the conditions require that the supports of  $\varrho_1$  and  $\varrho_2$  intersect. If this is the case Eq. 3 will be true for any pair  $\lambda, \lambda'$  in the intersection.

However, this is impossible since from probability conservation we must have  $\sum_{i=1}^4 P_M(\xi_i | \lambda, \lambda') = 1$  for every pair  $\lambda, \lambda'$ . Therefore, we must necessarily have

$$\varrho_2(\lambda) \cdot \varrho_1(\lambda) = 0 \quad \forall \lambda \quad (4)$$

i.e. that  $\varrho_1$  and  $\varrho_2$  have nonintersecting supports in the  $\lambda$ -space. Indeed, it is then obvious to see that Eq. 2 is satisfied if Eq. 4 is true. This constitutes the PBR theorem for the particular case of independent prepared states  $\Psi_1, \Psi_2$  defined before. PBR generalized their results for more arbitrary states using similar and astute procedures described in ref. 1.

If this theorem is true it would apparently make hidden variables completely redundant since it would be always possible to define a bijection or relation of equivalence between the  $\lambda$  space and the Hilbert space: (loosely speaking we could in principle make the correspondence  $\lambda \Leftrightarrow \psi$ ). Therefore it would be as if  $\lambda$  is nothing but a new name for  $\Psi$  itself. This would justify the label “ontic” given to this kind of interpretation in opposition to “epistemic” interpretations ruled out by the PBR result.

However, the PBR conclusion stated like that is too strong as it can be shown by carefully examining the assumptions necessary for the derivation of the theorem. Indeed, using the independence criterion and the well known Bayes-Laplace formula for conditional probability we deduce that the most general Bell's hidden variable probability space should obey the following rule

$$P_M(\xi_i; j, k) = \int P_M(\xi_i|\Psi_j, \Psi_k, \lambda, \lambda') \varrho_j(\lambda) \varrho_k(\lambda') d\lambda d\lambda' \quad (5)$$

in which, in contrast to equation 1, the transition probabilities  $P_M(\xi_i|\Psi_j, \Psi_k, \lambda, \lambda')$  now depend explicitly on the considered quantum states  $\Psi_j, \Psi_k$ . We point out that unlike  $\lambda$ ,  $\Psi$  is in this more general approach not a stochastic variable. This difference is particularly clear in the ontological interpretation of ref. 3 where  $\Psi$  plays the role of a dynamic guiding wave for the stochastic motion of the particle. Clearly, relaxing this PBR premise has a direct effect since we lose the ingredient necessary for the demonstration of Eq. 4. (more precisely we are no longer allowed to compare the product states  $|\Psi_j \otimes \Psi_k\rangle$  as it was done in ref. 1). Indeed, in order for Eq. 2 to be simultaneously true for the four states  $\xi_i$  (where  $P_M(\xi_i|\Psi_j, \Psi_k, \lambda, \lambda')$  now replace  $P_M(\xi_i|\lambda, \lambda')$ ) we must have

$$\left. \begin{aligned} P_M(\xi_1|\Psi_1, \Psi_1, \lambda, \lambda') = 0, P_M(\xi_2|\Psi_1, \Psi_2, \lambda, \lambda') = 0 \\ P_M(\xi_3|\Psi_2, \Psi_1, \lambda, \lambda') = 0, P_M(\xi_4|\Psi_2, \Psi_2, \lambda, \lambda') = 0 \end{aligned} \right\}. \quad (6)$$

Obviously, due to the explicit  $\Psi$  dependencies, Eq. 6 doesn't anymore enter in conflict with the conservation probability rule and therefore doesn't imply Eq. 4. In other words the reasoning leading to PBR theorem doesn't run if we abandon the axiom stating that

$$P_M(\xi_i|\Psi_j, \Psi_k, \lambda, \lambda') := P_M(\xi_i|\lambda, \lambda') \quad (7)$$

i.e. that the dynamic should be independent of  $\Psi_1, \Psi_2$ . This analysis clearly shows that Eq. 7 is a fundamental prerequisite (as important as the independence criterion at the preparation) for the validity of the PBR theorem [4]. In our knowledge this point was not yet discussed [5].

### 3 Discussion

Therefore, the PBR deduction presented in ref. 1 is actually limited to a very specific class of  $\Psi$ -epistemic interpretations. It fits well with the XIX<sup>th</sup> like hidden variable models using Liouville and Boltzmann approaches (i.e. models where the transition probabilities are independent of  $\Psi$ ) but it is not in agreement with neo-classical interpretations, e.g. the one proposed by de Broglie and Bohm [3], in which the transition probabilities  $P_M(\xi|\lambda, \Psi)$  and the trajectories depend explicitly and contextually on the quantum states  $\Psi$  (the de Broglie-Bohm theory being deterministic these probabilities can only reach values 0 or 1 for discrete observables  $\xi$ ). As an illustration, in the de Broglie Bohm model for a single particle the

spatial position  $\mathbf{x}$  plays the role of  $\lambda$ . This model doesn't require the condition  $\varrho_1(\lambda) \cdot \varrho_2(\lambda) = |\langle \mathbf{x} | \Psi_1 \rangle|^2 \cdot |\langle \mathbf{x} | \Psi_1 \rangle|^2 = 0$  for all  $\lambda$  in clear contradiction with Eq. 4. We point out that our reasoning doesn't contradict the PBR theorem *per se* since the central axiom associated with Eq. 7 is not true anymore for the model considered. In other words, if we recognize the importance of the second axiom discussed before (i.e. Eq. 7) the PBR theorem becomes a general result which can be stated like that:

i) If Eq. 7 applies then the deduction presented in ref. 1 shows that Eq. 4 results and therefore  $\lambda \leftrightarrow \Psi$  which means that epistemic interpretation of  $\Psi$  are equivalent to ontic interpretations. This means that a XIX<sup>th</sup> like hidden variable models is not really possible even if we accept Eq. 7 since we don't have any freedom on the hidden variable density  $\rho(\lambda)$ .

ii) However, if Eq. 7 doesn't apply then the ontic state of the wavefunction is already assumed - because it is a variable used in the definition of  $P_M(\xi|\lambda, \Psi)$ . This shows that ontic interpretation of  $\Psi$  is necessary. This is exemplified in the de Broglie-Bohm example: in this model, the "quantum potential" is assumed to be a real physical field which depends on the magnitude of the wavefunction, while the motion of the Bohm particle depends on the wavefunction's phase. This means that the wavefunction has ontological status in such a theory. This is consistent with the spirit of PBR's paper, but the authors didn't discussed that fundamental point.

We also point out that in the de Broglie-Bohm ontological approach the independence criterion at the preparation is respected in the regime considered by PBR. As a consequence, it is not needed to invoke retrocausality to save epistemic approaches.

It is important to stress how Eq. 4, which is a consequence of Eq. 7, contradicts the spirit of most hidden variable approaches. Consider indeed, a wave packet which is split into two well spatially localized waves  $\Psi_1$  and  $\Psi_2$  defined in two isolated regions 1 and 2. Now, the experimentalist having access to local measurements  $\xi_1$  in region 1 can define probabilities  $|\langle \xi_1 | \Psi_1 \rangle|^2$ . In agreement with de Broglie and Bohm most proponents of hidden variables would now say that the hidden variable  $\lambda$  of the system actually present in box 1 should not depends of the overall phase existing between  $\Psi_1$  and  $\Psi_2$ . In particular the density of hidden variables  $\varrho_\Psi(\lambda)$  in region 1 should be the same for  $\Psi = \Psi_1 + \Psi_2$  and  $\Psi' = \Psi_1 - \Psi_2$  since  $|\langle \xi_1 | \Psi \rangle|^2 = |\langle \xi_1 | \Psi' \rangle|^2$  for every local measurements  $\xi_1$  in region 1. This is a weak form of separability which is accepted even within the so exotic de Broglie Bohm's approach but which is rejected for those models accepting Eq. 4.

This point can be stated differently. Considering the state  $\Psi = \Psi_1 + \Psi_2$  previously discussed we can imagine a two-slits like interference experiment in which the probability for detecting outcomes  $x_0$ , i.e.,  $|\langle x_0 | \Psi \rangle|^2$  vanish for some values  $x_0$  while  $|\langle x_0 | \Psi_1 \rangle|^2$  do not. For those models satisfying Eq. 7 and forgetting one instant PBR theorem we deduce that in the hypothetical common support of  $\varrho_{\Psi_1}(\lambda)$  and  $\varrho_\Psi(\lambda)$  we must have

$P_M(\xi_0|\lambda) = 0$  since this transition probability should vanish in the support of  $\Psi$ . This allows us to present a “*poor-man*” version of the PBR’s theorem: The support of  $\varrho_{\Psi_1}(\lambda)$  can not be completely included in the support of  $\varrho_{\Psi}(\lambda)$  since otherwise  $P_M(\xi_0|\lambda) = 0$  would implies  $|\langle x_0|\Psi_1\rangle|^2 = 0$  in contradiction with the definition. PBR’s theorem is stronger than that since it shows that in the limit of validity of Eq. 7 the support of  $\varrho_{\Psi_1}(\lambda)$  and  $\varrho_{\Psi}(\lambda)$  are necessarily disjoint. Consequently, for those particular models the hidden variables involved in the observation of the observable  $\xi_0$  are not the same for the two states  $\Psi$  and  $\Psi_1$ . This is fundamentally different from de Broglie-Bohm approach where  $\lambda$  (e.g.  $\mathbf{x}(t_0)$ ) can be the same for both states.

This can lead to an interesting form of quantum correlation even with one single particle. Indeed, following the well known scheme of the Wheeler Gedanken experiment one is free at the last moment to either observe the interference pattern (i.e.  $|\langle x_0|\Psi\rangle|^2 = 0$ ) or to block the path 2 and destroy the interference (i.e.  $|\langle x_0|\Psi_1\rangle|^2 = 1/2$ ). In the model used by Bohm where  $\Psi$  acts as a guiding or pilot wave this is not surprising: blocking the path 2 induces a subsequent change in the propagation of the pilot wave which in turn affects the particle trajectories. Therefore, the trajectories will not be the same in these two experiments and there is no paradox. However, in the models considered by PBR there is no guiding wave since  $\Psi$  serves only to label the non overlapping density functions of hidden variable  $\varrho_{\Psi_1}(\lambda)$  and  $\varrho_{\Psi}(\lambda)$ . Since the beam block can be positioned after the particles leaved the source the hidden variable are already predefined (i.e. they are in the support of  $\varrho_{\Psi}(\lambda)$ ). Therefore, the trajectories are also predefined in those models and we apparently reach a contradiction since we should have  $P_M(\xi_0|\lambda) = 0$  while we experimentally record particles with properties  $\xi_0$ . The only way to solve the paradox is to suppose that some mysterious quantum influence is sent from the beam blocker to the particle in order to modify the path during the propagation and correlate it with presence or absence of the beam blocker. However, this will be just equivalent to the hypothesis of the de Broglie-Bohm guiding wave and quantum potential and contradicts apparently the spirit and the simplicity of  $\Psi$ -independent models satisfying Eq. 7.

#### 4 An example

We point out that despite these apparent contradictions it is easy to create an hidden variable model satisfying all the requirements of PBR theorem. Let any state  $|\Psi\rangle$  be defined at time  $t = 0$  in the complete basis  $|k\rangle$  of dimension  $N$  as  $|\Psi\rangle = \sum_k^N \Psi_k|k\rangle$  with  $\Psi_k = \Psi'_k + i\Psi''_k$ . We introduce two hidden variables  $\lambda$ , and  $\mu$  as the  $N$  dimensional real vectors  $\lambda := [\lambda_1, \lambda_2, \dots, \lambda_N]$  and  $\mu := [\mu_1, \mu_2, \dots, \mu_N]$ . We thus write the probability  $P_M(\xi, t, \Psi) = |\langle \xi|U(t)\Psi\rangle|^2$  of observing the out-

come  $\xi$  at time  $t$  as

$$\int P_M(\xi, t|\{\lambda_k, \mu_k\}_k) \prod_k^N \delta(\Psi'_k - \lambda_k)\delta(\Psi''_k - \mu_k)d\lambda_k d\mu_k \\ = P_M(\xi, t|\{\Psi'_k, \Psi''_k\}_k) = |\sum_k \langle \xi|U(t)|k\rangle \Psi_k|^2 \quad (8)$$

where  $U(t)$  is the Schrodinger evolution operator. Since  $\Psi$  can be arbitrary we thus generally have in this model

$$P_M(\xi, t|\{\lambda_k, \mu_k\}_k) = |\sum_k \langle \xi|U(t)|k\rangle (\lambda_k + i\mu_k)|^2.$$

The explicit time variation is associated with the unitary evolution  $U(t)$  which thus automatically includes contextual local or non local influences (coming from the beam blocker for example). We remark that this model is of course very formal and doesn’t provide a better understanding of the mechanism explaining the interaction processes. The hidden variable model we proposed is actually based on a earlier version shortly presented by Harrigan and Spekkens in ref. [2]. We completed the model by fixing the evolution probabilities and by considering the complex nature of wave function in the Dirac distribution. Furthermore, this model doesn’t yet satisfy the independence criterion if the quantum state is defined as  $|\Psi\rangle_{12} = |\Psi\rangle_1 \otimes |\Psi\rangle_2$  in the Hilbert tensor product space. Indeed, the hidden variables  $\lambda_{12,k}$  and  $\mu_{12,k}$  defined in Eq. 8 are global variables for the system 1,2. If we write

$$|\Psi\rangle_{12} = \sum_{n,p}^{N_1, N_2} \Psi_{12;n,p} |n\rangle_1 \otimes |p\rangle_2 \\ = \sum_{n,p}^{N_1, N_2} \Psi_{1;n} \Psi_{2;p} |n\rangle_1 \otimes |p\rangle_2 \quad (9)$$

the indices  $k$  previously used become a doublet of indices  $n, p$  and the probability

$$P_M(\xi, t|\Psi_{12}) = |\sum_{n,p}^{N_1, N_2} \langle \xi|U(t)|n, p\rangle_{12} \Psi_{12;n,p}|^2$$

in Eq. 8 reads now:

$$\int P_M(\xi, t|\{\lambda_{12;n,p}, \mu_{12;n,p}\}_{n,p}) \\ \times \prod_n^{N_1} \prod_p^{N_2} \delta(\Psi'_{12;n,p} - \lambda_{12;n,p}) \\ \times \delta(\Psi''_{12;n,p} - \mu_{12;n,p}) d\lambda_{12;n,p} d\mu_{12;n,p} \\ = P_M(\xi, t|\{\Psi'_{12;n,p}, \Psi''_{12;n,p}\}_{n,p}) \quad (10)$$

which indeed doesn’t show any explicit separation of the hidden variables density of states for subsystems 1 and 2. However, in the case where Eq. 9 is valid we can alternatively

introduce new hidden variable vectors  $\lambda_1, \lambda_2$  and  $\mu_1, \mu_2$  such that  $P_M(\xi, t|\Psi_{12})$  reads now:

$$\begin{aligned} & \int P_M(\xi, t|\{\lambda_{1;n}, \lambda_{2;p}, \mu_{1;n}, \mu_{2;n}\}_{n,p}) \\ & \times \prod_n^{N_1} \delta(\Psi'_{1;n} - \lambda_{1;n}) \delta(\Psi''_{1;n} - \mu_{1;n}) d\lambda_{1;n} d\mu_{1;n} \\ & \times \prod_p^{N_2} \delta(\Psi'_{2;p} - \lambda_{2;p}) \delta(\Psi''_{2;p} - \mu_{2;p}) d\lambda_{2;n} d\mu_{2;p} \\ & = P_M(\xi, t|\{\Psi'_{1;n}, \Psi'_{2;p}, \Psi''_{1;n}, \Psi''_{2;n}\}_{n,p}). \end{aligned} \quad (11)$$

Clearly here the density of probability  $\varrho_{12}(\lambda_1, \lambda_2, \mu_1, \mu_2)$  can be factorized as  $\varrho_1(\lambda_1, \mu_1) \cdot \varrho_2(\lambda_2, \mu_2)$  where

$$\begin{aligned} \varrho_1(\lambda_1, \mu_1) &= \prod_n^{N_1} \delta(\Psi'_{1;n} - \lambda_{1;n}) \delta(\Psi''_{1;n} - \mu_{1;n}) \\ \varrho_2(\lambda_2, \mu_2) &= \prod_p^{N_2} \delta(\Psi'_{2;n} - \lambda_{2;n}) \delta(\Psi''_{2;n} - \mu_{2;n}) \end{aligned} \quad (12)$$

Therefore, the independence criterion at the preparation (i.e. axiom 1) is here fulfilled.

Additionally, since by definition Eq. 8 and 10 are equivalent we have

$$\begin{aligned} P_M(\xi, t|\{\Psi'_{1;n}, \Psi'_{2;p}, \Psi''_{1;n}, \Psi''_{2;n}\}_{n,p}) \\ = P_M(\xi, t|\{\Psi'_{12;n,p}, \Psi''_{12;n,p}\}_{n,p}). \end{aligned} \quad (13)$$

Moreover, since  $\Psi_{1;n}$  and  $\Psi_{2;n}$  can have any complex values the following relation holds for any value of the hidden variables:

$$\begin{aligned} P_M(\xi, t|\{\lambda_{1;n}, \lambda_{2;p}, \mu_{1;n}, \mu_{2;n}\}_{n,p}) \\ = P_M(\xi, t|\{\lambda_{12;n,p}, \mu_{12;n,p}\}_{n,p}) \end{aligned} \quad (14)$$

with  $\lambda_{12;n,p} + i\mu_{12;n,p} = (\lambda_{1;n} + i\mu_{1;n})(\lambda_{2;p} + i\mu_{2;p})$ . This clearly define a bijection or relation of equivalence between the hidden variables  $[\lambda_{12}, \mu_{12}]$  on the one side and  $[\lambda_1, \mu_1, \lambda_2, \mu_2]$  on the second side. Therefore, we showed that it is always possible to define hidden variables satisfying the 2 PBR axioms: i) statistical independence at the sources or preparation

$$\varrho_{j,k}(\lambda, \lambda') = \varrho_j(\lambda) \varrho_k(\lambda')$$

(if Eq. 9 is true) and ii)  $\Psi$ -independence at the dynamic level, i.e., satisfying Eq. 7. We point out that the example discussed in this section proves that the PBR theorem is not only formal since we explicitly proposed a hidden variable model satisfying the two requirements of PBR theorem. This model is very important since it demonstrates that the de Broglie Bohm approach is not the only viable hidden variable theory. It is interesting to observe that our model corresponds to the case discussed in point i) of section 3 while Bohm's approach corresponds to the point labeled ii) in the same section 3. Additionally, the new model is fundamentally stochastic (since

the transition probabilities  $P_M(\xi|\lambda)$  have numerical values in general different from 1 or 0) while Bohm's approach is deterministic.

## 5 Conclusion

To conclude, we analyzed the PBR theorem and showed that beside the important independence criterion already pointed out in ref. 1 there is a second fundamental postulate associated with  $\Psi$ -independence at the dynamic level (that is our Eq. 7). We showed that by abandoning this prerequisite the PBR conclusion collapses. We also analyzed the nature of those models satisfying Eq. 7 and showed that despite their classical motivations they also possess counter intuitive features when compared for example to de Broglie Bohm model. We finally constructed an explicit model satisfying the PBR axioms. More studies would be necessary to understand the physical meaning of such hidden variable models.

Submitted on August 20, 2012 / Accepted on August 22, 2012

## References

1. Pusey M.F., Barrett J., Rudolph T. On the reality of the quantum state. *Nature Physics*, 2012, v. 8, 478–478.
2. Harrigan N., Spekkens R. W. Einstein, incompleteness, and the epistemic view of quantum states. *Foundations of Physics*, 2010, v.40, 125–157.
3. de Broglie L. La mécanique ondulatoire et la structure atomique de la matière et du rayonnement. *Journal de Physique et le Radium*, 1927, v. 8, 225–241.
4. We point out that we will not save the naive interpretation of PBR's theorem by using the "implicit" notation  $\Lambda = (\lambda, \Psi)$  and by writing  $\int P_M(\xi|\Lambda) \varrho(\Lambda) d\Lambda$  in order to hide the  $\Psi$  dependence  $P_M(\xi|\Lambda) := P_M(\xi|\lambda, \Psi)$ . Indeed, at the end of the day we have to compare different  $\Psi$  states and the explicit notation becomes necessary. The importance of Eq. 7 for PBR's result can therefore not be avoided.
5. See also A. Drezet, arXiv:1203.2475 (12 March 2012) for a detailed discussion of PBR's theorem.

# Relativistic Dynamics in the Vicinity of a Uniformly Charged Sphere

Chifu E. Ndikilar\* and Lucas W. Lumbi†

\*Department of Physics, Federal University Dutse, P.M.B. 7156, Dutse, Nigeria

†Department of Physics, Nasarawa State University, Nigeria

E-mail: ebenechifu@yahoo.com

The motion of test and photons in the vicinity of a uniformly charged spherically symmetric mass distribution is studied using a newly developed relativistic dynamical approach. The derived expressions for the mechanical energy and acceleration vector of test particles have correction terms of all orders of  $c^{-2}$ . The expression for the gravitational spectral shift also has additional terms which are functions of the electric potential on the sphere.

## 1 Introduction

In a recent article [1], the relativistic dynamical approach to the study of classical mechanics in homogeneous spherical distributions of mass (Schwarzschild's gravitational field) was introduced. Here, the relativistic dynamical theory of a combined gravitational and electric field within homogeneous spherical distributions of mass is developed.

## 2 Motion of test particles

According to Maxwell's theory of electromagnetism, the electric potential energy for a particle of non-zero rest mass in an electric field  $V_e$  is given by

$$V_e = q \Phi_e, \quad (1)$$

where  $q$  is the electric charge of the particle and  $\Phi_e$  is the electric scalar potential. Also, from Newton's dynamical theory, it is postulated [2] that the instantaneous mechanical energy for test particles in combined gravitational and electric fields is defined by

$$E = T + V_g + V_e, \quad (2)$$

where  $T$  is the total relativistic kinetic energy and  $V_g$  is the gravitational potential. From [1],  $T$  and  $V_g$  in Schwarzschild's gravitational field are given by

$$T = \left[ \left( 1 - \frac{u^2}{c^2} \right)^{-1/2} - 1 \right] m_0 c^2 \quad (3)$$

and the instantaneous relativistic gravitational potential energy ( $V_g$ ) for a particle of nonzero rest mass is

$$V_g = m_p \Phi_g = - \left( 1 - \frac{u^2}{c^2} \right)^{-1/2} \frac{GMm_0}{r}, \quad (4)$$

where  $\Phi_g = \frac{-GM}{r}$  is the gravitational scalar potential in a spherically symmetric gravitational field,  $r > R$ , the radius of the homogeneous sphere,  $G$  is the universal gravitational constant,  $c$  is the speed of light in vacuum,  $m_p$  is the passive mass of the test particle,  $M$  is the mass of the static homogeneous spherical mass,  $m_0$  is the rest mass of the test particle

and  $u$  is the instantaneous velocity of the test particle. Also, for a uniformly charged spherically symmetric mass the electric potential energy is given as

$$V_e = \frac{qQ}{4\pi\epsilon_0 r}, \quad (5)$$

where  $Q$  is the total charge on the sphere and  $q$  is the charge on the test particle. Thus, the instantaneous mechanical energy for the test particle can be written more explicitly as

$$E = m_0 c^2 \left[ \left( 1 - \frac{GM}{c^2 r} \right) \left( 1 - \frac{u^2}{c^2} \right)^{-1/2} - 1 \right] + \frac{qQ}{4\pi\epsilon_0 r}. \quad (6)$$

The expression for the instantaneous mechanical energy has post Newton and post Einstein correction terms of all orders of  $c^{-2}$ . The relativistic dynamical equation of motion for particles of non-zero rest masses in combined electric and gravitational fields is given as [2]

$$\frac{d}{d\tau} \bar{P} = -m_p \bar{\nabla} \Phi_g - q \bar{\nabla} \Phi_e, \quad (7)$$

where  $\bar{P}$  is the instantaneous linear momentum of the test particles. Thus, in this field, the relativistic dynamical equation of motion for test particles is given explicitly as

$$\begin{aligned} \frac{d}{d\tau} \left[ \left( 1 - \frac{u^2}{c^2} \right)^{-1/2} \bar{u} \right] &= \\ &= - \left( 1 - \frac{u^2}{c^2} \right)^{-1/2} \bar{\nabla} \Phi_g - \frac{q}{m_0} \bar{\nabla} \Phi_e \end{aligned} \quad (8)$$

or

$$\begin{aligned} \bar{a} + \frac{1}{2c^2} \left( 1 - \frac{u^2}{c^2} \right)^{-1} \frac{d}{d\tau} (u^2) \bar{u} &= \\ &= \frac{GM}{r^2} - \frac{q}{m_0} \left( 1 - \frac{u^2}{c^2} \right)^{1/2} \bar{\nabla} \Phi_e, \end{aligned} \quad (9)$$

where  $\bar{a}$  is the instantaneous acceleration vector of the test particles and thus the time equation of motion is obtained as

$$a_{x_0} + \frac{1}{2c^2} \left( 1 - \frac{u^2}{c^2} \right)^{-1} \frac{d}{d\tau} (u^2) u_{x_0} = 0. \quad (10)$$

The azimuthal equation of motion is

$$\dot{r} \sin \theta \dot{\phi} + r \cos \theta \dot{\theta} \dot{\phi} + r \sin \theta \ddot{\phi} + \frac{1}{2c^2} \left(1 - \frac{u^2}{c^2}\right)^{-1} \frac{d}{d\tau}(u^2) u_\phi = 0. \quad (11)$$

The polar equation of motion is given as

$$r \ddot{\theta} + \dot{r} \dot{\theta} + \frac{1}{2c^2} \left(1 - \frac{u^2}{c^2}\right)^{-1} \frac{d}{d\tau}(u^2) u_\theta = 0 \quad (12)$$

and the radial equation of motion is

$$a_r + \frac{1}{2c^2} \left(1 - \frac{u^2}{c^2}\right)^{-1} \frac{d}{d\tau}(u^2) u_r = -\frac{GM}{r^2} - \frac{q}{m_0} \left(1 - \frac{u^2}{c^2}\right)^{1/2} \bar{\nabla} \Phi_e. \quad (13)$$

As in [1], the equations have correction terms not found in the general relativistic approach. It is also worth remarking that the homogeneous charge distribution on the sphere and the charge on the test particle affects only the radial component of the motion and hence the other components are the same as those of an uncharged sphere [1].

### 3 Motion of photons

From [1], it can be deduced that the instantaneous gravitational potential energy of a photon is given as

$$V_g = -\frac{h\nu}{c^2} \frac{GM}{r}. \quad (14)$$

The instantaneous electric potential energy of the photon is given [2] as

$$V_e = -\frac{h\nu}{c^2} \bar{\nabla} \Phi_e \quad (15)$$

or more explicitly in this field as

$$V_e = -\frac{h\nu}{c^2} \frac{Q}{4\pi\epsilon_0 r}. \quad (16)$$

Also, the instantaneous kinetic energy of the photon [1] is given as

$$T = h(\nu - \nu_0). \quad (17)$$

Thus, the instantaneous mechanical energy of a photon in this combined gravitational and electric field is obtained as

$$E = h(\nu - \nu_0) - \frac{h\nu}{c^2 r} \left( GM + \frac{Q}{4\pi\epsilon_0} \right). \quad (18)$$

Suppose at  $r = r_0$ ,  $E = E_0$  then

$$E_0 = -\frac{kh\nu_0}{c^2 r_0}, \quad (19)$$

where

$$k = GM + \frac{Q}{4\pi\epsilon_0}. \quad (20)$$

Thus, from the principle of conservation of mechanical energy

$$-\frac{kh\nu_0}{c^2 r_0} = h(\nu - \nu_0) - \frac{kh\nu}{c^2 r} \quad (21)$$

or

$$\nu = \nu_0 \left(1 - \frac{k}{c^2 r_0}\right) \left(1 - \frac{k}{c^2 r}\right)^{-1}. \quad (22)$$

Equation (22) is the expression for spectral shift in this field with contributions from the gravitational and electric potentials. It has corrections of all orders of  $c^{-2}$ .

Also, for photons, the instantaneous linear momentum is given [1] as

$$\bar{P} = \frac{h\nu}{c^2} \bar{u}. \quad (23)$$

Hence, as in Newton's dynamical theory, the equation of motion of photons in this field is obtained from equation (7) as

$$\frac{d}{d\tau}(\nu \bar{u}) = -\nu \bar{\nabla} \Phi_g - \frac{qc^2}{h} \bar{\nabla} \Phi_e. \quad (24)$$

Thus the presence of an electric field introduces an additional term to the expression for the equation of motion of photons.

### 4 Conclusion

This article provides a crucial link between gravitational and electric fields. It also introduces, hitherto unknown corrections of all orders of  $c^{-2}$  to the expressions of instantaneous mechanical energy, spectral shift and equations of motion for test particles and photons in combined spherically symmetric gravitational and electric field.

Submitted on August 17, 2012 / Accepted on August 22, 2012

### References

1. Chifu E.N. Relativistic Dynamical Theory for Test Particles and Photons in Static Spherically Symmetric Gravitational Fields. *Progress in Physics*, 2012, v. 2, 3-5.
2. Howusu S.X.K. Complete Dynamical Theories of Physics. Jos University Press, Jos, 2010.

# A Bipolar Model of Oscillations in a Chain System for Elementary Particle Masses

Andreas Ries

Universidade Federal de Pernambuco, Centro de Tecnologia e Geociências, Laboratório de Dispositivos e Nanoestruturas,  
Rua Acadêmico Hélio Ramos s/n, 50740-330 Recife – PE, Brazil  
E-mail: andreasries@yahoo.com

The philosophical idea of a bipolar nature (the Chinese “Yin and Yang”) is combined with the mathematical formalism of a fractal scaling model originally published by Müller in this journal. From this extension new rules for the calculation of proton and electron resonances via continued fractions are derived. The set of the 117 most accurately determined elementary particle masses (all with error < 0.13%) was expressed through this type of continued fractions. Only one outlier was found, in all other cases the numerical errors were smaller than the standard deviation. Speaking in terms of oscillation properties, the results suggest that the electron is an inverted or mirrored oscillation state of the proton and vice versa. A complete description of elementary particle masses by the model of oscillations in a chain system is only possible when considering both, proton and electron resonances.

## 1 Introduction

The mass distribution of elementary particles is still an unsolved mystery of physics. According to the Standard Model, mass is given by arbitrary variable couplings to the Higgs boson, and the coupling is then adequately adjusted to reproduce the experimentally observed mass.

However, the particle mass spectrum is not completely chaotic, and some groupings are clearly visible. Several attempts have already been made to obtain equations to describe regularities in the set of elementary particle masses.

For instance Greulich [1] calculated the masses of all fundamental elementary particles (those with a lifetime > 10<sup>-24</sup> seconds) with an inaccuracy of approximately 1% using the equation

$$\frac{m_{particle}}{m_{electron}} = \frac{N}{2\alpha},$$

where  $\alpha$  is the fine structure constant ( $= 1/137.036$ ), and  $N$  is an integer variable.

Paasch [2] assigned each elementary particle mass a position on a logarithmic spiral. As a result, particles then accumulate on straight lines.

A study from India [3] revealed a tendency for successive mass differences between particles to be close to an integer multiple or integer fraction of 29.315 MeV. The value 29.315 MeV is the mass difference between a muon and a neutral pion.

Even more recently Boris Tatischeff published a series of articles [4–8] dealing with fractal properties of elementary particle masses. He even predicted tentatively the masses of some still unobserved particles [5].

An other fractal scaling model was used in a previous article of the present author [9], and a set of 78 accurately measured elementary particle masses was expressed in the

form of continued fractions. This underlying model was originally published by Müller [10–12], and its very basic idea is to treat all protons as fundamental oscillators connected through the physical vacuum. This leads to the idea of a chain of equal harmonic proton oscillators with an associated logarithmic spectrum of eigenfrequencies which can be expressed through continued fractions. Particle masses are interpreted as proton resonance states and expressed in continued fraction form. However, the results obtained in reference [9] were not completely satisfying since around 14% of the masses were outliers, i.e. could not be reproduced by this model.

A more recent article [13] revealed that electron resonance states exist analogously which serves now as the basis for further extensions of Müller’s model. From this starting point, the present article proposes a new version of the model developed with the objective to reproduce all elementary particle masses.

## 2 Data sources and computational details

Masses of elementary particles (including the proton and electron reference masses) were taken from the Particle Data Group website [14] and were expressed in GeV throughout the whole article. An electronic version of these data is available for downloading. Quark masses were eliminated from the list because it has not been possible to isolate quarks.

Some of the listed particle masses are extremely accurate and others have a quite high measurement error. Figure 1 shows an overview of the particle masses and their standard deviations (expressed in % of the particle mass). It can be roughly estimated that more or less 60% of the particles have a standard deviation (SD) below 0.13%; this set of excellent measurements consists of 117 particles and only this selection of very high quality data was used for the numerical analysis and extension of Müller’s model.

Table 1: Continued fraction representations of the lepton masses ( $x = -1.75083890054$ )

Particle	Mass $\pm$ SD [GeV] Continued fraction representation(s)	Numerical error [GeV]
electron	$5.10998910 \times 10^{-4} \pm 1.3 \times 10^{-11}$ P [x; -6   12, -6]	$1.21 \times 10^{-15}$
$\mu^-$	$1.05658367 \times 10^{-1} \pm 4.0 \times 10^{-9}$ P [x; 0   -6, -9, -e-1, 12, -6, -15] E [-x; 3   e+1, e+1, -e-1, e+1, 9, -48, e+1, -e-1]	$2.45 \times 10^{-10}$  $3.06 \times 10^{-9}$
$\tau^-$	$1.77682 \pm 1.6 \times 10^{-4}$ P [0; 0   e+1, 6, -e-1, e+1, -e-1, -e-1] P [x; 3   -e-1, -e-1, 231] E [0; 9   -e-1, 6, -e-1, -e-1, -6] E [-x; 6   6, e+1, -45]	$4.52 \times 10^{-5}$ $2.50 \times 10^{-6}$ $6.81 \times 10^{-5}$ $1.92 \times 10^{-5}$

Fig. 1: Overview of particle masses on the logarithmic number line together with their standard deviations expressed in % of the mass. Note that a few particles with very low or high mass or percentage error were omitted for clarity (e.g. electron, muon, proton, gauge bosons).

For consistency with previous articles on this topic, the following abbreviations and conventions for the numerical analysis hold:

#### Calculation method:

The considered particle mass is transformed into a continued fraction according to the equations

$$\ln \frac{m_{particle}}{m_{electron}} = p + S, \quad \ln \frac{m_{particle}}{m_{proton}} = p + S,$$

where  $p$  is the phase shift and  $S$  is the continued fraction ( $e$  is Euler's number)

$$S = n_0 + \frac{e}{n_1 + \frac{e}{n_2 + \frac{e}{n_3 + \dots}}}. \quad (1)$$

The continued fraction representation  $p+S$  is abbreviated as  $[p; n_0 | n_1, n_2, n_3, \dots]$ , where the free link  $n_0$  is allowed to be  $0, \pm 3, \pm 6, \pm 9, \dots$  and all partial denominators  $n_i$  can take the values  $e+1, -e-1, \pm 6, \pm 9, \pm 12, \dots$ . In the tables these abbreviations were marked with P or E, in order to indicate proton or electron resonance states.

For practical reasons only 18 partial denominators were determined. Next, the particle mass was repeatedly calculated from the continued fraction, every time considering one more partial denominator. As soon as the calculated mass value (on the linear scale) was in the interval "mass  $\pm$  standard deviation", no further denominators were considered and the resulting fractions are displayed in the tables. In some rare cases, this procedure provides a mass value just a little inside the interval and considering the next denominator would

Table 2: Continued fraction representations of the boson masses ( $x = -1.75083890054$ )

Particle	Mass $\pm$ SD [GeV] Continued fraction representation(s)	Numerical error [GeV]
$W^+$	$8.0399 \times 10^1 \pm 2.3 \times 10^{-2}$ E [0; 12   -81, e+1, (24)]	$3.23 \times 10^{-5}$
$Z^0$	$9.11876 \times 10^1 \pm 2.1 \times 10^{-3}$ P [x; 6   9, -e-1, -15, -e-1, e+1] E [0; 12   30, -6, (12)]	$1.01 \times 10^{-3}$ $7.23 \times 10^{-4}$

match the measured value almost exactly. In such cases this denominator is then additionally given in brackets.

The numerical error is always understood as the absolute value of the difference between the measured particle mass and the mass calculated from the corresponding continued fraction representation.

In order to avoid machine based rounding errors, numerical values of continued fractions were always calculated using the the Lenz algorithm as indicated in reference [15].

#### Outliers:

A particle mass is considered as an outlier (i.e. does not fit into the here extended Müller model) when its mass, as calculated from the corresponding continued fraction representation provides a value outside the interval "particle mass  $\pm$  standard deviation".

### 3 Results and discussion

#### 3.1 Fundamental philosophical idea

Chinese philosophy is dominated by the concept of "Yin and Yang" describing an indivisible whole of two complementary effects (male–female, day–night, good–bad, etc.). This means that everything has two opposite poles, and both poles are necessary to understand the whole thing (e.g. male can only be understood completely because female also exists as the opposite).

Table 3: Continued fraction representations of the light unflavored mesons ( $x = -1.75083890054$ )

Particle	Mass $\pm$ SD [GeV] Continued fraction representation(s)	Numerical error [GeV]
$\pi^+$	$1.3957018 \times 10^{-1} \pm 3.5 \times 10^{-7}$ P [x; 0   -18, 6, 6, (-117)] E [0; 6   -6, -e-1, e+1, -e-1, 48]	$7.67 \times 10^{-10}$ $1.68 \times 10^{-7}$
$\pi^0$	$1.349766 \times 10^{-1} \pm 6.0 \times 10^{-7}$ E [0; 6   -6, -6, -6, 6, -e-1]	$2.49 \times 10^{-7}$
$\eta^0$	$5.47853 \times 10^{-1} \pm 2.4 \times 10^{-5}$ P [0; 0   -6, e+1, -e-1, 6, -e-1, 12] E [0; 6   e+1, -e-1, e+1, -6, -e-1, e+1, (24)]	$6.52 \times 10^{-7}$ $2.51 \times 10^{-7}$
$\rho(770)^{0,+}$	$7.7549 \times 10^{-1} \pm 3.4 \times 10^{-4}$ P [0; 0   -15, e+1, (-174)]	$1.73 \times 10^{-7}$
$\omega(782)^0$	$7.8265 \times 10^{-1} \pm 1.2 \times 10^{-4}$ P [0; 0   -15, (243)] E [-x; 6   -6, -6, e+1, -9, (135)]	$2.10 \times 10^{-7}$ $4.51 \times 10^{-11}$
$\eta'(958)^0$	$9.5778 \times 10^{-1} \pm 6.0 \times 10^{-5}$ P [0; 0   132, (30)] E [-x; 6   -12, -e-1, -6, (-24)]	$6.81 \times 10^{-7}$ $4.66 \times 10^{-7}$
$\phi(1020)^0$	$1.019455 \pm 2.0 \times 10^{-5}$ P [0; 0   33, -12, e+1]	$4.92 \times 10^{-6}$
$f_2(1270)^0$	$1.2751 \pm 1.2 \times 10^{-3}$ P [0; 0   9, -21] P [x; 3   -e-1, e+1, -6, (36)] E [-x; 6   39, -e-1]	$3.84 \times 10^{-4}$ $1.87 \times 10^{-5}$ $3.78 \times 10^{-4}$
$f_1(1285)^0$	$1.2818 \pm 6.0 \times 10^{-4}$ P [0; 0   9, -9, -6] P [x; 3   -e-1, e+1, -6, -e-1, e+1] E [-x; 6   36, -6]	$2.46 \times 10^{-5}$ $9.88 \times 10^{-5}$ $1.20 \times 10^{-4}$
$a_2(1320)^{0,+}$	$1.3183 \pm 5.0 \times 10^{-4}$ P [0; 0   9, -e-1, e+1, -e-1, e+1, -e-1, e+1] P [x; 3   -e-1, e+1, 186] E [-x; 6   27, -e-1, e+1, -e-1]	$4.50 \times 10^{-4}$ $5.66 \times 10^{-6}$ $2.98 \times 10^{-4}$
$f_1(1420)^0$	$1.4264 \pm 9.0 \times 10^{-4}$ P [0; 0   6, 6, -6, (-39)] P [x; 3   -e-1, 6, 24] E [-x; 6   15, -15]	$1.64 \times 10^{-6}$ $9.34 \times 10^{-5}$ $3.29 \times 10^{-5}$
$\rho_3(1690)^{0,+}$	$1.6888 \pm 2.1 \times 10^{-3}$ P [0; 0   e+1, e+1, -e-1, (-51)] P [x; 3   -e-1, -6, -e-1, e+1] E [0; 9   -e-1, e+1, 12]	$1.95 \times 10^{-5}$ $5.29 \times 10^{-4}$ $8.78 \times 10^{-4}$

In physics we can find a number of analogous dualities, for instance: positive and negative charges, north and south magnetic poles, particles and antiparticles, emission and absorption of quanta, destructive and constructive interference of waves, nuclear fusion and fission, and in the widest sense also Newton's principle "action = reaction".

From these observations an interesting question arises: does such a duality also exist in the model of oscillations in a chain system, and how must this model be extended to make the "Yin-Yang" obvious and visible?

Applying this idea to Müller's model, it must be claimed

Table 4: Continued fraction representations of masses of the strange mesons ( $x = -1.75083890054$ )

Particle	Mass $\pm$ SD [GeV] Continued fraction representation(s)	Numerical error [GeV]
$K^+$	$4.93677 \times 10^{-1} \pm 1.6 \times 10^{-5}$ P [0; 0   -e-1, -6, e+1, 45] E [0; 6   e+1, -e-1, -e-1, 15, -e-1] E [-x; 6   -e-1, e+1, e+1, 6, e+1, -6]	$5.65 \times 10^{-7}$ $6.96 \times 10^{-6}$ $4.04 \times 10^{-6}$
$K^0, K_S^0, K_L^0$	$4.97614 \times 10^{-1} \pm 2.4 \times 10^{-5}$ E [-x; 6   -e-1, e+1, e+1, -e-1, -e-1, e+1, e+1]	$4.73 \times 10^{-6}$
$K^*(892)^+$	$8.9166 \times 10^{-1} \pm 2.6 \times 10^{-4}$ P [0; 0   -54, e+1] E [-x; 6   -9, -6, 6]	$6.63 \times 10^{-5}$ $6.13 \times 10^{-5}$
$K^*(892)^0$	$8.9594 \times 10^{-1} \pm 2.2 \times 10^{-4}$ P [0; 0   -60, e+1, -e-1] E [-x; 6   -9, -e-1, -6]	$1.47 \times 10^{-4}$ $5.48 \times 10^{-5}$
$K_2^*(1430)^+$	$1.4256 \pm 1.5 \times 10^{-3}$ P [0; 0   6, 6, -6] P [x; 3   -e-1, 6, 30] E [-x; 6   15, -21]	$7.56 \times 10^{-4}$ $1.08 \times 10^{-4}$ $1.40 \times 10^{-4}$
$K_2^*(1430)^0$	$1.4324 \pm 1.3 \times 10^{-3}$ P [0; 0   6, 6, 6] P [x; 3   -e-1, 6, 9, (-e-1)] E [-x; 6   15, -6, e+1, (36)]	$3.72 \times 10^{-4}$ $6.31 \times 10^{-4}$ $5.37 \times 10^{-7}$

that the fundamental spectrum of proton resonances must have an opposite, an anti-oscillation or inverted oscillation spectrum. What could it be?

We know that these proton master-oscillations are stable, so the theorized counter-oscillations must belong to a particle with similar lifetime than the proton. Consequently the electron is the only particle that could be a manifestation of such an inverted oscillation.

Now the concept of an inverted oscillation must be translated into a mathematical equation. According to Müller's standard model, we can express the electron mass as a proton resonance and the proton mass as an electron resonance:

$$\ln \frac{m_{electron}}{m_{proton}} = p + S_p,$$

$$\ln \frac{m_{proton}}{m_{electron}} = p + S_e,$$

where  $p$  is the phase shift (with value 0 or 1.5) and  $S$  the continued fraction as discussed in previous papers (given in equation (1)). Obviously for  $p \neq 0$ ,  $S_p \neq S_e$ , and this is the starting point for the further modification of the model. We have to adjust the phase shift (when different from zero) in such a way that both continued fractions become opposite in the sense of oscillation information. This means that the denominators of  $S_p$  and  $S_e$  must be the same, but with opposite

sign. If

$$S_p = n_0 + \frac{e}{n_1 + \frac{e}{n_2 + \frac{e}{n_3 + \dots}}}$$

then must hold for  $S_e$ :

$$S_e = -n_0 + \frac{e}{-n_1 + \frac{e}{-n_2 + \frac{e}{-n_3 + \dots}}}$$

Mathematically it is now obvious that one equation must be modified by a minus sign and we have to write:

$$\ln \frac{m_{electron}}{m_{proton}} = p + S_p, \tag{2}$$

$$\ln \frac{m_{proton}}{m_{electron}} = -p + S_e, \tag{3}$$

However, this is not yet a complete set of rules to find new continued fraction representations of the proton and electron; in order to arrive at a conclusion, it is absolutely necessary to develop further physical ideas.

**Idea 1 – Length of continued fractions**

The resulting continued fractions  $S_p$  and  $S_e$  should be short. A previous article already suggested that short fractions are associated with stability [9]. However, the fractions must not be too short. The fundamental oscillators must be represented by the simplest variant of a chain of oscillators. This is a single mass hold via two massless flexible strings between two motionless, fixed walls. This setup leads to 3 parameters determining the eigenfrequency of the chain, the mass value and the two different lengths of the strings. Consequently the continued fraction also should have 3 free parameters (the free link and two denominators). This idea solves the conceptual problem of a “no information oscillation”. When expressing the electron mass as a proton resonance, then  $\ln \frac{m_{electron}}{m_{proton}} = p + S$ , and  $p$  must not have values determining  $S$  as zero or any other integer number ( $\pm 3, \pm 6, \pm 9, \dots$ ). In such a case no continued fraction can be written down, and the oscillation would not have any property.

**Idea 2 – Small denominators**

According to Müller’s theory, a high positive or negative denominator locates the data point in a fluctuating zone. Consequently the considered property should be difficult to be kept constant. From all our observations, it is highly reasonable to believe that proton and electron masses are constant even over very long time scales. Therefore their masses cannot be located too deep inside a fluctuation zone. In this study, the maximum value of the denominators was tentatively limited to  $\pm 18$ .

**Idea 3 – The free link**

The calculation

$$\ln \frac{m_{electron}}{m_{proton}} \approx -7.51$$

Table 5: Continued fraction representations of masses of the charmed, and charmed strange mesons ( $x = -1.75083890054$ )

Particle	Mass $\pm$ SD [GeV] Continued fraction representation(s)	Numerical error [GeV]
$D^+$	$1.86957 \pm 1.6 \times 10^{-4}$ P [0; 0   e+1, 12, 27] E [0; 9   -e-1, 9, 39] E [-x; 6   6, -213]	$2.92 \times 10^{-5}$ $5.45 \times 10^{-6}$ $1.95 \times 10^{-8}$
$D^0$	$1.86480 \pm 1.4 \times 10^{-4}$ P [0; 0   e+1, 12, -e-1, -6] E [0; 9   -e-1, 9, -12, e+1] E [-x; 6   6, 129]	$1.03 \times 10^{-4}$ $1.29 \times 10^{-4}$ $6.40 \times 10^{-6}$
$D^*(2007)^0$	$2.00693 \pm 1.6 \times 10^{-4}$ P [0; 0   e+1, -18, -e-1, e+1, -e-1] P [x; 3   -6, 6, 15] E [0; 9   -e-1, -78] E [-x; 6   6, -e-1, 6, e+1, 6]	$8.59 \times 10^{-5}$ $7.91 \times 10^{-5}$ $3.94 \times 10^{-5}$ $2.21 \times 10^{-5}$
$D^*(2010)^+$	$2.01022 \pm 1.4 \times 10^{-4}$ P [0; 0   e+1, -18, (-102)] P [x; 3   -6, 6, 6, (-21)] E [0; 9   -e-1, -63, (6)] E [-x; 6   6, -e-1, 6, -12]	$4.53 \times 10^{-7}$ $5.72 \times 10^{-6}$ $3.23 \times 10^{-7}$ $1.62 \times 10^{-4}$
$D_1(2420)^0$	$2.4213 \pm 6.0 \times 10^{-4}$ P [0; 0   e+1, -e-1, 6, -e-1, 6] P [x; 3   -9, -102] E [0; 9   -6, e+1, -e-1, 9, -e-1] E [-x; 6   e+1, 27, e+1, -e-1, e+1]	$4.56 \times 10^{-4}$ $3.68 \times 10^{-6}$ $4.37 \times 10^{-4}$ $4.10 \times 10^{-4}$
$D_2^*(2460)^0$	$2.4626 \pm 7.0 \times 10^{-4}$ P [0; 0   e+1, -e-1, e+1, 18, -9] E [0; 9   -6, e+1, -15] E [-x; 6   e+1, 348]	$5.21 \times 10^{-6}$ $9.58 \times 10^{-5}$ $1.02 \times 10^{-5}$
$D_2^*(2460)^+$	$2.4644 \pm 1.9 \times 10^{-3}$ P [0; 0   e+1, -e-1, e+1, 24] P [x; 3   -9, -e-1, -e-1, (e+1, 18)] E [0; 9   -6, e+1, -18] E [-x; 6   e+1, 663]	$7.45 \times 10^{-5}$ $2.40 \times 10^{-6}$ $1.14 \times 10^{-4}$ $1.95 \times 10^{-6}$
$D_s^+$	$1.96845 \pm 3.3 \times 10^{-4}$ P [0; 0   e+1, -54, (-e-1, -15)] P [x; 3   -6, e+1, 6, (-63)] E [0; 9   -e-1, 42, e+1, -e-1] E [-x; 6   6, -e-1, -e-1, -6]	$3.13 \times 10^{-7}$ $6.81 \times 10^{-7}$ $2.34 \times 10^{-4}$ $2.00 \times 10^{-4}$
$D_s^{*+}$	$2.1123 \pm 5.0 \times 10^{-4}$ P [x; 3   -6, -12, -e-1] E [0; 9   -e-1, -9, 6, -e-1, (-18, -45)] E [-x; 6   e+1, e+1, -e-1, e+1, -e-1, e+1, -e-1]	$4.00 \times 10^{-4}$ $3.42 \times 10^{-9}$ $4.70 \times 10^{-4}$
$D_{s0}^*(2317)^+$	$2.3178 \pm 6.0 \times 10^{-4}$ P [0; 0   e+1, -e-1, -27] E [0; 9   -e-1, -e-1, e+1, -e-1, -39]	$4.57 \times 10^{-4}$ $1.50 \times 10^{-5}$
$D_{s1}(2460)^+$	$2.4595 \pm 6.0 \times 10^{-4}$ P [0; 0   e+1, -e-1, e+1, 12, (15)] P [x; 3   -9, -6, e+1, (-9)] E [0; 9   -6, e+1, -12, e+1, (12)] E [-x; 6   e+1, 189]	$1.19 \times 10^{-6}$ $5.71 \times 10^{-5}$ $4.66 \times 10^{-6}$ $5.06 \times 10^{-5}$
$D_{s1}(2536)^+$	$2.53528 \pm 2.0 \times 10^{-4}$ P [0; 0   e+1, -e-1, e+1, -e-1, e+1, e+1, -6] E [0; 9   -6, 6, -36] E [-x; 6   e+1, -21, e+1, -e-1, (-e-1)]	$3.89 \times 10^{-5}$ $1.87 \times 10^{-5}$ $1.88 \times 10^{-5}$
$D_{s2}^*(2573)^+$	$2.5726 \pm 9.0 \times 10^{-4}$ P [x; 3   -12, e+1, 15] E [0; 9   -6, 9, 6]	$8.95 \times 10^{-5}$ $2.24 \times 10^{-4}$

Table 6: Continued fraction representations of masses of the bottom mesons (including strange and charmed mesons) ( $x = -1.75083890054$ )

Particle	Mass $\pm$ SD [GeV] Continued fraction representation(s)	Numerical error [GeV]
$B^+$	$5.27917 \pm 2.9 \times 10^{-4}$ P [x; 3   6, -9, 6, 6]	$8.81 \times 10^{-5}$
$B^0$	$5.27950 \pm 3.0 \times 10^{-4}$ P [x; 3   6, -9, 6, (33)]	$4.56 \times 10^{-6}$
$B^{*0,+}$	$5.3251 \pm 5.0 \times 10^{-4}$ P [x; 3   6, -6, -6, e+1, e+1]	$1.09 \times 10^{-4}$
$B_{2^*}(5747)^{0,+}$	$5.743 \pm 5.0 \times 10^{-3}$ E [0; 9   9, -e-1, -12]	$2.95 \times 10^{-4}$
$B_s^0$	$5.3663 \pm 6.0 \times 10^{-4}$ P [x; 3   6, -6, e+1, (9)]	$4.93 \times 10^{-6}$
$B_s^{*0}$	$5.4154 \pm 1.4 \times 10^{-3}$ P [x; 3   6, -e-1, -e-1, 12]	$2.19 \times 10^{-5}$
$B_{s2^*}(5840)^0$	$5.8397 \pm 6.0 \times 10^{-4}$ P [x; 3   e+1, e+1, -e-1, e+1, -9, (-6)]	$4.08 \times 10^{-5}$
$B_c^+$	$6.277 \pm 6.0 \times 10^{-3}$ P [x; 3   e+1, 6, -153] E [0; 9   6, 6, -e-1, e+1, (63)]	$1.21 \times 10^{-5}$ $1.71 \times 10^{-6}$

leads to a value between the principal nodes -6 and -9. From this it follows that in the continued fractions, the free link  $n_0$  can only take the values  $\pm 6$  and  $\pm 9$ .

#### Idea 4 – Effect of canceling denominators

Elementary particles can be divided in two groups: the vast majority with an extremely short half-life, and a small set with comparable longer lifetime. When analyzing the more stable particles with Müller's standard model, already a striking tendency can be discovered that especially the sum of the free link and the first denominators tends to be zero.

Examples:

The  $\tau$  can be interpreted as proton resonance and the full continued fraction representation, as calculated by the computer is: P [0; 0 | e+1, 6, -e-1, e+1, -e-1, -e-1, (6)]. Note that in the end, every determination of a continued fraction results in an infinite periodical alternating sequence of the denominators e+1 and -e-1, which is always omitted here. Without significantly changing the mass value, the fraction can be rewritten: P [0; 0 | e+1, 6, -e-1, e+1, -e-1, -e-1, (e+1, -6)], and then the sum of all denominators equals zero.

The full continued fraction for the charged pion is:

E [0; 6 | -6, -e-1, e+1, -e-1, 48, (-e-1, 6, -24, e+1, -e-1, 12)]. It can be seen that the free link and the first 3 denominators cancel successively. Then this changes. A minimal manipulation leads to:

E [0; 6 | -6, -e-1, e+1, -e-1, 48, (-e-1, 6, -48, e+1, -6, e+1)].

The full continued fraction for the neutral pion is:

E [0; 6 | -6, -6, -6, 6, -e-1, (12, -12, e+1, -e-1, e+1, 45, 6)]. Here we have only to eliminate the 11<sup>th</sup> denominator (45) and

Table 7: Continued fraction representations of masses of the  $c\bar{c}$  mesons ( $x = -1.75083890054$ )

Particle	Mass $\pm$ SD [GeV] Continued fraction representation(s)	Numerical error [GeV]
$\eta_c(1S)^0$	$2.9803 \pm 1.2 \times 10^{-3}$ P [x; 3   -30, e+1, -e-1] E [0; 9   -9, e+1, (-216)] E [-x; 6   e+1, -e-1, 18, -e-1, e+1]	$6.56 \times 10^{-5}$ $7.34 \times 10^{-7}$ $8.84 \times 10^{-4}$
$J/\psi(1S)^0$	$3.096916 \pm 1.1 \times 10^{-5}$ E [-x; 6   e+1, -e-1, e+1, 6, -e-1, e+1, 6, e+1, (-18)]	$1.19 \times 10^{-8}$
$\chi_{c0}(1P)^0$	$3.41475 \pm 3.1 \times 10^{-4}$ P [x; 3   63, e+1, (57)] E [0; 9   -15, e+1, -e-1, (-12)]	$6.99 \times 10^{-8}$ $9.48 \times 10^{-6}$
$\chi_{c1}(1P)^0$	$3.51066 \pm 7.0 \times 10^{-5}$ no continued fraction found	outlier
$h_c(1P)^0$	$3.52541 \pm 1.6 \times 10^{-4}$ P [x; 3   36, 6, (-24)]	$1.94 \times 10^{-6}$
$\chi_{c2}(1P)^0$	$3.55620 \pm 9.0 \times 10^{-5}$ P [x; 3   33, -9, e+1, -e-1, e+1] E [0; 9   -18, 21, -e-1]	$7.52 \times 10^{-5}$ $5.36 \times 10^{-5}$
$\eta_c(2S)^0$	$3.637 \pm 4.0 \times 10^{-3}$ E [0; 9   -21, (66)]	$5.00 \times 10^{-6}$
$\psi(2S)^0$	$3.68609 \pm 4.0 \times 10^{-5}$ E [0; 9   -24, e+1, e+1, e+1, e+1]	$6.30 \times 10^{-6}$
$\psi(3770)^0$	$3.77292 \pm 3.5 \times 10^{-4}$ E [0; 9   -30, e+1, (-12)]	$5.90 \times 10^{-5}$
$\chi_{c2}(2P)^0$	$3.9272 \pm 2.6 \times 10^{-3}$ P [x; 3   15, -27] E [0; 9   -51, -9, e+1]	$1.47 \times 10^{-4}$ $1.10 \times 10^{-4}$
$\psi(4040)^0$	$4.0390 \pm 1.0 \times 10^{-3}$ P [x; 3   12, e+1, -e-1, (495)] E [0; 9   -108, -e-1]	$3.14 \times 10^{-8}$ $5.66 \times 10^{-4}$
$\psi(4160)^0$	$4.1530 \pm 3.0 \times 10^{-3}$ P [x; 3   12, -e-1, -e-1, (6)] E [0; 9   915]	$1.88 \times 10^{-5}$ $1.36 \times 10^{-5}$
$\psi(4415)^0$	$4.421 \pm 4.0 \times 10^{-3}$ P [x; 3   9, 81] E [0; 9   42, -6]	$4.82 \times 10^{-5}$ $3.64 \times 10^{-4}$

the sum equals zero.

The full continued fraction for the  $\eta^0$  is:

P [0; 0 | -6, e+1, -e-1, 6, -e-1, 12, (-9, -12, -e-1, e+1, -e-1, -e-1, e+1, -e-1, e+1, e+1)].

Again the first 4 denominators form a zero sum, then the 7<sup>th</sup> denominator (-9) interrupts this canceling. Without significant change of the numerical value, this fraction could be shortened and rewritten: P [0; 0 | -6, e+1, -e-1, 6, -e-1, 12, (-12, e+1)].

When interpreting  $\eta^0$  as electron resonance, again adding the free link to the first 5 denominators gives zero:

E [0; 6 | e+1, -e-1, e+1, -6, -e-1, e+1, (24)]. We can add and rewrite: E [0; 6 | e+1, -e-1, e+1, -6, -e-1, e+1, (24, -e-1, -24)].

A completely different case is the neutron; here the con-

Table 8: Continued fraction representations of masses of the  $b\bar{b}$  mesons ( $x = -1.75083890054$ )

Particle	Mass $\pm$ SD [GeV] Continued fraction representation(s)	Numerical error [GeV]
$\Upsilon(1S)^0$	$9.46030 \pm 2.6 \times 10^{-4}$ P [0; 3   -e-1, -12, -87] E [-x; 9   -e-1, e+1, -12, -63]	$1.02 \times 10^{-5}$ $9.33 \times 10^{-6}$
$\chi_{b0}(1P)^0$	$9.8594 \pm 5.0 \times 10^{-4}$ E [0; 9   e+1, -e-1, -e-1, e+1, -9, -e-1] E [-x; 9   -e-1, e+1, 6, -e-1, 6, e+1]	$1.96 \times 10^{-4}$ $3.40 \times 10^{-4}$
$\chi_{b1}(1P)^0$	$9.8928 \pm 4.0 \times 10^{-4}$ E [0; 9   e+1, -e-1, -e-1, 6, (-75)] E [-x; 9   -e-1, e+1, e+1, e+1, -12]	$4.52 \times 10^{-6}$ $3.00 \times 10^{-4}$
$\chi_{b2}(1P)^0$	$9.9122 \pm 4.0 \times 10^{-4}$ P [0; 3   -e-1, -6, e+1, 15, -e-1] E [0; 9   e+1, -e-1, -e-1, 12, -6] E [-x; 9   -e-1, e+1, e+1, 6]	$8.26 \times 10^{-5}$ $1.07 \times 10^{-5}$ $2.21 \times 10^{-6}$
$\Upsilon(2S)^0$	$1.002326 \times 10^1 \pm 3.1 \times 10^{-4}$ P [0; 3   -e-1, -e-1, -e-1, e+1, -75] E [0; 9   e+1, -e-1, -6, e+1, e+1, e+1, (-18)] E [-x; 9   -e-1, e+1, e+1, -e-1, 6, -e-1, e+1, -e-1, e+1]	$1.86 \times 10^{-6}$ $1.28 \times 10^{-6}$ $2.49 \times 10^{-4}$
$\chi_{b0}(2P)^0$	$1.02325 \times 10^1 \pm 6.0 \times 10^{-4}$ P [0; 3   -e-1, -e-1, 327] E [0; 9   e+1, -e-1, -30] E [-x; 9   -e-1, 6, -e-1, -e-1, -e-1, -e-1]	$1.29 \times 10^{-6}$ $9.85 \times 10^{-5}$ $2.80 \times 10^{-4}$
$\chi_{b1}(2P)^0$	$1.02555 \times 10^1 \pm 5.0 \times 10^{-4}$ P [0; 3   -e-1, -e-1, 30] E [0; 9   e+1, -e-1, -54] E [-x; 9   -e-1, 6, -6, e+1, -e-1, -6]	$2.78 \times 10^{-4}$ $4.85 \times 10^{-4}$ $8.02 \times 10^{-5}$
$\chi_{b2}(2P)^0$	$1.02686 \times 10^1 \pm 5.0 \times 10^{-4}$ P [0; 3   -e-1, -e-1, 21, -e-1, 9] E [0; 9   e+1, -e-1, -93] E [-x; 9   -e-1, 6, -6, 9, (-12)]	$1.11 \times 10^{-5}$ $2.07 \times 10^{-5}$ $4.33 \times 10^{-6}$
$\Upsilon(3S)^0$	$1.03552 \times 10^1 \pm 5.0 \times 10^{-4}$ P [0; 3   -e-1, -e-1, 6, e+1, 6] E [-x; 9   -e-1, 6, -30, -e-1]	$3.94 \times 10^{-5}$ $1.75 \times 10^{-4}$
$\Upsilon(4S)^0$	$1.05794 \times 10^1 \pm 1.2 \times 10^{-3}$ P [0; 3   -e-1, -e-1, e+1, -e-1, e+1, -15] E [0; 9   e+1, -e-1, 6, e+1, 21]	$9.28 \times 10^{-5}$ $4.37 \times 10^{-5}$
$\Upsilon(10860)^0$	$1.0876 \times 10^1 \pm 1.1 \times 10^{-2}$ E [0; 9   e+1, -e-1, e+1, 24]	$8.32 \times 10^{-5}$
$\Upsilon(11020)^0$	$1.1019 \times 10^1 \pm 8.0 \times 10^{-3}$ P [0; 3   -6, e+1, -e-1, 6, e+1] E [0; 9   e+1, -e-1, e+1, -6, (-18)]	$3.60 \times 10^{-3}$ $3.89 \times 10^{-5}$

tinued fraction is: P [0; 0 | 1974, -e-1, -e-1, (-24)]. As the first denominator is very high, the following denominators can make only minor changes of the numerical value of the fraction. So here it would be easily possible adding denominators to force the sum to be zero. Actually many particle representations fall in that category, so from looking only at these examples, the fundamental idea of a vanishing sum of denominators does not come out at all.

### Hypothesis:

From all these examples we can theorize that for a permanently stable particle such as the proton and electron, the sum of the free link and all partial denominators must be zero.

### 3.2 Rules for constructing continued fractions

With these physical ideas, we can express the proton and electron through a very limited set of 10 pairs of continued fractions (Table 12), which can all be written down. For every continued fraction, the phase shift  $p$  can be calculated, so that equations (2) and (3) hold. Then, new rules for the interpretation of elementary particle masses can be derived. First, a mass can be either a proton or an electron resonance, and second, this newly found phase shift must now be considered.

When interpreting particle masses as proton resonance states we write ( $x$  is the new phase shift):

$$\ln \frac{m_{particle}}{m_{proton}} = (0 \text{ or } x) + S \quad (4)$$

and for electron resonances holds:

$$\ln \frac{m_{particle}}{m_{electron}} = (0 \text{ or } -x) + S. \quad (5)$$

The basic rule that the phase shift can be zero, is fundamental and will not be changed.

Now for every of these 10 different phase shifts, the new model must be checked. We have to find out to what extent other elementary particles are compatible to one of these 10 new versions of the model and still accumulate in spectral nodes. There is a set of 18 particle masses, which cannot be expressed as proton or electron resonances with phase shift zero; these are:  $\mu^-$ ,  $K^0$ ,  $B^+$ ,  $B^0$ ,  $B^{*0,+}$ ,  $B_s^0$ ,  $B_s^{*0}$ ,  $B_{s2}^{*0}(5840)^0$ ,  $J/\psi(1S)^0$ ,  $\chi_{c1}(1P)^0$ ,  $h_c(1P)^0$ ,  $\Lambda(1520)^0$ ,  $\Sigma^0$ ,  $\Sigma(1385)^+$ ,  $\Xi^-$ ,  $\Lambda_c^+$ ,  $\Sigma_b^{*0,+}$  and  $\Sigma_b^{*-}$ . The question is now: which of the 10 possible phase shifts can reproduce these 18 masses best, with the lowest number of outliers?

By trial and error it was found that there is indeed such a "best possibility", providing only one outlier:

$$\ln \frac{m_{electron}}{m_{proton}} = x + (-6) + \frac{e}{12 + \frac{e}{-6}} \quad (6)$$

$$\ln \frac{m_{proton}}{m_{electron}} = -x + 6 + \frac{e}{-12 + \frac{e}{6}}. \quad (7)$$

The phase shift  $x$  equals  $-1.75083890054$  and the numerical errors are very small (see Tables 1 and 9).

Tables 1 to 11 show the continued fraction representations for the considered data set (117 particles, 107 different masses) All possible fractions are given for both, proton and electron resonances with the phase shifts 0 and  $\pm x$ . For completeness, Table 12 displays the 10 alternative continued fraction representations together with the calculated phase shifts

and the number of outliers when trying to reproduce the aforementioned set of 18 masses.

A single outlier is a very satisfying result when comparing to 14% outliers, which have been found with the standard version of Müller's model [9]. Since the spectra of electron and proton resonances overlap, most particles can even expressed as both, proton and electron resonances. This demonstrates that it makes only sense to analyze high accuracy data, otherwise easily a continued fraction representation can be found.

As expected, the principle of "Yin and Yang" has not been found anymore in this set of particles. There are no other pairs of particles with opposite oscillation information. It seems to be that this fundamental concept is only applicable to longterm stable systems or processes. Further research on other data sets should confirm this.

### 3.3 Model discussion

Is the principle of "Yin and Yang" really necessary to obtain continued fraction representations for most elementary particle masses? The critical reader could argue that alone the additional consideration of electron resonances greatly enhances the chances to express particle masses via standard continued fractions (with phase shift 0 and 3/2). This is true, however, the author has found that the 14% outliers were very little reduced when considering such additional electron resonances. So another phase shift is definitively required.

But, are the electron resonances really necessary? Would it not be possible to write only

$$\ln \frac{m_{particle}}{m_{proton}} = (0 \text{ or } p) + S \quad (8)$$

where p is just any other phase shift different from the standard value 3/2 (between 0 and  $\pm 3$ )? This was exactly the author's first attempt to modify Müller's model. It was found that such phase shift does not exist.

For that reason the problem can only be solved through a new physical or philosophical idea. Every good physical theory consists of two parts, equivalent to a soul and a body. The soul represents a fundamental physical law or a philosophical principle, while always mathematics is the body.

From this viewpoint the author is particularly satisfied having found the "Yin-Yang" principle as an adequate extension of the proton resonance concept. It clearly justifies the importance of electron resonances and distinguishes the model from numerology.

Regarding the selection of the appropriate phase shift, a very critical reader could note that there is only one outlier difference between

$$\ln \frac{m_{electron}}{m_{proton}} = [x_1; -9 | -9, 18] \quad (2 \text{ outliers})$$

and the best variant

$$\ln \frac{m_{electron}}{m_{proton}} = [x_2; -6 | 12, -6], \quad (1 \text{ outlier})$$

Table 9: Continued fraction representations of masses of the N,  $\Delta$ ,  $\Lambda$ ,  $\Sigma$ ,  $\Xi$  and  $\Omega$  baryons ( $x = -1.75083890054$ )

Particle	Mass $\pm$ SD [GeV] Continued fraction representation(s)	Numerical error [GeV]
$p^+$	$9.38272013 \times 10^{-1} \pm 2.3 \times 10^{-8}$ E [-x; 6   -12, 6]	$2.22 \times 10^{-12}$
$n^0$	$9.39565346 \times 10^{-1} \pm 2.3 \times 10^{-8}$ P [0; 0   1974, -e-1, -e-1, (-24)]	$7.85 \times 10^{-11}$
$\Delta(1232)^{-0,+;++}$	$1.2320 \pm 1.0 \times 10^{-3}$ P [0; 0   9, e+1, -e-1, e+1] P [x; 3   -e-1, e+1, -e-1, 6, e+1, -e-1] E [-x; 6   75]	$4.29 \times 10^{-4}$ $7.12 \times 10^{-4}$ $8.61 \times 10^{-4}$
$\Lambda^0$	$1.115683 \pm 6.0 \times 10^{-6}$ P [0; 0   15, e+1, 15, -6]	$9.92 \times 10^{-8}$
$\Lambda(1405)^0$	$1.4051 \pm 1.3 \times 10^{-3}$ P [0; 0   6, e+1] P [x; 3   -e-1, 6, -e-1, -e-1]	$2.50 \times 10^{-5}$ $6.44 \times 10^{-4}$
$\Lambda(1520)^0$	$1.5195 \pm 1.0 \times 10^{-3}$ P [x; 3   -e-1, 15, e+1] E [-x; 6   12, -e-1, e+1, -e-1]	$5.71 \times 10^{-4}$ $4.36 \times 10^{-4}$
$\Sigma^+$	$1.18937 \pm 7.0 \times 10^{-5}$ P [0; 0   12, -6, e+1, -e-1, 6]	$5.70 \times 10^{-6}$
$\Sigma^0$	$1.192642 \pm 2.4 \times 10^{-5}$ E [-x; 6   606]	$1.24 \times 10^{-5}$
$\Sigma^-$	$1.197449 \pm 3.0 \times 10^{-5}$ P [0; 0   12, -e-1, 6, -e-1, e+1, -e-1, (93)] E [-x; 6   321, -e-1]	$5.89 \times 10^{-9}$ $1.22 \times 10^{-5}$
$\Sigma(1385)^+$	$1.3828 \pm 4.0 \times 10^{-4}$ E [-x; 6   18, -15 (-e-1)]	$8.96 \times 10^{-5}$
$\Sigma(1385)^0$	$1.3837 \pm 1.0 \times 10^{-3}$ P [0; 0   6, e+1, -e-1, e+1, -e-1] E [-x; 6   18, -12, (e+1, 60)]	$6.88 \times 10^{-4}$ $2.95 \times 10^{-8}$
$\Sigma(1385)^-$	$1.3872 \pm 5.0 \times 10^{-4}$ P [0; 0   6, e+1, -e-1, e+1, e+1] E [-x; 6   18, -6, e+1]	$3.03 \times 10^{-4}$ $1.66 \times 10^{-4}$
$\Xi^0$	$1.31486 \pm 2.0 \times 10^{-4}$ P [0; 0   9, -e-1, e+1, -6] P [x; 3   -e-1, e+1, -93] E [-x; 6   27, -9, e+1]	$1.42 \times 10^{-4}$ $2.86 \times 10^{-5}$ $1.53 \times 10^{-4}$
$\Xi^-$	$1.32171 \pm 7.0 \times 10^{-5}$ P [x; 3   -e-1, e+1, 45, e+1]	$5.35 \times 10^{-5}$
$\Xi(1530)^0$	$1.53180 \pm 3.2 \times 10^{-4}$ P [0; 0   6, -6, (165)] E [0; 9   -e-1, e+1, -e-1, e+1, -e-1, -e-1, -e-1]	$1.35 \times 10^{-6}$ $5.19 \times 10^{-5}$
$\Xi(1530)^-$	$1.5350 \pm 6.0 \times 10^{-4}$ P [0; 0   6, -6, 9, (-12)] P [x; 3   -e-1, 21, 6] E [0; 9   -e-1, e+1, -e-1, e+1, -6, (-54)]	$1.09 \times 10^{-5}$ $1.01 \times 10^{-4}$ $1.18 \times 10^{-6}$
$\Omega^-$	$1.67245 \pm 2.9 \times 10^{-4}$ P [0; 0   e+1, e+1, -e-1, e+1, -e-1, -e-1] P [x; 3   -e-1, 9, e+1, -9] E [0; 9   -e-1, e+1, 48]	$1.09 \times 10^{-4}$ $1.50 \times 10^{-4}$ $1.23 \times 10^{-4}$

Table 10: Continued fraction representations of masses of the charmed baryons ( $x = -1.75083890054$ )

Particle	Mass $\pm$ SD [GeV] Continued fraction representation(s)	Numerical error [GeV]
$\Lambda_c^+$	$2.28646 \pm 1.4 \times 10^{-4}$ E [-x; 6   e+1, 6, 9, -e-1, (-e-1)]	$8.64 \times 10^{-6}$
$\Lambda_c(2595)^+$	$2.5954 \pm 6.0 \times 10^{-4}$ P [x; 3   -12, 9, e+1] E [0; 9   -6, 15, (66)] E [-x; 6   e+1, -12, e+1, -9]	$5.64 \times 10^{-4}$ $1.23 \times 10^{-6}$ $1.13 \times 10^{-4}$
$\Sigma_c(2455)^{++}$	$2.45403 \pm 1.8 \times 10^{-4}$ P [x; 3   -9, -6, -39] E [0; 9   -6, e+1, -9, e+1, -e-1] E [-x; 6   e+1, 105]	$8.51 \times 10^{-7}$ $2.02 \times 10^{-5}$ $7.84 \times 10^{-5}$
$\Sigma_c(2455)^+$	$2.4529 \pm 4.0 \times 10^{-4}$ P [0; 0   e+1, -e-1, e+1, 6, e+1, -e-1, e+1] P [x; 3   -9, -6, -9] E [-x; 6   e+1, 96]	$2.84 \times 10^{-4}$ $1.07 \times 10^{-4}$ $1.02 \times 10^{-4}$
$\Sigma_c(2455)^0$	$2.45376 \pm 1.8 \times 10^{-4}$ P [x; 3   -9, -6, -24] E [0; 9   -6, e+1, -9, e+1, -e-1, e+1] E [-x; 6   e+1, 102, (e+1)]	$3.06 \times 10^{-5}$ $1.48 \times 10^{-4}$ $8.05 \times 10^{-5}$
$\Sigma_c(2520)^{++}$	$2.5184 \pm 6.0 \times 10^{-4}$ P [0; 0   e+1, -e-1, e+1, -e-1, -18] E [0; 9   -6, 6, -e-1, e+1, (18)] E [-x; 6   e+1, -27, e+1, (6)]	$1.44 \times 10^{-4}$ $1.05 \times 10^{-5}$ $1.68 \times 10^{-5}$
$\Sigma_c(2520)^+$	$2.5175 \pm 2.3 \times 10^{-3}$ P [0; 0   e+1, -e-1, e+1, -e-1, -15, e+1] E [0; 9   -6, 6, -e-1, e+1, (-6)] E [-x; 6   e+1, -27]	$1.01 \times 10^{-4}$ $7.02 \times 10^{-5}$ $4.20 \times 10^{-4}$
$\Sigma_c(2520)^0$	$2.5180 \pm 5.0 \times 10^{-4}$ P [0; 0   e+1, -e-1, e+1, -e-1, -15] E [0; 9   -6, 6, -e-1, e+1, (-21)] E [-x; 6   e+1, -27, 6]	$2.46 \times 10^{-4}$ $8.75 \times 10^{-6}$ $2.10 \times 10^{-5}$
$\Xi_c^+$	$2.4678 \pm 4.0 \times 10^{-4}$ P [0; 0   e+1, -e-1, e+1, 60] P [x; 3   -9, -e-1, -e-1, e+1, e+1] E [0; 9   -6, e+1, -33] E [-x; 6   e+1, -933]	$5.29 \times 10^{-5}$ $2.82 \times 10^{-4}$ $8.89 \times 10^{-6}$ $1.45 \times 10^{-6}$
$\Xi_c^0$	$2.47088 \pm 3.4 \times 10^{-4}$ P [0; 0   e+1, -e-1, e+1, -162] P [x; 3   -9, -e-1, -9, (-9)] E [0; 9   -6, e+1, -141] E [-x; 6   e+1, -294]	$2.87 \times 10^{-7}$ $1.73 \times 10^{-5}$ $6.33 \times 10^{-6}$ $5.91 \times 10^{-6}$
$\Xi_c^{'+}$	$2.5756 \pm 3.1 \times 10^{-3}$ P [x; 3   -12, e+1, 6] E [0; 9   -6, 9, e+1] E [-x; 6   e+1, -12, -e-1, e+1]	$4.33 \times 10^{-4}$ $1.02 \times 10^{-3}$ $1.40 \times 10^{-3}$
$\Xi_c^{'0}$	$2.5779 \pm 2.9 \times 10^{-3}$ P [x; 3   -12, e+1, e+1] E [-x; 6   e+1, -12, -e-1]	$5.26 \times 10^{-4}$ $8.16 \times 10^{-4}$
$\Xi_c(2645)^{0,+}$	$2.6459 \pm 5.0 \times 10^{-4}$ P [x; 3   -12, -e-1, 9] E [0; 9   -6, -39, (-330)] E [-x; 6   e+1, -9, e+1, 6]	$7.47 \times 10^{-6}$ $1.13 \times 10^{-8}$ $2.50 \times 10^{-4}$
$\Omega_c^0$	$2.6952 \pm 1.7 \times 10^{-3}$ P [x; 3   -15, e+1, -e-1, e+1] E [0; 9   -6, -9, e+1, (-12)] E [-x; 6   e+1, -6, e+1]	$6.84 \times 10^{-4}$ $3.15 \times 10^{-6}$ $9.61 \times 10^{-4}$
$\Omega_c(2770)^0$	$2.7659 \pm 2.0 \times 10^{-3}$ E [0; 9   -6, -e-1, (93)] E [-x; 6   e+1, -6, e+1, e+1]	$9.99 \times 10^{-6}$ $3.47 \times 10^{-4}$

Table 11: Continued fraction representations of masses of the bottom baryons ( $x = -1.75083890054$ )

Particle	Mass $\pm$ SD [GeV] Continued fraction representation(s)	Numerical error [GeV]
$\Lambda_b^0$	$5.6202 \pm 1.6 \times 10^{-3}$ P [x; 3   6, e+1, -e-1, e+1, 9] E [0; 9   9, -27]	$1.25 \times 10^{-4}$ $3.49 \times 10^{-4}$
$\Sigma_b^+$	$5.8078 \pm 2.7 \times 10^{-3}$ E [0; 9   9, -e-1, e+1, -e-1, (-27)]	$2.47 \times 10^{-6}$
$\Sigma_b^-$	$5.8152 \pm 2.0 \times 10^{-3}$ E [0; 9   9, -e-1, e+1, -e-1, e+1, (-e-1, 24)]	$4.30 \times 10^{-6}$
$\Sigma_b^{*+}, \Sigma_b^{*0}$	$5.8290 \pm 3.4 \times 10^{-3}$ P [x; 3   e+1, e+1, -e-1, e+1]	$8.39 \times 10^{-4}$
$\Sigma_b^{*-}$	$5.8364 \pm 2.8 \times 10^{-3}$ P [x; 3   e+1, e+1, -e-1, e+1, -6]	$7.39 \times 10^{-5}$
$\Xi_b^{-,0}$	$5.7905 \pm 2.7 \times 10^{-3}$ E [0; 9   9, -e-1, e+1, 9]	$2.20 \times 10^{-4}$

Table 12: List of the 10 possible continued fraction representations of the electron mass when considering the rules that denominators must be small and their sum including the free link equals zero, together with their associate phase shifts and the number of outliers when considering the following set of 18 particles:  $\mu^-$ ,  $K^0$ ,  $B^+$ ,  $B^0$ ,  $B^{*0,+}$ ,  $B_s^0$ ,  $B_s^{*0}$ ,  $B_{s2}^{*0}(5840)^0$ ,  $J/\psi(1S)^0$ ,  $\chi_{c1}(1P)^0$ ,  $h_c(1P)^0$ ,  $\Lambda(1520)^0$ ,  $\Sigma^0$ ,  $\Sigma(1385)^+$ ,  $\Xi^-$ ,  $\Lambda_c^+$ ,  $\Sigma_b^{*0,+}$  and  $\Sigma_b^{*-}$ 

Continued fraction representation for $\ln \frac{m_{electron}}{m_{proton}} = x + S$	phase shift x	number of outliers
P [x; -9   15, -6]	1.29770965366	3
P [x; -9   -6, 15]	1.95172884111	5
P [x; -9   18, -9]	1.33097940724	4
P [x; -9   -9, 18]	1.79175802145	2 $\mu^-$ , $\Sigma^0$
P [x; -6   -6, 12]	-1.04460536299	6
P [x; -6   12, -6]	-1.75083890054	1 $\chi_{c1}(1P)^0$
P [x; -6   -9, 15]	-1.20718990898	6
P [x; -6   15, -9]	-1.70037040878	6
P [x; -6   18, -12]	-1.66836807753	3
P [x; -6   -12, 18]	-1.2860171871	4

so one single outlier might not be sufficiently significant to make a clear decision. Here it is now worth looking at the outlier particles. In the first case, the two outliers are the muon and the  $\Sigma^0$ . The muon has a comparatively long mean lifetime of  $2.2 \mu s$ . So it is far more stable than the average elementary particle. Therefore it is reasonable to request that the muon mass is reproduced by the model, i.e. the muon must not be an outlier.

#### 4 Conclusions

The here presented bipolar version of Müller's continued fraction model is so far the best description of elementary particle masses. It demonstrates two facts: first, electron and

proton can be interpreted as a manifestation of the “Yin and Yang” principle in nature. They both can be interpreted as fundamental reference points in the model of a chain of harmonic oscillations. Second, the proton resonance idea alone is an incomplete concept and we have to recognize that electron resonances also play an important role in the universe.

These results can be obtained only when strictly considering the individual measurement errors of the particles and all similar future analyses should be based on the most accurate data available.

Until now, this bipolar version of Müller’s model has reproduced only one data set. It is obvious that this alone cannot be considered as a full proof of correctness of this model variant and much more data should be analyzed.

### Acknowledgments

The author greatly acknowledges the financial support from the Brazilian governmental funding agencies FACEPE and CNPq.

Submitted on September 6, 2012 / Accepted on September 11, 2012

### References

1. Greulich K.O. Calculation of the masses of all fundamental Elementary Particles with an accuracy of approx. 1%. *Journal of Modern Physics*, 2010, v. 1, 300–302.
2. Paasch K. The logarithmic potential and an exponential mass function for Elementary Particles. *Progress in Physics*, 2009, v. 1 36–39.
3. Shah G.N. and Mir T.A. Are Elementary Particle masses related? *29th International Cosmic Ray Conference Pune*, 2005, v. 9, 219–222.
4. Tatischeff B. Use of nuclei fractal properties for help to determine some unknown particle spins and unknown nuclei excited level spins. arXiv: 1112.1586v1.
5. Tatischeff B. Fractals and log-periodic corrections applied to masses and energy levels of several nuclei. arXiv: 1107.1976v1.
6. Tatischeff B. Fractal properties applied to hadron spectroscopy. arXiv: 1105.2034v1.
7. Tatischeff B. Fractal properties in fundamental force coupling constants, in atomic energies, and in elementary particle masses. arXiv: 1104.5379v1.
8. Tatischeff B. and Brissaud I. Relations between elementary particle masses. arXiv: 1005.0238v1.
9. Ries A., Fook M.V.L. Fractal structure of nature’s preferred masses: Application of the model of oscillations in a chain system. *Progress in Physics*, 2010, v. 4, 82–89.
10. Müller H. Fractal scaling Models of resonant oscillations in chain systems of harmonic oscillators. *Progress in Physics*, 2009, v. 2, 72–76.
11. Müller H. Fractal scaling models of natural oscillations in chain systems and the mass distribution of the celestial bodies in the solar system. *Progress in Physics*, 2010, v. 1, 62–66.
12. Müller H. Fractal scaling models of natural oscillations in chain systems and the mass distribution of particles. *Progress in Physics*, 2010, v. 3, 61–66.
13. Ries A. The radial electron density in the Hydrogen atom and the model of oscillations in a chain system. *Progress in Physics*, 2012, v. 3, 29–34.
14. Nakamura K. et al. Review of Particle Physics. *Journal of Physics G*, 2010, v. 37, 075021. <http://pdg.lbl.gov>
15. Press W.H., Teukolsky S.A., Vetterling W.T., Flannery B.P. Numerical recipes in C. Cambridge University Press, Cambridge, 1992.

# Galaxy S-Stars Exhibit Orbital Angular Momentum Quantization per Unit Mass

Franklin Potter

Sciencegems.com, 8642 Marvale Drive, Huntington Beach, CA 92646 USA. E-mail: frank11hb@yahoo.com

The innermost stars of our Galaxy, called S-stars, are in Keplerian orbits. Quantum celestial mechanics (QCM) predicts orbital angular momentum quantization *per unit mass* for each of them. I determine the quantization integers for the 27 well-measured S-stars and the total angular momentum of this nearly isolated QCM system within the Galactic bulge.

## 1 Introduction

The innermost stars of our Galaxy, called S-stars, are in Keplerian orbits about a proposed [1] black hole of mass  $4.3 \pm 0.3$  million solar masses. Their orbital planes appear to have random orientations, their orbital eccentricities range from 0.131 to 0.963 with no apparent pattern, and their origins of formation remain an issue. The star labelled S0-2 has the smallest semi-major axis of about 1020 AU and has been monitored for one complete revolution of its orbit, thereby allowing a determination of the position of the Galactic center Sgr A\* at a distance of  $8.33 \pm 0.36$  kpc.

In this brief report I use the orbital distances of the 27 well-measured S-stars revolving about the Galactic Center as a test of the orbital angular momentum quantization *per unit mass* predicted by the quantum celestial mechanics (QCM) introduced by H.G. Preston and F. Potter in 2003 [2, 3]. For the derivation of QCM from the general relativistic Hamilton-Jacobi equation, see the published articles online [2, 4].

In a Schwarzschild metric approximation, their proposed gravitational wave equation (GWE) reduces to a Schrödinger-like equation in the  $r$ -coordinate while the angular coordinates  $(\theta, \phi)$  dictate the angular momentum quantization per unit mass. In particular, a body of mass  $\mu$  orbiting a central mass  $M$  has an orbital angular momentum  $L$  that obeys

$$\frac{L}{\mu} = m c H, \quad (1)$$

where  $m$  is the quantization integer and  $c$  is the speed of light. We assume that over millions of years the orbit has reached a QCM equilibrium distance  $r$  that agrees in angular momentum value with its Newtonian value  $L = \mu \sqrt{GM}r$ .

$H$  is the Preston gravitational distance, a different constant for each separate gravitationally bound system, equal to the system's total angular momentum  $L_T$  divided by its total mass  $M_T$

$$H = \frac{L_T}{M_T c}. \quad (2)$$

Note that  $H$  is not a universal constant, unlike  $\hbar$ , and that QCM is not quantum gravity. Also recall that the GWE in the free particle limit becomes the standard Schrödinger equation of quantum mechanics.

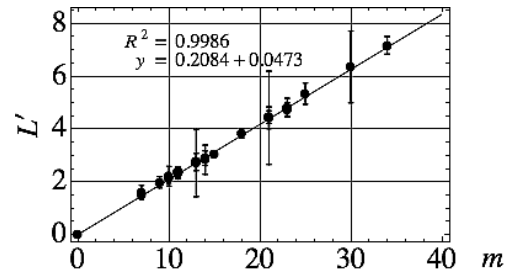


Fig. 1: QCM fit of S-stars at the Galactic Center.

## 2 S-star Orbital Quantization

The pertinent orbital parameters [5] for the 27 S-stars are listed in Table 1. Note that some uncertainties in both the semi-major axis column and in the eccentricity column are quite a large percentage of the mean values. These uncertainties will become smaller as more of these stars complete their orbits in the decades to come. More than an additional 100 S-stars are being studied in order to determine their orbital parameters. S0-16, whose orbital parameters are still being determined, has come the closest [1] to the Galactic Center Sgr A\* at 45 AU ( $6.75 \times 10^{12}$  m) with a tangential velocity of  $1.2 \times 10^7$  m/sec!

I assume that each S-star is in a QCM equilibrium orbit in order to use the Newtonian values for the plot of  $L' = L/\mu c$  versus  $m$  in Figure 1. The linear regression measure  $R^2 = 0.9986$  indicates an excellent fit. I did not take the proposed black hole mass for  $M$  but used one solar mass instead as a reference. The slope  $H = 6.59 \times 10^7$  meters for one solar mass, which becomes  $H_{BH} = 1.30 \times 10^{11}$  meters (0.87 AU) for the proposed central black hole mass. For comparison, the Schwarzschild radius for this BH is  $1.27 \times 10^{10}$  meters.

Stars having the same QCM values for  $m$ , such as the six stars with  $m = 11$ , have orbits in different planes. I.e., their orbital angular momentum vectors point in different directions. There might be orbital resonances among stars with different  $m$  values even though their orbital planes have quite different orientations. With much more S-star orbital data to be determined, future fits to the QCM angular momentum quantization constraint should be very interesting.

S-star	$m$	$a$ ["]	$\epsilon$
S0-2	7	$0.123 \pm 0.001$	$0.880 \pm 0.003$
S0-38	7	$0.139 \pm 0.041$	$0.802 \pm 0.041$
S0-21	9	$0.213 \pm 0.041$	$0.784 \pm 0.028$
S0-5	10	$0.250 \pm 0.042$	$0.842 \pm 0.017$
S0-14	10	$0.256 \pm 0.010$	$0.963 \pm 0.006$
S0-18	10	$0.265 \pm 0.080$	$0.759 \pm 0.052$
S0-9	11	$0.293 \pm 0.050$	$0.825 \pm 0.020$
S0-13	11	$0.297 \pm 0.012$	$0.490 \pm 0.023$
S0-4	11	$0.298 \pm 0.019$	$0.406 \pm 0.022$
S0-31	11	$0.298 \pm 0.044$	$0.934 \pm 0.007$
S0-12	11	$0.308 \pm 0.008$	$0.900 \pm 0.003$
S0-17	11	$0.311 \pm 0.004$	$0.364 \pm 0.015$
S0-29	13	$0.397 \pm 0.335$	$0.916 \pm 0.048$
S0-33	13	$0.410 \pm 0.088$	$0.731 \pm 0.039$
S0-8	13	$0.411 \pm 0.004$	$0.824 \pm 0.014$
S0-6	14	$0.436 \pm 0.153$	$0.886 \pm 0.026$
S0-27	14	$0.454 \pm 0.078$	$0.952 \pm 0.006$
S0-1	15	$0.508 \pm 0.028$	$0.496 \pm 0.028$
S0-19	18	$0.798 \pm 0.064$	$0.844 \pm 0.062$
S0-24	21	$1.060 \pm 0.178$	$0.933 \pm 0.010$
S0-71	21	$1.061 \pm 0.765$	$0.844 \pm 0.075$
S0-67	21	$1.095 \pm 0.102$	$0.368 \pm 0.041$
S0-66	23	$1.210 \pm 0.126$	$0.178 \pm 0.039$
S0-87	23	$1.260 \pm 0.001$	$0.880 \pm 0.003$
S0-96	25	$1.545 \pm 0.209$	$0.131 \pm 0.054$
S0-97	30	$2.186 \pm 0.844$	$0.302 \pm 0.308$
S0-83	34	$2.785 \pm 0.234$	$0.657 \pm 0.096$

Table 1: Galaxy Center S-star orbital parameters.

### 3 Total Angular Momentum

If there exists the BH at the center, from the value of  $H_{BH}$  we calculate the predicted QCM total angular momentum  $L_T$  of this system to be about  $3.35 \times 10^{56}$  kg m<sup>2</sup>/s. The rotating BH can contribute a maximum angular momentum of  $J = GM^2/c$ , about  $1.64 \times 10^{55}$  kg m<sup>2</sup>/s, meaning that the orbiting stars dominate the angular momentum of this system.

Spectroscopic measurements to determine S-star types indicate that their masses lie between 10 and 30 solar masses, so assuming about 100 such stars randomly distributed within 10 times the orbital radius of S0-83, one estimates an average total contribution of about  $1.4 \times 10^{56}$  kg m<sup>2</sup>/s, large enough to accommodate the QCM predicted total angular momentum value. Therefore, most of the system angular momentum is in the orbital motion of the S-stars.

Just how big radially is this gravitationally bound system involving the S-stars according to the QCM fit? Obviously, the angular momentum totals indicate that this gravitationally bound system does not extend significantly into the Galactic bulge, otherwise, the system's predicted  $H$  value will increase by many orders of magnitude with increases in radial dis-

tance. The Preston gravitational distance for the Galaxy,  $H_{Gal} = 1.2 \times 10^{17}$  meters, may be the partition distance between this nearly isolated inner system and the rest of the Galaxy.

Therefore, this S-star system behaves as a nearly isolated system obeying QCM in the larger system called the Galaxy (or perhaps the Galaxy Bulge). Such QCM smaller systems within larger QCM systems already exist in the Solar System, e.g., the satellite systems of the planets [2], including the Jovian systems and the moons of Pluto [6]. Our Solar System [6] is a QCM system out on one spiral arm of the Galaxy, which is itself a QCM system requiring a different metric [4]. This hierarchy of QCM systems even applies to clusters of galaxies [7] and the Universe [8].

### 4 Final Comments

QCM predicts the orbital angular momentum quantization exhibited by the 27 S-stars nearest the Galactic Center. The result does not disagree with the proposed black hole mass of about 4.3 million solar masses there. The consequence is that the S-stars seem to be in their own nearly isolated QCM gravitationally bound system within the larger system of the Galaxy and the Galaxy bulge.

### Acknowledgements

Generous support from Sciencegems.com is deeply appreciated.

Submitted on September 04, 2012 / Accepted on September 07, 2012

### References

1. Ghez A. M., Salim S., Hornstein S. D., Tanner A., Lu J. R., Morris M., Becklin E. E., Duchêne G. Stellar Orbits around the Galactic Center Black Hole. *The Astrophysical Journal*, 2005, v. 620 (2), 744–757. arXiv: astro-ph/0306130.
2. Preston H. P., Potter F. Exploring Large-scale Gravitational Quantization without h-bar in Planetary Systems, Galaxies, and the Universe. arXiv: gr-qc/030311v1.
3. Potter F., Preston H. G. Quantum Celestial Mechanics: large-scale gravitational quantization states in galaxies and the Universe. *1st Crisis in Cosmology Conference: CCC-I*, Lerner E. J. and Almeida J. B., eds., AIP CP822, 2006, 239–252.
4. Potter F., Preston H. G. Gravitational Lensing by Galaxy Quantization States. arXiv: gr-qc/0405025v1.
5. Gillessen S., Eisenhauer F., Trippe S., Alexander T., Genzel R., Martins F., Ott T. Monitoring Stellar Orbits around the Massive Black Hole in the Galactic Center. arXiv: 0810.4674v1.
6. Potter F. Pluto Moons exhibit Orbital Angular Momentum Quantization per Mass. *Progress in Physics*, 2012, v. 4, 3–4.
7. Potter F., Preston H. G. Quantization State of Baryonic Mass in Clusters of Galaxies. *Progress in Physics*, 2007, v. 1, 61–63.
8. Potter F., Preston H. G. Cosmological Redshift Interpreted as Gravitational Redshift. *Progress in Physics*, 2007, v. 2, 31–33.

# Does the Equivalence between Gravitational Mass and Energy Survive for a Quantum Body?

Andrei G. Lebed

Department of Physics, University of Arizona, 1118 E. 4th Street, Tucson, AZ 85721, USA. E-mail: lebed@physics.arizona.edu

We consider the simplest quantum composite body, a hydrogen atom, in the presence of a weak external gravitational field. We show that passive gravitational mass operator of the atom in the post-Newtonian approximation of general relativity does not commute with its energy operator, taken in the absence of the field. Nevertheless, the equivalence between the expectations values of passive gravitational mass and energy is shown to survive at a macroscopic level for stationary quantum states. Breakdown of the equivalence between passive gravitational mass and energy at a microscopic level for stationary quantum states can be experimentally detected by studying unusual electromagnetic radiation, emitted by the atoms, supported and moved in the Earth gravitational field with constant velocity, using spacecraft or satellite.

## 1 Introduction

Formulation of a successful quantum gravitation theory is considered to be one of the most important problems in modern physics and the major step towards the so-called “Theory of Everything”. On the other hand, fundamentals of general relativity and quantum mechanics are so different that there is a possibility that it will not be possible to unite these two theories in a feasible future. In this difficult situation, it seems to be important to suggest a combination of quantum mechanics and some non-trivial approximation of general relativity. In particular, this is important in the case where such theory can be experimentally tested. To the best of our knowledge, so far only quantum variant of the trivial Newtonian approximation of general relativity has been tested experimentally in the famous COW [1] and ILL [2] experiments. As to such important and nontrivial quantum effects in general relativity as the Hawking radiation [3] and the Unruh effect [4], they are still very far from their direct and unequivocal experimental confirmations.

The notion of gravitational mass of a composite body is known to be non-trivial in general relativity and related to the following paradoxes. If we consider a free photon with energy  $E$  and apply to it the so-called Tolman formula for gravitational mass [5], we will obtain  $m^g = 2E/c^2$  (i.e., two times bigger value than the expected one) [6]. If a photon is confined in a box with mirrors, then we have a composite body at rest. In this case, as shown in Ref. [6], we have to take into account a negative contribution to  $m^g$  from stress in the box walls to restore the Einstein equation,  $m^g = E/c^2$ . It is important that the later equation is restored only after averaging over time. A role of the classical virial theorem in establishing of the equivalence between averaged over time gravitational mass and energy is discussed in detail in Refs. [7, 8] for different types of classical composite bodies. In particular, for electrostatically bound two bodies with bare masses  $m_1$  and

$m_2$ , it is shown that gravitational field is coupled to a combination  $3K + 2U$ , where  $K$  is kinetic energy,  $U$  is the Coulomb potential energy. Since the classical virial theorem states that the following time average is equal to zero,  $\langle 2K + U \rangle_t = 0$ , then we conclude that averaged over time gravitational mass is proportional to the total amount of energy [7, 8]:

$$\langle m^g \rangle_t = m_1 + m_2 + \langle 3K + 2U \rangle_t / c^2 = E/c^2. \quad (1)$$

## 2 Goal

The main goal of our paper is to study a quantum problem about passive gravitational mass of a composite body. As the simplest example, we consider a hydrogen atom in the Earth gravitational field, where we take into account only kinetic and Coulomb potential energies of an electron in a curved spacetime. We claim three main results in the paper (see also Refs. [9, 10]). Our first result is that the equivalence between passive gravitational mass and energy in the absence of gravitational field survives at a macroscopic level in a quantum case. More strictly speaking, we show that the expectation value of the mass is equal to  $E/c^2$  for stationary quantum states due to the quantum virial theorem. Our second result is a breakdown of the equivalence between passive gravitational mass and energy at a microscopic level for stationary quantum states due to the fact that the mass operator does not commute with energy operator, taken in the absence of gravitational field. As a result, there exist a non-zero probability that a measurement of passive gravitational mass gives value, which is different from  $E/c^2$ , given by the Einstein equation. Our third result is a suggestion of a realistic experiment to detect this inequivalence by measurements of electromagnetic radiation, emitted by a macroscopic ensemble of hydrogen atoms, supported and moved in the Earth gravitational field, using spacecraft or satellite.

### 3 Gravitational Mass in Classical Physics

Below, we derive the Lagrangian and Hamiltonian of a hydrogen atom in the Earth gravitational field, taking into account couplings of kinetic and potential Coulomb energies of an electron with a weak centrosymmetric gravitational field. Note that we keep only terms of the order of  $1/c^2$  and disregard magnetic force, radiation of both electromagnetic and gravitational waves as well as all tidal and spin dependent effects. Let us write the interval in the Earth centrosymmetric gravitational field, using the so-called weak field approximation [11]:

$$ds^2 = -\left(1+2\frac{\phi}{c^2}\right)(cdt)^2 + \left(1-2\frac{\phi}{c^2}\right)(dx^2 + dy^2 + dz^2), \quad (2)$$

$$\phi = -\frac{GM}{R},$$

where  $G$  is the gravitational constant,  $c$  is the velocity of light,  $M$  is the Earth mass,  $R$  is a distance between a center of the Earth and a center of mass of a hydrogen atom (i.e., proton). We pay attention that to calculate the Lagrangian (and later — the Hamiltonian) in a linear with respect to a small parameter  $\phi(R)/c^2$  approximation, we do not need to keep the terms of the order of  $[\phi(R)/c^2]^2$  in metric (2), in contrast to the perihelion orbit procession calculations [11].

Then, in the local proper spacetime coordinates,

$$\begin{aligned} x' &= \left(1 - \frac{\phi}{c^2}\right)x, & y' &= \left(1 - \frac{\phi}{c^2}\right)y, \\ z' &= \left(1 - \frac{\phi}{c^2}\right)z, & t' &= \left(1 + \frac{\phi}{c^2}\right)t, \end{aligned} \quad (3)$$

the classical Lagrangian and action of an electron in a hydrogen atom have the following standard forms:

$$L' = -m_e c^2 + \frac{1}{2}m_e(\mathbf{v}')^2 + \frac{e^2}{r'}, \quad S' = \int L' dt', \quad (4)$$

where  $m_e$  is the bare electron mass,  $e$  and  $\mathbf{v}'$  are the electron charge and velocity, respectively;  $r'$  is a distance between electron and proton. It is possible to show that the Lagrangian (4) can be rewritten in coordinates  $(x, y, z, t)$  as

$$L = -m_e c^2 + \frac{1}{2}m_e \mathbf{v}^2 + \frac{e^2}{r} - m_e \phi - \left(3m_e \frac{\mathbf{v}^2}{2} - 2\frac{e^2}{r}\right) \frac{\phi}{c^2}. \quad (5)$$

Let us calculate the Hamiltonian, corresponding to the Lagrangian (5), by means of a standard procedure,  $H(\mathbf{p}, \mathbf{r}) = \mathbf{p}\mathbf{v} - L(\mathbf{v}, \mathbf{r})$ , where  $\mathbf{p} = \partial L(\mathbf{v}, \mathbf{r})/\partial \mathbf{v}$ . As a result, we obtain:

$$H = m_e c^2 + \frac{\mathbf{p}^2}{2m_e} - \frac{e^2}{r} + m_e \phi + \left(3\frac{\mathbf{p}^2}{2m_e} - 2\frac{e^2}{r}\right) \frac{\phi}{c^2}, \quad (6)$$

where canonical momentum in a gravitational field is  $\mathbf{p} = m_e \mathbf{v}(1 - 3\phi/c^2)$ . [Note that, in the paper, we disregard all

tidal effects (i.e., we do not differentiate gravitational potential with respect to electron coordinates,  $\mathbf{r}$  and  $\mathbf{r}'$ , corresponding to a position of an electron in the center of mass coordinate system). It is possible to show that this means that we consider the atom as a point-like body and disregard all effects of the order of  $|\phi/c^2|(r_B/R) \sim 10^{-26}$ , where  $r_B$  is the Bohr radius (i.e., a typical size of the atom).] From the Hamiltonian (6), averaged over time electron passive gravitational mass,  $\langle m_e^g \rangle_t$ , defined as its weight in a weak centrosymmetric gravitational field (2), can be expressed as

$$\begin{aligned} \langle m_e^g \rangle_t &= m_e + \left\langle \frac{\mathbf{p}^2}{2m_e} - \frac{e^2}{r} \right\rangle_t \frac{1}{c^2} + \left\langle 2\frac{\mathbf{p}^2}{2m_e} - \frac{e^2}{r} \right\rangle_t \frac{1}{c^2} \\ &= m_e + \frac{E}{c^2}, \end{aligned} \quad (7)$$

where  $E = \mathbf{p}^2/2m_e - e^2/r$  is an electron energy. We pay attention that averaged over time third term in Eq. (7) is equal to zero due to the classical virial theorem. Thus, we conclude that in classical physics averaged over time passive gravitational mass of a composite body is equivalent to its energy, taken in the absence of gravitational field [7, 8].

### 4 Gravitational Mass in Quantum Physics

The Hamiltonian (6) can be quantized by substituting a momentum operator,  $\hat{\mathbf{p}} = -i\hbar\partial/\partial\mathbf{r}$ , instead of canonical momentum,  $\mathbf{p}$ . It is convenient to write the quantized Hamiltonian in the following form:

$$\hat{H} = m_e c^2 + \frac{\hat{\mathbf{p}}^2}{2m_e} - \frac{e^2}{r} + \hat{m}_e^g \phi, \quad (8)$$

where we introduce passive gravitational mass operator of an electron to be proportional to its weight operator in a weak centrosymmetric gravitational field (2),

$$\hat{m}_e^g = m_e + \left(\frac{\hat{\mathbf{p}}^2}{2m_e} - \frac{e^2}{r}\right) \frac{1}{c^2} + \left(2\frac{\hat{\mathbf{p}}^2}{2m_e} - \frac{e^2}{r}\right) \frac{1}{c^2}. \quad (9)$$

Note that the first term in Eq. (9) corresponds to the bare electron mass,  $m_e$ , the second term corresponds to the expected electron energy contribution to the mass operator, whereas the third nontrivial term is the virial contribution to the mass operator. It is important that the operator (9) does not commute with electron energy operator, taken in the absence of the field. It is possible to show that Eqs. (8), (9) can be also obtained directly from the Dirac equation in a curved spacetime, corresponding to a weak centrosymmetric gravitational field (2). For example, the Hamiltonian (8), (9) can be obtained [9, 10] from the Hamiltonian (3.24) of Ref. [12], where different physical problem is considered, by omitting all tidal terms.

Below, we discuss some consequences of Eq. (9). Suppose that we have a macroscopic ensemble of hydrogen atoms with each of them being in a ground state with energy  $E_1$ .

Then, as follows from Eq. (9), the expectation value of the gravitational mass operator per one electron is

$$\langle \hat{m}_e^g \rangle = m_e + \frac{E_1}{c^2} + \left\langle 2 \frac{\hat{\mathbf{p}}^2}{2m_e} - \frac{e^2}{r} \right\rangle \frac{1}{c^2} = m_e + \frac{E_1}{c^2}, \quad (10)$$

where the third term in Eq. (10) is zero in accordance with the quantum virial theorem [13]. Therefore, we conclude that the equivalence between passive gravitational mass and energy in the absence of gravitational field survives at a macroscopic level for stationary quantum states.

Let us discuss how Eqs. (8), (9) break the equivalence between passive gravitational mass and energy at a microscopic level. First of all, we recall that the mass operator (9) does not commute with electron energy operator, taken in the absence of gravitational field. This means that, if we create a quantum state of a hydrogen atom with definite energy, it will not be characterized by definite passive gravitational mass. In other words, a measurement of the mass in such quantum state may give different values, which, as shown, are quantized. Here, we illustrate the above mentioned inequivalence, using the following thought experiment. Suppose that at  $t = 0$  we create a ground state wave function of a hydrogen atom, corresponding to the absence of gravitational field,

$$\Psi_1(r, t) = \Psi_1(r) \exp(-iE_1 t / \hbar). \quad (11)$$

In a weak centrosymmetric gravitational field (2), wave function (11) is not anymore a ground state of the Hamiltonian (8), (9), where we treat gravitational field as a small perturbation in an inertial system [7–12]. It is important that for inertial observer, in accordance with Eq. (3), a general solution of the Schrodinger equation, corresponding to the Hamiltonian (8), (9), can be written as

$$\begin{aligned} \Psi(r, t) &= (1 - \phi/c^2)^{3/2} \sum_{n=1}^{\infty} a_n \Psi_n[(1 - \phi/c^2)r] \\ &\times \exp[-im_e c^2(1 + \phi/c^2)t/\hbar] \\ &\times \exp[-iE_n(1 + \phi/c^2)t/\hbar]. \end{aligned} \quad (12)$$

We pay attention that wave function (12) is a series of eigenfunctions of passive gravitational mass operator (9), if we take into account only linear terms with respect to the parameter  $\phi/c^2$ . Here, factor  $1 - \phi/c^2$  is due to a curvature of space, whereas the term  $E_n(1 + \phi/c^2)$  represents the famous red shift in gravitational field and is due to a curvature of time.  $\Psi_n(r)$  is a normalized wave function of an electron in a hydrogen atom in the absence of gravitational field, corresponding to energy  $E_n$ . [Note that, due to symmetry of our problem, an electron from  $1S$  ground state of a hydrogen atom can be excited only into  $nS$  excited states. We also pay attention that the wave function (12) contains a normalization factor  $(1 - \phi/c^2)^{3/2}$ .]

In accordance with the basic principles of the quantum mechanics, probability that, at  $t > 0$ , an electron occupies excited state with energy  $m_e c^2(1 + \phi/c^2) + E_n(1 + \phi/c^2)$  is

$$\begin{aligned} P_n &= |a_n|^2, \\ a_n &= \int \Psi_1^*(r) \Psi_n[(1 - \phi/c^2)r] d^3 \mathbf{r} \\ &= -(\phi/c^2) \int \Psi_1^*(r) r \Psi_n'(r) d^3 \mathbf{r}. \end{aligned} \quad (13)$$

Note that it is possible to demonstrate that for  $a_1$  in Eq. (13) a linear term with respect to gravitational potential,  $\phi$ , is zero, which is a consequence of the quantum virial theorem. Taking into account that the Hamiltonian is a Hermitian operator, it is possible to show that for  $n \neq 1$ :

$$\begin{aligned} \int \Psi_1^*(r) r \Psi_n'(r) d^3 \mathbf{r} &= \frac{V_{n,1}}{\hbar \omega_{n,1}}, \\ \hbar \omega_{n,1} &= E_n - E_1, \quad n \neq 1, \end{aligned} \quad (14)$$

where  $V_{n,1}$  is a matrix element of the virial operator,

$$V_{n,1} = \int \Psi_1^*(r) \hat{V}(r) \Psi_n(r) d^3 \mathbf{r}, \quad \hat{V}(r) = 2 \frac{\hat{\mathbf{p}}^2}{2m_e} - \frac{e^2}{r}. \quad (15)$$

It is important that, since the virial operator (15) does not commute with the Hamiltonian, taken in the absence of gravitational field, the probabilities (13)–(15) are not equal to zero for  $n \neq 1$ .

Let us discuss Eqs. (12)–(15). We pay attention that they directly demonstrate that there is a finite probability,

$$P_n = |a_n|^2 = \left( \frac{\phi}{c^2} \right)^2 \left( \frac{V_{n,1}}{E_n - E_1} \right)^2, \quad n \neq 1, \quad (16)$$

that, at  $t > 0$ , an electron occupies  $n$ -th ( $n \neq 1$ ) energy level, which breaks the expected Einstein equation,  $m_e^g = m_e + E_1/c^2$ . In fact, this means that measurement of passive gravitational mass (i.e., weight in the gravitational field (2)) in a quantum state with a definite energy (11) gives the following quantized values:

$$m_e^g(n) = m_e + E_n/c^2, \quad (17)$$

corresponding to the probabilities (16). [Note that, as it follows from quantum mechanics, we have to calculate wave function (12) in a linear approximation with respect to the parameter  $\phi/c^2$  to obtain probabilities (16), (22), (23), which are proportional to  $(\phi/c^2)^2$ . A simple analysis shows that an account in Eq. (12) terms of the order of  $(\phi/c^2)^2$  would change electron passive gravitational mass of the order of  $(\phi/c^2)m_e \sim 10^{-9}m_e$ , which is much smaller than the distance between the quantized values (17),  $\delta m_e^g \sim \alpha^2 m_e \sim 10^{-4}m_e$ , where  $\alpha$  is the fine structure constant.] We also point out that, although the probabilities (16) are quadratic with respect to gravitational potential and, thus, small, the changes of the

passive gravitational mass (17) are large and of the order of  $\alpha^2 m_e$ . We also pay attention that small values of probabilities (16),  $P_n \sim 10^{-18}$ , do not contradict the existing Eötvös type measurements [11], which have confirmed the equivalence principle with the accuracy of the order of  $10^{-12}$ - $10^{-13}$ . For our case, it is crucial that the excited levels of a hydrogen atom spontaneously decay with time, therefore, one can detect the quantization law (17) by measuring electromagnetic radiation, emitted by a macroscopic ensemble of hydrogen atoms. The above mentioned optical method is much more sensitive than the Eötvös type measurements and we, therefore, hope that it allows to detect the breakdown of the equivalence between energy and passive gravitational mass, revealed in the paper.

## 5 Suggested Experiment

Here, we describe a realistic experiment [9, 10]. We consider a hydrogen atom to be in its ground state at  $t = 0$  and located at distance  $R'$  from a center of the Earth. The corresponding wave function can be written as

$$\begin{aligned} \tilde{\Psi}_1(r, t) &= (1 - 2\phi')^{3/2} \Psi_1[(1 - \phi'/c^2)r] \\ &\times \exp[-im_e c^2(1 + \phi'/c^2)t/\hbar] \\ &\times \exp[-iE_1(1 + \phi'/c^2)t/\hbar], \end{aligned} \quad (18)$$

where  $\phi' = \phi(R')$ . The atom is supported in the Earth gravitational field and moved from the Earth with constant velocity,  $v \ll ac$ , by spacecraft or satellite. As follows from Ref. [7], the extra contributions to the Lagrangian (5) are small in this case in an inertial system, related to a center of mass of a hydrogen atom (i.e., proton). Therefore, electron wave function and time dependent perturbation for the Hamiltonian (8), (9) in this inertial coordinate system can be expressed as

$$\begin{aligned} \tilde{\Psi}(r, t) &= (1 - 2\phi')^{3/2} \sum_{n=1}^{\infty} \tilde{a}_n(t) \Psi_n[(1 - \phi'/c^2)r] \\ &\times \exp[-im_e c^2(1 + \phi'/c^2)t/\hbar] \\ &\times \exp[-iE_n(1 + \phi'/c^2)t/\hbar], \end{aligned} \quad (19)$$

$$\hat{U}(\mathbf{r}, t) = \frac{\phi(R' + vt) - \phi(R')}{c^2} \left( 3 \frac{\hat{\mathbf{p}}^2}{2m_e} - 2 \frac{e^2}{r} \right). \quad (20)$$

We pay attention that in a spacecraft (satellite), which moves with constant velocity, gravitational force, which acts on each hydrogen atom, is compensated by some non-gravitational forces. This causes very small changes of a hydrogen atom energy levels and is not important for our calculations. Therefore, the atoms do not feel directly gravitational acceleration,  $\mathbf{g}$ , but feel, instead, gravitational potential,  $\phi(R' + vt)$ , changing with time due to a spacecraft (satellite) motion in the Earth gravitational field. Application of

the time-dependent quantum mechanical perturbation theory gives the following solutions for functions  $\tilde{a}_n(t)$  in Eq. (19):

$$\tilde{a}_n(t) = \frac{\phi(R' + vt) - \phi(R')}{c^2} \frac{V_{n,1}}{\hbar\omega_{n,1}} \exp(i\omega_{n,1}t), \quad n \neq 1, \quad (21)$$

where  $V_{n,1}$  and  $\omega_{n,1}$  are given by Eqs. (14), (15);  $\omega_{n,1} \gg v/R'$ .

It is important that, if excited levels of a hydrogen atom were strictly stationary, then a probability to find the passive gravitational mass to be quantized with  $n \neq 1$  (17) would be

$$\tilde{P}_n(t) = \left( \frac{V_{n,1}}{\hbar\omega_{n,1}} \right)^2 \frac{[\phi(R' + vt) - \phi(R')]^2}{c^4}, \quad n \neq 1. \quad (22)$$

In reality, the excited levels spontaneously decay with time and, therefore, it is possible to observe the quantization law (17) indirectly by measuring electromagnetic radiation from a macroscopic ensemble of the atoms. In this case, Eq. (22) gives a probability that a hydrogen atom emits a photon with frequency  $\omega_{n,1} = (E_n - E_1)/\hbar$  during the time interval  $t$ . [We note that dipole matrix elements for  $nS \rightarrow 1S$  quantum transitions are zero. Nevertheless, the corresponding photons can be emitted due to quadrupole effects.]

Let us estimate the probability (22). If the experiment is done by using spacecraft or satellite, then we may have  $|\phi(R' + vt)| \ll |\phi(R')|$ . In this case Eq. (22) is reduced to Eq. (16) and can be rewritten as

$$\tilde{P}_n = \left( \frac{V_{n,1}}{E_n - E_1} \right)^2 \frac{\phi^2(R')}{c^4} \approx 0.49 \times 10^{-18} \left( \frac{V_{n,1}}{E_n - E_1} \right)^2, \quad (23)$$

where, in Eq. (23), we use the following numerical values of the Earth mass,  $M \approx 6 \times 10^{24}$  kg, and its radius,  $R_0 \approx 6.36 \times 10^6$  m. It is important that, although the probabilities (23) are small, the number of photons,  $N$ , emitted by macroscopic ensemble of the atoms, can be large since the factor  $V_{n,1}^2/(E_n - E_1)^2$  is of the order of unity. For instance, for 1000 moles of hydrogen atoms,  $N$  is estimated as

$$N_{n,1} = 2.95 \times 10^8 \left( \frac{V_{n,1}}{E_n - E_1} \right)^2, \quad N_{2,1} = 0.9 \times 10^8, \quad (24)$$

which can be experimentally detected, where  $N_{n,1}$  stands for a number of photons, emitted with energy  $\hbar\omega_{n,1} = E_n - E_1$ .

## 6 Summary

To summarize, we have demonstrated that passive gravitational mass of a composite quantum body is not equivalent to its energy due to quantum fluctuations, if the mass is defined to be proportional to a weight of the body. We have also discussed a realistic experimental method to detect this inequivalency. If the corresponding experiment is done, to the best of our knowledge, it will be the first experiment, which directly tests some nontrivial combination of general relativity and quantum mechanics. We have also shown that

the corresponding expectation values are equivalent to each other for stationary quantum states. It is important that our results are due to different couplings of kinetic and potential energy with an external gravitational field. Therefore, the current approach is completely different from that discussed in Refs. [12, 14, 15], where small corrections to electron energy levels are calculated for a free falling hydrogen atom [14, 15] or for a hydrogen atom supported in a gravitational field [12]. Note that phenomena suggested in the paper are not restricted by atomic physics, but also have to be observed in solid state, nuclear, and particle physics.

### Acknowledgements

We are thankful to N. N. Bagmet (Lebed), V. A. Belinski, and Li-Zhi Fang for useful discussions. This work was supported by the NSF under Grant DMR-1104512.

Submitted on September 04, 2012 / Accepted on September 07, 2012

### References

1. Colella R., Overhauser A. W., Werner S. A. Observation of gravitationally induced quantum interference. *Physical Review Letters*, 1975, v. 34 (23), 1472–1474.
2. Nesvizhevsky V. V., Borner H. G., Petukhov A. K., Abele H., Baebler S., Rueb F. J., Stoferle Th., Westphal A., Gagarski A. M., Petrov G. A., Strelkov A. V. Quantum states of neutrons in the Earth's gravitational field. *Nature*, 2002, v. 415 (January 17), 297–299.
3. Hawking S. W. Black hole explosions? *Nature*, 1974, v. 248 (March 1), 30–31.
4. Unruh W. G. Notes on black-hole evaporation. *Physical Review D*, 1976, v. 14 (4), 870–892.
5. Landau L. D., Lifshitz E. M. *The Classical Theory of Fields*. Butterworth-Heinemann, Amsterdam, 2003.
6. Misner C. W., Putnam P. Active Gravitational Mass. *Physical Review*, 1959, v. 116 (4), 1045–1046.
7. Nordtvedt K. Post-Newtonian gravity: its theory-experiment interference. *Classical and Quantum Gravity*, 1994, v. 11, A119–A132.
8. Carlip S. Kinetic energy and the equivalence principle. *American Journal of Physics*, 1998, v. 66 (5), 409–413.
9. Lebed A. G. Is Gravitational Mass of a Composite Quantum Body Equivalent to its Energy? arXiv: gr-qc/1111.5365v1; Breakdown of the Equivalence between Energy Content and Weight in a Weak Gravitational Field for a Quantum Body. arXiv: gr-qc/1205.3134v1.
10. Lebed A. G. "Breakdown of the Equivalence between Passive Gravitational Mass and Energy for a Quantum Body", in the Proceedings of the 13th Marcel Grossmann Meeting on Recent Developments in Theoretical and Experimental General Relativity, to be published. arXiv: gr-qc/1208.5756v1.
11. Misner C. W., Thorne K. S., Wheeler J. A. *Gravitation*. W. H. Freeman and Co, San Francisco, 1973.
12. Fischbach E., Freeman B. S., Cheng W. K. General-relativistic effects in hydrogenic systems. *Physical Review D*, 1981, v. 23 (10), 2157–2180.
13. Park D. *Introduction to the Quantum Theory*. Dover Publications, New York, 2005.
14. Pinto F. Rydberg Atoms in Curved Space-Time. *Physical Review Letters*, 1993, v. 70 (25), 3839–3843.
15. Parker L. One-Electron Atom in Curved Space-Time. *Physical Review Letters*, 1980, v. 44 (23), 1559–1562.

## Genesis of the “Critical-Acceleration of MOND” and Its Role in “Formation of Structures”

Hasmukh K. Tank

Indian Space Research Organization, 22/693, Krishna Dham-2, Vejalpur, Ahmedabad-380015, India  
E-mail: tank.hasmukh@rediffmail.com, hasmukh.tank1@gmail.com

As an attempt to explain the “flattening of galaxies rotation-curves”, Milgrom proposed a Modification of Newtonian Dynamics MOND, in which he needed a new constant of nature  $a_0$ , termed as “critical-acceleration-of MOND”, in his best-fit empirical formula. But so far it has been an ad-hoc introduction of a new constant. Whereas this article proposes: (i) a genesis of this constant; (ii) explains its recurrences in various physical situations; and (iii) its role in determining the size and radii of various structures, like: the electron, the proton, the nucleus-of-atom, the globular-clusters, the spiral-galaxies, the galactic-clusters and the whole universe. In this process we get a new interpretation of “the cosmological-red-shift”, that the linear part of the cosmological-red-shift may not be due to “metric-expansion-of-space”; and even the currently-believed “accelerated-expansion” may be slowing down with time.

### 1 Introduction

The observations of “flattening of galaxies rotation curves” are generally explained by assuming the presence of “dark-matter”, but there is no way to directly detect it other than its presumed gravitational effect. M. Milgrom [1] proposed an alternative explanation for the “galaxies rotation curves”, by modifying Newton’s law of gravitation, for which he needed an ad-hoc introduction of a new constant of nature  $a_0$ , termed as “critical-acceleration of MOND”, of the order of magnitude:  $1.2 \times 10^{-10}$  meter per seconds squared. But so far it has been an ad-hoc introduction of a new constant; and there has been no explanation for why its value is this much. Sivaram noticed its recurrences in various physical situations. This author has been of the opinion that the matching of values of the “anomalous decelerations of the four space-probes”: Pioneer-10, Pioneer-11, Galileo and Ulysses and the “deceleration of cosmologically-red-shifting-photons” can not be an accidental coincidence. Now, this article presents a genesis of this “critical-acceleration of MOND”. And based on this genesis, the formation of various structures, like the electron, the proton, the nucleus-of-atom, the globular-clusters, the spiral-galaxies, the galactic-clusters and the whole universe, are explained here.

### 2 Genesis of the “critical acceleration of MOND”

R.K. Adair, in his book “Concepts in Physics” [2] has given a derivation, that the sum of “gravitational-potential-energy” and “energy-of-mass” of the whole universe is, strikingly, zero! i.e.

$$M_0 c^2 - \frac{GM_0 M_0}{R_0} = 0 \quad (1)$$

where  $M_0$  and  $R_0$  are total-mass and radius of the universe respectively, and  $G$  is Newton’s gravitational constant; i.e.

$$\frac{GM_0 m}{R_0} = mc^2. \quad (2)$$

Where  $m$  is mass of any piece of matter. That is, the relativistic-energy of any piece of matter of mass  $m$  is equal to its “cosmic-gravitational-potential-energy”. So the “cosmic-gravitational-force” experienced by every piece of matter is:

$$\frac{GM_0 m}{R_0^2} = m \frac{c^2}{R_0}. \quad (3)$$

We know that  $R_0 H_0 = c$ , so,  $R_0 = c/H_0$ . Here  $H_0$  is Hubble’s constant; i.e.

$$\frac{GM_0 m}{R_0^2} = m H_0 c \quad (4)$$

where  $m$  is mass of any object; and  $H_0 c$  is a “cosmic-constant-of-acceleration”.  $H_0 c = 6.87 \times 10^{-10}$  meter/second<sup>2</sup>. In the next section we will see the recurrences of this “cosmic-constant-of-acceleration” in various physical situations.

### 3 Observable recurrences of “the cosmic-constant-of-acceleration”

Inter-galactic-photons experience the “cosmological red-shift”. We can express the cosmological red-shift  $z_c$  in terms of de-acceleration experienced by the photon [3, 4], as follows:

$$z_c = \frac{f_0 - f}{f} = \frac{H_0 D}{c}$$

i.e.

$$\frac{h \Delta f}{hf} = \frac{H_0 D}{c}$$

i.e.

$$h \Delta f = \frac{hf}{c^2} (H_0 c) D. \quad (5)$$

Here:  $h$  is Planck’s constant,  $f_0$  is frequency of photon at the time of its emission,  $f$  is the red-shifted frequency measured on earth,  $H_0$  is Hubble’s constant, and  $D$  the luminosity-distance.

That is, the loss in energy of the photon is equal to its mass ( $hf/c^2$ ) times the acceleration  $a = H_0c$ , times the distance  $D$  travelled by it. Where:  $H_0$  is Hubble-parameter. And the value of constant acceleration  $a$  is:  $a = H_0c$ ,  $a = 6.87 \times 10^{-10}$  meter/sec<sup>2</sup>.

Now, we will verify that the accelerations experienced by the Pioneer-10, Pioneer-11, Galileo and Ulysses space-probes do match significantly with the “cosmic-constant-of-acceleration”. Slightly higher value of decelerations of the space-probes is then explained.

Carefully observed values of de-accelerations [5]:

For Pioneer-10:

$$a = (8.09 \pm 0.2) \times 10^{-10} \text{ m/s}^2 = H_0c. \quad (6)$$

For Pioneer-11:

$$a = (8.56 \pm 0.15) \times 10^{-10} \text{ m/s}^2 = H_0c. \quad (7)$$

For Ulysses:

$$a = (12 \pm 3) \times 10^{-10} \text{ m/s}^2 = H_0c. \quad (8)$$

For Galileo:

$$a = (8 \pm 3) \times 10^{-10} \text{ m/s}^2 = H_0c. \quad (9)$$

For Cosmologically-red-shifted-photon,

$$a = 6.87 \times 10^{-10} \text{ m/s}^2 = H_0c. \quad (10)$$

This value of acceleration is also the “critical acceleration” of modified Newtonian dynamics MOND,

$$a_0 = H_0c \quad (11)$$

and the rate of “accelerated-expansion of the universe”

$$a_{exp} = H_0c. \quad (12)$$

According to Weinberg, mass of a fundamental-particle can be obtained from the “fundamental-constants” as follows: Mass of a fundamental-particle,

$$m = \left( \frac{h^2 H_0}{cG} \right)^{1/3}$$

i.e.

$$\frac{Gm}{(h/mc)^2} = H_0c. \quad (13)$$

That is, the self-gravitational-acceleration of Weinberg’s [7] “fundamental-particle” is also equal to the “cosmic-constant-of-acceleration”.

**Reason why the apparent value of deceleration of the cosmic-photon is slightly small:**

When the extra-galactic-photon enters our own milky-way-galaxy, the photon also experiences the gravitational-blue-shift, because of the gravitational-pull of our galaxy. The photon of a given frequency, if it has come from a near-by-galaxy, then it gets more blue-shifted, compared to the photon which has come from very-very far-distant-galaxy; so the galaxy which is at closer distance, appears at more closer distance, than the galaxies at far-away-distances. That is, the cosmic photon decelerated during its long inter-galactic-journey, and then accelerated because of the gravitational-pull of our milky-way galaxy; so we measure slightly lesser value of  $H_0$ ;  $H_0c = 6.87 \times 10^{-10}$  meter per seconds squared. But if we could send the Hubble-like Space-Telescope out-side our milky-way-galaxy, then the value of  $H_0c$  will match perfectly with the value of deceleration of all the four space-probes;  $= 8.5 \times 10^{-10}$  meters per seconds squared.

Currently, the whole values of “anomalous accelerations of the space-probes” are “explained” in terms of radiation-pressure, gas-leakage... etc. So here we can explain the slight differences in their values of decelerations in terms of radiation-pressure, gas-leakage etc! Thus, the matching of values of decelerations of all the four space-probes is itself an interesting observation; and its matching with the deceleration of cosmologically-red-shifting-photons can not be ignored by a scientific mind as a coincidence. There is one more interesting thing about the value of this deceleration as first noticed by Milgrom, that: with this value of deceleration, an object moving with the speed of light would come to rest exactly after the time  $T_0$  which is the age of the universe.

#### 4 Formation of structures

Sivaram [6] has noticed that:

$$\begin{aligned} \frac{G M_0}{R_0^2} &= \frac{G m_p}{r_p^2} = \frac{G m_e}{r_e^2} = \frac{G m_n}{r_n^2} \\ &= \frac{G M_{gc}}{R_{gc}^2} = \frac{G M_{gal}}{R_{gal}^2} = \frac{G M_{cg}}{R_{cg}^2} \end{aligned} \quad (14)$$

= the “critical-acceleration” of MOND  
=  $H_0c$ .

(Here:  $M_0$  and  $R_0$  are mass and radius of the universe respectively,  $m_p$  and  $r_p$  are mass and radius of the proton,  $m_e$  and  $r_e$  are mass and radius of the electron,  $m_n$  and  $r_n$  are mass and radius of the nucleus of an atom,  $M_{gc}$  and  $R_{gc}$  are mass and radius of the globular-clusters,  $M_{gal}$  and  $R_{gal}$  are mass and radius of the spiral-galaxies, and  $M_{cg}$  and  $R_{cg}$  are mass and radius of the galactic-clusters respectively).

That is, the self-gravitational-pulling-force experienced by all the above bodies will be: Self-gravitational-force  $F =$  (mass of the body, say a galaxy) times (a constant value of deceleration  $H_0c$ ).

For the formation of a stable structure, the “self-gravitational-acceleration” of a body of mass  $m$  should be equal to

the value of “cosmic-constant-of-acceleration”  $H_0c$ . In the expressions of eq. 14 above we found that: at the “surface” of the electron, the proton, the nucleus-of-atom, the globular-clusters, the spiral-galaxies, and the galactic-clusters this condition is beautifully satisfied. That is:

$$\frac{GM}{R^2} = H_0c. \quad (15)$$

Where  $M$  and  $R$  represent mass and radius of the above objects. And the size and radius of the above structures get decided as follows: i.e.

$$\frac{GM}{R^2} = H_0c = \frac{c^2}{R_0}$$

i.e.

$$R^2 = \frac{GM}{c^2} R_0$$

i.e.

$$R = (r_G R_0)^{1/2} \quad (16)$$

where  $r_G$  is “gravitational-radius” of the above objects. This is how all the structures get formed, beginning from the electron to the galactic-clusters.

## 5 Explanation for the “flattening of galaxies rotation-curves”

As seen in the expression-15, the condition for the formation of a stable structure is:  $GM/R^2 = H_0c$  where  $M$  and  $R$  are mass and radius of a galaxy. That is, the centripetal acceleration at the surface of a structure is:

$$\frac{v^2}{R} = \frac{GM}{R^2} = H_0c \quad (17)$$

i.e.

$$v^2 = RH_0c. \quad (18)$$

Now, by dividing both the sides of the above expression by a distance  $r$  greater than  $R$ , the acceleration towards the center of spiral-galaxy experienced by a star at a distance  $r$  from the center is:

$$\frac{v^2}{r} = \frac{R}{r} H_0c. \quad (19)$$

Where  $r > R$ .

So, the velocity of the stars at the out-skirts of spiral galaxies is:

$$v = \left[ \left( \frac{GM}{c^2} \frac{GM_0}{c^2} \right)^{1/2} a_0 \right]^{1/2} \quad (20)$$

i.e.

$$v = \left[ \left( \frac{GM}{c^2} R_0 \right)^{1/2} \frac{c^2}{R_0} \right]^{1/2} \quad (21)$$

i.e.

$$v = \left[ \frac{M}{M_0} \right]^{1/4} c, \quad (22)$$

a constant velocity. The above expression-22 is equal to Milgrom’s expression:  $(v^2/r) = [(GM/r^2)a_0]^{1/2}$  because  $a_0 = GM_0/R_0^2$ . This is how we can explain the “flattening of galaxies rotation-curves”.

## 6 Conclusion

We presented here the genesis or root of the “critical acceleration of MOND”, that it follows from the equality of “gravitational potential-energy” and “energy-of-mass” of the universe; and showed that there are as many as fifteen physical situations where we find recurrences of this “cosmic-constant-of-acceleration”. The sizes of various structures like the electron, the proton, the nucleus-of-atom, the globular-clusters, the spiral-galaxies, the galactic-clusters and the whole universe get decided based on the condition that: the “self-gravitational-acceleration” of them all should be equal to the “cosmic-constant-of-acceleration”  $H_0c$ . The flattening of galaxies rotation curves at the out skirts of spiral galaxies also emerge from the above-mentioned equality.

We are sure that the space-probes Pioneer-10 et al. did show decelerations of the order  $H_0c$ . Now, similar to the space-probes, if the cosmologically red-shifting photons also decelerate due to the “cosmic-gravitational-force” then the linear part of the cosmological-red-shift may not be due to the “metric-expansion-of-space”; only the recently-discovered accelerated-expansion may be due to the “metric-expansion-of-space”; and its rate  $H_0c$  suggests that even the receding galaxies may be getting decelerated like the space-probes! Thus we may be able to explain even the “accelerated-expansion of the universe” without any need for dark-energy.

Submitted on: September 6, 2012 / Accepted on: September 13, 2012

## References

1. Milgrom M. A modification of the Newtonian dynamics as a possible alternative to the hidden mass hypothesis. *Astrophysical Journal*, 1983, v. 270, 365.
2. Adair R.K. Concepts in Physics. Academic Press, New York, (1969), p. 775.
3. Tank H.K. A new law emerging from the recurrences of the “critical-acceleration” of MOND, suggesting a clue to unification of fundamental forces. *Astrophysics and Space Science*, 2010, v. 330, 203–205.
4. Tank H.K. Some clues to understand MOND and the accelerated expansion of the universe. *Astrophysics and Space Science*, 2011, v. 336, no. 2, 341–343.
5. Anderson J.D., Laing P.A., Lau E.L., Liu A.S., Nieto M.M., and Turyshch, S.G. Indication, from Pioneer 10, 11, Galileo, and Ulysses Data, of an Apparent Anomalous, Weak, Long-Range Acceleration. *Physical Review Letters*, 1998, v. 81, 2858–2861 [(Comment by Katz J.L.: *Physical Review Letters*, 1999, v. 83, 1892; Reply: *Physical Review Letters*, 1999, v. 83, 1893)].
6. Sivaram C. Some aspects of MOND and its consequences for cosmology. *Astrophysics and Space Science*, 1994, v. 215, 185–189.
7. Weinberg S. Gravitation and Cosmology. John Wiley & Sons, (1972), p. 620.

# Identical Bands and $\Delta I = 2$ Staggering in Superdeformed Nuclei in $A \sim 150$ Mass Region Using Three Parameters Rotational Model

A.M. Khalaf\*, M.M. Taha†, and M. Kotb‡

\*Physics Department, Faculty of Science, Al-Azhar University, Cairo, Egypt. E-mail: Profkhalaf@gmail.com

†Mathematics and Theoretical Physics Department, NRC, Atomic Energy Authority, P.No. 13759, Cairo, Egypt. E-mail: mahmoudmt@hotmail.com

‡Physics Department, Faculty of Science, Al-Azhar University, Cairo, Egypt. E-mail: mahmoudkottb@gmail.com

By using a computer simulated search program, the experimental gamma transition energies for superdeformed rotational bands (SDRB's) in  $A \sim 150$  region are fitted to proposed three-parameters model. The model parameters and the spin of the bandhead were obtained for the selected ten SDRB's namely:  $^{150}\text{Gd}$  (yrast and excited SD bands),  $^{151}\text{Tb}$  (yrast and excited SD bands),  $^{152}\text{Dy}$  (yrast SD bands),  $^{148}\text{Gd}$  (SD-1, SD-6),  $^{149}\text{Gd}$  (SD-1),  $^{153}\text{Dy}$  (SD-1) and  $^{148}\text{Eu}$  (SD-1). The Kinematic  $J^{(1)}$  and dynamic  $J^{(2)}$  moments of inertia are studied as a function of the rotational frequency  $\hbar\omega$ . From the calculated results, we notice that the excited SD bands have identical energies to their  $Z+1$  neighbours for the twinned SD bands in  $N=86$  nuclei. Also the analysis done allows us to confirm  $\Delta I = 2$  staggering in the yrast SD bands of  $^{148}\text{Gd}$ ,  $^{149}\text{Gd}$ ,  $^{153}\text{Dy}$ , and  $^{148}\text{Eu}$  and in the excited SD bands of  $^{148}\text{Gd}$ , by performing a staggering parameter analysis. For each band, we calculated the deviation of the gamma ray energies from smooth reference representing the finite difference approximation to the fourth derivative of the gamma ray transition energies at a given spin.

## 1 Introduction

The superdeformed (SD) nuclei is one of the most interesting topics of nuclear structure studies. Over the past two decades, many superdeformed rotational bands (SDRB's) have been observed in several region of nuclear chart [1]. At present although a general understanding of these SDRB's have been achieved, there are still many open problems. For example the spin, parity and excitation energy relative to the ground state of the SD bands have not yet been measured. The difficulty lies with observing the very weak discrete transitions which link SD levels with normal deformed (ND) levels. Until now, only several SD bands have been identified to exist the transition from SD levels to ND levels. Many theoretical approaches to predict the spins of these SD bands have been proposed [2–11].

Several SDRB's in the  $A \sim 150$  region exhibit a rather surprising feature of a  $\Delta I = 2$  staggering [12–25] in its transition energies, *i.e.* sequences of states differing by four units of angular momentum are displaced relative to each other. The phenomenon of  $\Delta I = 2$  staggering has attracted much attention and interest, and has thus become one of the most frequently considerable subjects. Within a short period, a considerable amount of effort has been spent on understanding its physical implication based on various theoretical ideas [9, 26–41]. Despite such efforts, definite conclusions have not yet been reached until present time.

The discovery of the phenomenon of identical bands (IB's) [42, 43] at high spin in SD states in even-even and odd-A nuclei aroused a considerable interest. It was found that the transition energies and moments of inertia in neighboring nuclei much close than expected. This has created much theo-

retical interest [44, 45]. The first interpretation [46] to IB's was done within the framework of the strong coupling limit of the particle-rotor model, in which one or more particles are coupled to a rotating deformed core and follow the rotation adiabatically. Investigation also suggest that the phenomena of IB's may result from a cancelation of contributions to the moment of inertia occurring in mean field method [47].

In the present paper we suggest a three-particle model to predict the spins of the rotational bands and to study the properties of the SDRB's and to investigate the existence of  $\Delta I = 2$  staggering and also investigate the presence of IB's observed in the  $A \sim 150$  mass region.

## 2 Nuclear SDRB's in framework of three parameters rotational model

In the present work, the energies of the SD nuclear RB's  $E(I)$  as a function of the unknown spin  $I$  are expressed as:

$$E(I) = E_0 + a[[1 + b\hat{I}^2]^{1/2} - 1] + c\hat{I}^2 \quad (1)$$

with  $\hat{I}^2 = I(I + 1)$ , where  $a, b$  and  $c$  are the parameters of the model. The rotational frequency  $\hbar\omega$  is defined as the derivative of the energy  $E$  with respect to the angular momentum  $\hat{I}$

$$\begin{aligned} \hbar\omega &= \frac{dE}{d\hat{I}} \\ &= [2c + ab[1 + bI(I + 1)]^{1/2}]I(I + 1)^{-1/2}. \end{aligned} \quad (2)$$

Two possible types of nuclear moments of inertia have been suggested which reflect two different aspects of nuclear dynamics. The kinematic moment of inertia  $J^{(1)}$ , which is

Table 1: The adopted best parameters  $a, b, c$  of the model and the band-head spin assignment  $I_0$  of our ten SDRB's. The rms deviations are also shown.

SD Band	$E\gamma(I+2 \rightarrow I)$ (keV)	$I_0$ ( $\hbar$ )	$a$ (keV)	$b$ (keV)	$c$ (keV)	$\chi$
$^{148}\text{Gd}$ (SD-1)	699.9	31	-0.313446E+07	0.163069E-04	0.311027E+02	7.387009E-01
(SD-6)	802.2	39	-0.106162E+06	0.107495E-03	0.105003E+02	2.104025E-01
$^{150}\text{Gd}$ (SD-1)	815.0	47	-0.148586E+06	-0.517219E-04	0.954401E-01	5.250988E-01
(SD-2)	727.9	31	-0.617154E+06	-0.134929E-04	0.163288E+01	1.734822E+00
$^{152}\text{Dy}$ (SD-1)	602.4	26	-0.144369E+06	0.207972E-04	0.733270E+01	5.217181E-01
$^{149}\text{Gd}$ (SD-1)	617.8	27.5	-0.825976E+05	-0.698261E-04	0.285641E+01	4.559227E-01
$^{148}\text{Eu}$ (SD-1)	747.7	29	-0.131028E+06	0.432608E-04	0.928191E+01	7.010767E-01
$^{151}\text{Tb}$ (SD-1)	726.5	30.5	-0.852833E+06	-0.546382E-05	0.364770E+01	2.023767E+00
(SD-2)	602.1	26.5	-0.136986E+07	-0.431179E-05	0.289128E+01	6.644767E-01
$^{153}\text{Dy}$ (SD-1)	721.4	30.5	-0.671437E+06	-0.386442E-05	0.464507E+01	2.171267E+00

equal to the inverse of the slope of the curve of energy  $E$  versus  $\hat{I}$ :

$$\begin{aligned} J^{(1)} &= \hbar^2 \hat{I} \left( \frac{dE}{d\hat{I}} \right)^{-1} \\ &= \frac{\hbar^2}{ab} [1 + bI(I+1)]^{1/2} + \frac{1}{2c} \end{aligned} \quad (3)$$

and the dynamic moment of inertia  $J^{(2)}$ , which is related to the curvature in the curve of  $E$  versus  $\hat{I}$ :

$$\begin{aligned} J^{(2)} &= \hbar^2 \left( \frac{d^2E}{d\hat{I}^2} \right)^{-1} \\ &= \frac{\hbar^2}{ab} [1 + bI(I+1)]^{3/2} + \frac{1}{2c}. \end{aligned} \quad (4)$$

For the SD bands, one can extract the rotational frequency, dynamic and kinematic moment of inertia by using the experimental interband E2 transition energies as follows:

$$\hbar\omega = \frac{1}{4} [E_\gamma(I+2) + E_\gamma(I)], \quad (5)$$

$$J^{(2)}(I) = \frac{4\hbar^2}{\Delta E_\gamma}, \quad (6)$$

$$J^{(1)}(I-1) = \frac{\hbar^2(2I-1)}{E_\gamma}, \quad (7)$$

where

$$E_\gamma = E(I) - E(I-2),$$

$$\Delta E_\gamma = E_\gamma(I+2) - E_\gamma(I).$$

It is seen that whereas the extracted  $J^{(1)}$  depends on  $I$  proposition,  $J^{(2)}$  does not.

### 3 Analysis of the $\Delta I = 2$ staggering effects

It has been found that some SD rotational bands in different mass region show an unexpected  $\Delta I = 2$  staggering effects in the gamma ray energies [12–25]. The effect is best seen in

long rotational sequences, where the expected regular behavior of the energy levels with respect to spin or to rotational frequency is perturbed. The result is that the rotational sequence is split into two parts with states separated by  $\Delta I = 4$  (bifurcation) shifting up in energy and the intermediate states shifting down in energy. The curve found by smoothly interpolating the band energy of the spin sequence  $I, I+4, I+8, \dots$  is somewhat displaced from the corresponding curve of the sequence  $I+2, I+6, I+10, \dots$

To explore more clearly the  $\Delta I = 2$  staggering, for each band the deviation of the transition energies from a smooth reference  $\Delta E_\gamma$  is determined by calculating the fourth derivative of the transition energies  $E_\gamma(I)$  at a given spin  $I$  by

$$\begin{aligned} \Delta E_\gamma(I) &= \frac{3}{8} \left( E_\gamma(I) - \frac{1}{6} [4E_\gamma(I-2) + 4E_\gamma(I+2) \right. \\ &\quad \left. - E_\gamma(I-4) - E_\gamma(I+4)] \right). \end{aligned} \quad (8)$$

This expression was previously used in [15] and is identical to the expression for  $\Delta^4 E_\gamma(I)$  in Ref. [33]. We chose to use the expression above in order to be able to follow higher order changes in the moments of inertia of the SD bands.

### 4 Superdeformed identical bands

A particularly striking feature of SD nuclei is the observation of numerous bands with nearly identical transition energies in nuclei differing by one or two mass unit [42–45]. To determine whether a pair of bands is identical or not, one must compare the dynamical moment of inertia or compare the E2 transition energies of the two bands.

### 5 Numerical calculations and discussions

Nine SDRB's observed in nuclei of mass number  $A \sim 150$  have been analyzed in terms of our three parameter model. The experimental transition energies are taken from Ref. [1]. The studied SDRB's are namely:

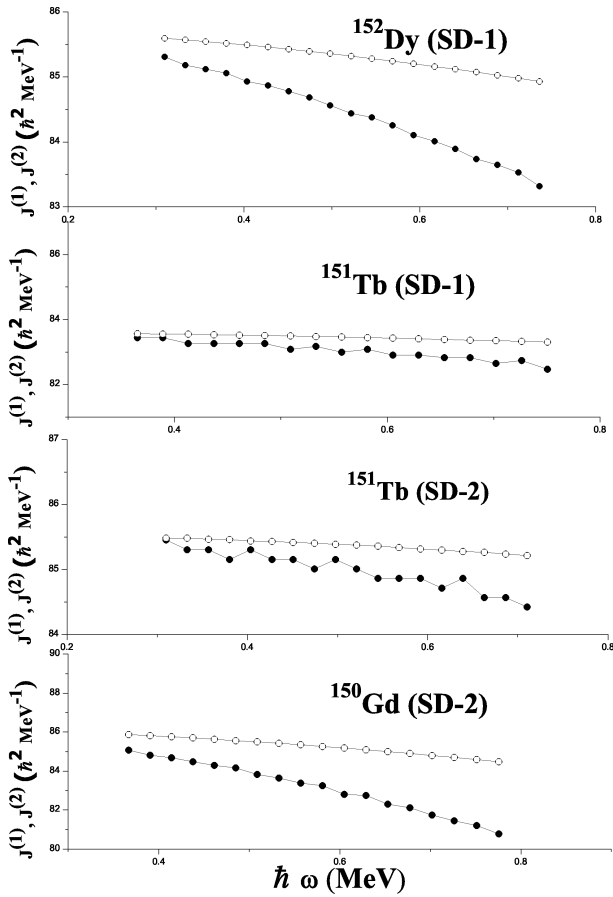


Fig. 1: Calculated Kinematic  $J^{(1)}$  (open circles) and dynamic  $J^{(2)}$  (closed circles) moments of inertia as a function of rotational frequency  $\hbar\omega$  for the set of identical bands  $^{151}\text{Tb}(\text{SD-1})$ ,  $^{152}\text{Dy}(\text{SD-1})$ ,  $^{150}\text{Gd}(\text{SD-3})$  and  $^{151}\text{Tb}(\text{SD-2})$ .

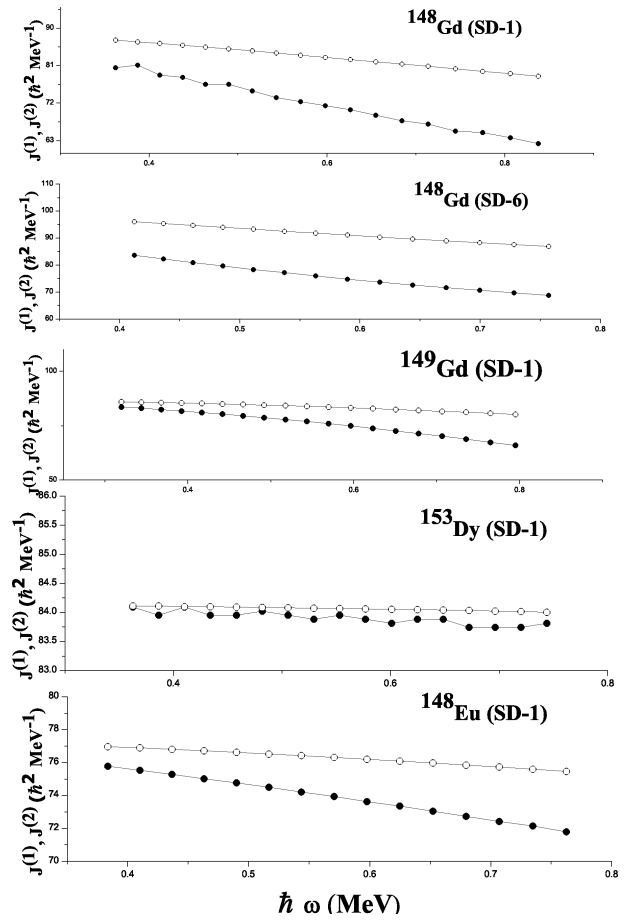


Fig. 2: Calculated Kinematic  $J^{(1)}$  (open circles) and dynamic  $J^{(2)}$  (closed circles) moments of inertia as a function of rotational frequency  $\hbar\omega$  for the SDRB's  $^{148}\text{Gd}(\text{SD-1, SD-6})$ ,  $^{149}\text{Gd}(\text{SD-1})$ ,  $^{153}\text{Dy}(\text{SD-1})$  and  $^{148}\text{Eu}(\text{SD-1})$ .

$^{150}\text{Gd}(\text{SD1, SD2})$ ,  $^{151}\text{Tb}(\text{SD1, SD2})$ ,  $^{152}\text{Dy}(\text{SD1})$ ,  $^{148}\text{Gd}(\text{SD1, SD6})$ ,  $^{149}\text{Gd}(\text{SD1})$ ,  $^{153}\text{Dy}(\text{SD1})$  and  $^{148}\text{Eu}(\text{SD1})$ . The difference between the SD bands in various mass region are obviously evident through the behavior of the dynamical  $J^{(2)}$  and kinematic  $J^{(1)}$  moments of inertia seems to be very useful to the understanding of the properties of the SD bands. The bandhead moment of inertia  $J_0$  at  $J^{(2)} = J^{(1)}$  is a sensitive guideline parameter for the spin proposition.

A computer simulated search program has been used to get a minimum root mean square (rms) deviation between the experimental transition energies  $E_\gamma^{exp}$  and the calculated ones derived from our present three parameter model  $E_\gamma^{cal}$ :

$$\chi = \frac{1}{N} \left[ \sum_{i=1}^n \left| \frac{E_\gamma^{cal}(I_i) - E_\gamma^{exp}(I_i)}{\delta E_\gamma^{exp}(I_i)} \right|^2 \right]^{1/2} \quad (9)$$

where  $N$  is the number of data points enters in the fitting procedure and  $\delta E_\gamma^{exp}(i)$  is the uncertainties in the  $\gamma$ -transitions. For each SD band the optimized best fitted four parameters

$a, b, c$  and the bandhead spin  $I_0$  were obtained by the adopted fit procedure. The procedure is repeated for several sets of trial values  $a, b, c$  and  $I_0$ . The spin  $I_0$  is taken as the nearest integer number, then another fit with only  $a, b$  and  $c$  as free parameters is made to determine their values. The lowest bandhead spin  $I_0$  and the best parameters of the model  $a, b, c$  for each band is listed in Table(1). The SD bands are identified by the lowest gamma transition energies  $E_\gamma(I_0 + 2 \rightarrow I_0)$  observed.

The dynamical  $J^{(2)}$  and kinematic  $J^{(1)}$  moments of inertia using our proposed model at the assigned spin values are calculated as a function of rotational frequency  $\hbar\omega$  and illustrated in Figs. (1,2).  $J^{(2)}$  mostly decrease with a great deal of variation from nucleus to nucleus. The properties of the SD bands are mainly influenced by the number of the high- $N$  intruder orbitals occupied. For example the large slopes of  $J^{(2)}$  against  $\hbar\omega$  in  $^{150}\text{Gd}$  and  $^{151}\text{Tb}$  are due to the occupation of  $\pi 6_2, \nu 7_2$  orbitals, while in  $^{152}\text{Dy}$  the  $\pi 6_4$  level is also occupied and this leads to a more constant  $J^{(2)}$  against  $\hbar\omega$ . A plot of

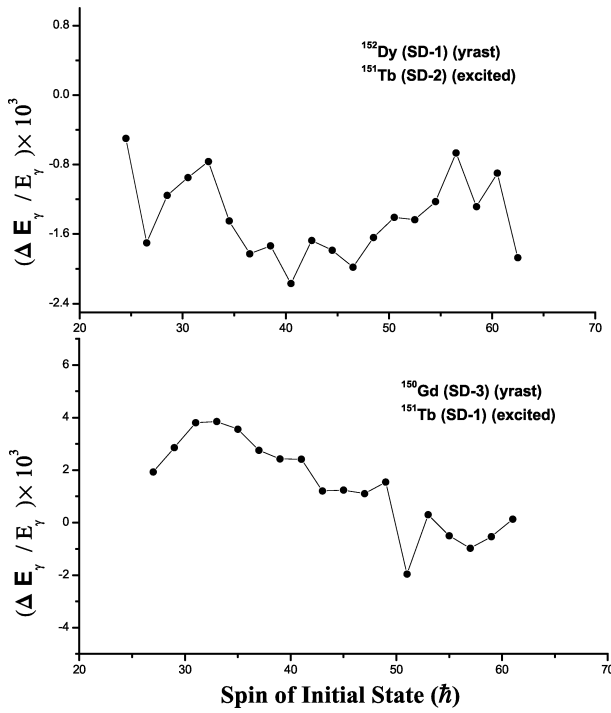


Fig. 3: Percentage differences  $\Delta E_\gamma/E_\gamma$  in transition energies  $E_\gamma = E(I) - E(I - 2)$  as a function of spin  $I$  for the set of identical bands ( $^{151}\text{Tb}(\text{SD-2})$ ,  $^{152}\text{Dy}(\text{SD-1})$ ) and ( $^{150}\text{Gd}(\text{SD-2})$ ,  $^{151}\text{Tb}(\text{SD-1})$ ).

$J^{(2)}$  against  $\hbar\omega$  for the excited SD band in  $^{151}\text{Tb}$  gives a curve that is practically constant and which closely follows the  $J^{(2)}$  curved traced out by the yrast SD band in  $^{152}\text{Dy}$  but which is very different from the yrast SD band in  $^{151}\text{Tb}$ . Similarly the  $^{150}\text{Gd}$  excited SD band has  $J^{(2)}$  values which resemble those observed in the  $^{151}\text{Tb}$  yrast SD band. It is concluded that the  $N=86$  isotones SD nuclei have identical supershell structures:

Nucleus	Yrast band	Excited band
$^{150}_{64}\text{Gd}$	$\pi(3)^0[(4)^{10}(5)^{12}](i_{13/2})^2$	$\pi(3)^1[(4)^{10}(5)^{12}](i_{13/2})^3$
$^{151}_{65}\text{Tb}$	$\pi(3)^0[(4)^{10}(5)^{12}](i_{13/2})^3$	$\pi(3)^1[(4)^{10}(5)^{12}](i_{13/2})^4$
$^{152}_{66}\text{Dy}$	$\pi(3)^0[(4)^{10}(5)^{12}](i_{13/2})^4$	$\pi(3)^1[(4)^{10}(5)^{12}](i_{13/2})^5$

## 6 Identical bands in the isotones nuclei $N=86$

A particularly striking feature of SD nuclei is the observation of a numerous bands with nearly identical transition energies in neighboring nuclei. Because of the large single particle SD gaps at  $Z=66$  and  $N=86$ , the nucleus  $^{152}\text{Dy}$  is expected to be a very good doubly magic SD core. The difference in  $\gamma$ -ray energies  $\Delta E_\gamma$  between transition in the two pairs of  $N=86$  isotones (excited  $^{151}\text{Tb}$  (SD-2), yrast  $^{152}\text{Dy}$  (SD-1)) and (excited  $^{150}\text{Gd}$  (SD-2), yrast  $^{151}\text{Tb}$  (SD-1)) were calculated.

The gamma transition energies of the excited band (SD-2) in  $^{151}\text{Tb}$  are almost identical to that of the yrast band (SD-1) in  $^{152}\text{Dy}$ . This twin band has been associated with a  $[301]1/2$

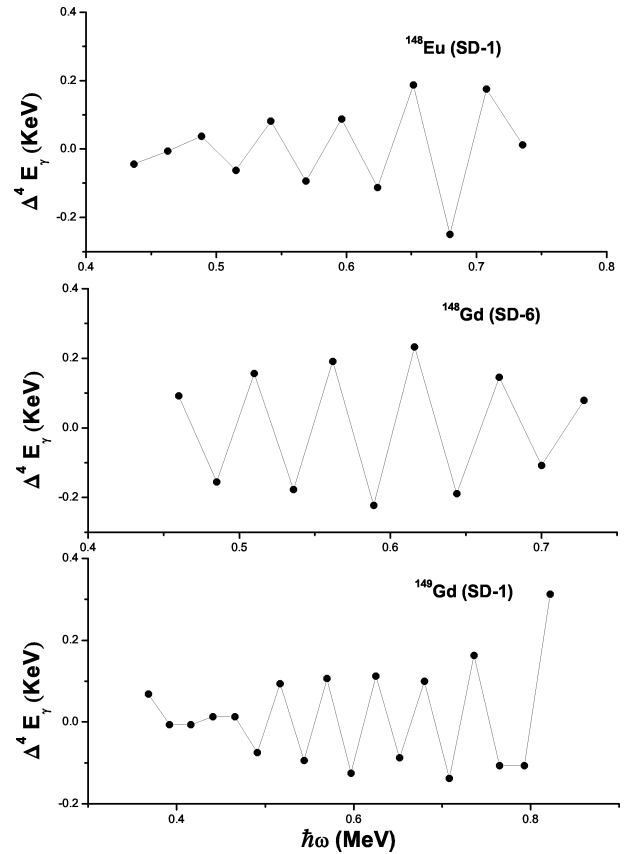


Fig. 4: The calculated  $\Delta^4 E_\gamma$  staggering as a function of rotational frequency  $\hbar\omega$  of the SDRB's  $^{148}\text{Eu}(\text{SD-1})$ ,  $^{148}\text{Gd}(\text{SD-6})$ ,  $^{149}\text{Gd}(\text{SD-1})$ .

hole in the  $^{152}\text{Dy}$  core. The orbitals  $\pi 6_2$  and  $\nu 7_2$  are occupied in  $^{151}\text{Tb}$ , while in  $^{152}\text{Dy}$  the  $\pi 6_4$  level is occupied and this leads to a more constant in dynamic moment of inertia  $J^{(2)}$ . Clearly the  $J^{(2)}$  values for the excited SD bands are very similar to the yrast SD bands in their  $Z+1$ ,  $N=86$  isotones. The plot of percentage differences  $\Delta E_\gamma/E_\gamma$  in transition energies versus spin for the two pairs ( $^{151}\text{Tb}(\text{SD-2})$ ,  $^{152}\text{Dy}(\text{SD-1})$ ) and ( $^{150}\text{Gd}(\text{SD-2})$ ,  $^{151}\text{Tb}(\text{SD-1})$ ) are illustrated in Fig. (3).

## 7 $\Delta I = 2$ Staggering

Another result of the present work is the observation of a  $\Delta I = 2$  staggering effects in the  $\gamma$ -ray energies, where the two sequences for spins  $I = 4j, 4j + 1$  ( $j=0,1,2,\dots$ ) and  $I = 4j + 2$  ( $j=0,1,2,\dots$ ) are bifurcated. For each band the deviation of the  $\gamma$ -ray energies from a smooth reference  $\Delta E_\gamma$  is determined by calculating the fourth derivative of the  $\gamma$ -ray energies  $\Delta E_\gamma(I)$  at a given spin  $\Delta^4 E_\gamma$ . The staggering in the  $\gamma$ -ray energies is indeed found for the SD bands in  $^{148}\text{Eu}(\text{SD-1})$ ,  $^{148}\text{Gd}(\text{SD-6})$  and  $^{149}\text{Gd}(\text{SD-1})$  in Fig. (4).

Submitted on June 11, 2012 / Accepted on June 25, 2012

## References

1. Balraj Singh, Roy Zywine, Richard B. Firestone. Table of Superdeformed Nuclear Bands and Fission Isomers. *Nuclear Data Sheets*, 2002, v. 97, 241–592.
2. Becker J.A. et al. Level spin and moments of inertia in superdeformed nuclei near  $A = 194$ . *Nuclear Physics*, 1990, v. A520 c187–c194.
3. Draper J.E., et al. Spins in superdeformed bands in the mass 190 region. *Physical Review*, 1994, v. c42 R1791–R1795.
4. Khalaf A.M., et al. Band Head of the Superdeformed Bands in the  $A \sim 150$  Mass region Nuclei. *Egypt Journal of Physics*, 2002, v. 33 (1), 67–87.
5. Khalaf A.M., et al. Spin Prediction and Systematics of Moments of inertia of superdeformed Nuclear Rotational Band in the Mass Region  $A \sim 190$ . *Egypt Journal of Physics*, 2002, v. 33 (3), 585–602.
6. Khalaf A.M., et al. Description of Rotational Bands in Superdeformed Nuclei by Using Two-parameter Empirical Formula. *Egypt Journal of Physics*, 2003, v. 34 (2), 159–177.
7. Khalaf A.M., et al. Properties of Superdeformed Rotational Bands of Odd Nuclei in the Mass-190 Region Using Harris Expansion. *Egypt Journal of Physics*, 2003, v. 34 (2), 195–215.
8. Khalaf A.M., et al. Analysis of Rotational Bands in Superdeformed Nuclei Using sdg Interacting Boson Model. *Egypt Journal of Physics*, 2004, v. 34 (1), 79–104.
9. Khalaf A.M., and Sirag M.M. Prediction of Nuclear Superdeformed Rotational Bands Using Incremental Alignments. *Egypt Journal of Physics*, 2006, v. 37 (3), 277–293.
10. Khalaf A.M., Allam M.A., and Saber E. Signature Partners in Odd Superdeformed Nuclei in Mass Region  $A \sim 190$ . *Egypt Journal of Physics*, 2008, v. 39 (1), 41–65.
11. Khalaf A.M., Allam M.A., and Sirag M.M. Bandhead Spin Determination and Moments of inertia of Superdeformed Nuclei in Mass Region 60-90 Using Variable Moment of inertia Model. *Egypt Journal of Physics*, 2010, v. 41 (2), 13–27.
12. Khalaf A.M., and Sirag M.M. Analysis of  $\Delta I = 2$  Staggering in Nuclear Superdeformed Rotational Bands. *Egypt Journal of Physics*, 2004, v. 35 (2), 359–375.
13. Sirag M.M. A Reexamination of  $\Delta I = 2$  Energy Staggering in Nuclear Superdeformed Rotational Bands. *Egypt Journal of Physics*, 2007, v. 38 (1), 1–14.
14. Flibolte S., et al.  $\Delta I = 4$  bifurcation in a superdeformed band: Evidence for a  $C_4$  symmetry. *Physical Review Letters*, 1993, v. 71 4299–4302.
15. Cederwall B., et al. New features of superdeformed bands in  $^{194}\text{Hg}$ . *Physical Review Letters*, 1994, v. 72 3150–3153.
16. Flibolte S., et al. Multi-particle excitations in the superdeformed  $^{149}\text{Gd}$  nucleus. *Nuclear Physics*, 1995, v. A584 (2), 373–396.
17. Carpenter M.P., et al. Identification of the unfavored  $N=7$  superdeformed band in  $^{191}\text{Hg}$ . *Physical Review*, 1995, v. C51 2400–2405.
18. Farris L.P., et al. Neutron blocking and delayed proton pair alignment in superdeformed  $^{195}\text{Pb}$ . *Physical Review*, 1995, v. C51 R2288–R2292.
19. Bernstien L.A., et al. Superdeformation in  $^{154}\text{Er}$ . *Physical Review*, 1995, v. C52 R1171–R1174.
20. Angelis G., et al. Spectroscopy in the second well of the  $^{148}\text{Gd}$  nucleus: Two quasiparticle and collective excitations. *Physical Review*, 1996, v. C53 679–688.
21. Fischer S.M., et al. Alignment additivity in the two-quasiparticle superdeformed bands of  $^{192}\text{Tl}$ . *Physical Review*, 1996, v. C53 2126–2133.
22. Semple A.T., et al. Energy Staggering in Superdeformed Bands in  $^{131}\text{Ce}$ ,  $^{132}\text{Ce}$ , and  $^{133}\text{Ce}$ . *Physical Review Letters*, 1996, v. 76 3671–3674.
23. Krucken R., et al. Test of  $\Delta I=2$  staggering in the superdeformed bands of  $^{194}\text{Hg}$ . *Physical Review*, 1996, v. C54 R2109–R2113.
24. Cederwall B., et al. Properties of superdeformed bands in  $^{153}\text{Dy}$ . *Physics Letters*, 1995, v. B346 (3-4), 244–250.
25. Haslip D.S., et al.  $\Delta I=4$  Bifurcation in Identical Superdeformed Bands. *Physical Review Letters*, 1997, v. 78 3447–3450.
26. Hamamoto I. and Moltelran B. Superdeformed rotational bands in the presence of  $Y_{44}$  deformation. *Physics Letters*, 1994, v. B333 294–298.
27. Pavlicherkov I.M. and Flibolte S.  $C_4$  Symmetry and bifurcation in superdeformed bands. *Physical Review*, 1995, v. C51 R460–R464.
28. Macchiavelli A.O., et al.  $C_4$  Symmetry effects in nuclear rotational motion. *Physical Review*, 1995, v. C51 R1–R4.
29. Sun Y., Zhang J. and Guidry M.  $\Delta I=4$  Bifurcation without Explicit Fourfold Symmetry. *Physical Review Letters*, 1995, v. 75 3398–3401.
30. Burzynski K., et al. Hexadecapole interaction and the  $\Delta I = 4$  staggering effect in rotational bands. *Physica Scripta*, 1995, v. T56 228–230.
31. Magierski P., Burzynski K. and Dobaczewski J. The  $\Delta I=4$  bifurcation in superdeformed bands. *Acta Physica Polonica*, 1995, v. B26 291–296.
32. Mikhailov I.N. and Quentin P. Band Staggering in Some Superdeformed States and Intrinsic Vortical Motion. *Physical Review Letters*, 1995, v. 74 3336–3340.
33. Reviol W., Jin H.Q. and Rieendinger L.L. Transition energy staggering and band interaction in rare-earth nuclei. *Physical Letters*, 1996, v. B371 19–24.
34. Pavlicherkov I.M. Nonadiabatic mean field effects in the  $\Delta I=2$  staggering of superdeformed bands. *Physical Review*, 1997, v. C55 1275–1281.
35. Magierski P., et al. Quadrupole and hexadecapole correlations in rotating nuclei studied within the single-j shell model. *Physical Review*, 1997, v. C55 1236–1245.
36. Kota V.K.B. Interacting boson model basis and Hamiltonian for  $\Delta L=4$  staggering. *Physical Review*, 1996, v. C53 2550–2553.
37. Liu Y.X., et al. Description of superdeformed nuclear states in the interacting boson model. *Physical Review*, 1997, v. C56 1370–1379.
38. Hara K. and Lalazissis. Analysis of  $\Delta I=2$  staggering in nuclear rotational spectra. *Physical Review*, 1997, v. C55 1789–1796.
39. Toki H. and Wu L.A.  $\Delta I=4$  Bifurcation in Ground Bands of Even-Even Nuclei and the Interacting Boson Model. *Physical Review Letters*, 1997, v. 79 2006–2009.
40. Luo W.D., et al. Microscopic study of a  $C_4$ -symmetry hypothesis in  $A = 150$  superdeformed nuclei: Deformed Woods-Saxon mean field. *Physical Review*, 1995, v. C52 2989–3001.
41. Donou F., Frouendorf S. and Merg J. Can hexadecapole deformation lead to  $\Delta I = 2$  staggering in superdeformed bands. *Physics Letters*, 1996, v. B387 667–672.
42. Byrski T., et al. Observation of identical superdeformed bands in  $N=86$  nuclei. *Physical Review Letters*, 1990, v. 64 1650–1653.
43. Baktash C., Hars B. and Nazarewicz N. Identical Bands in Normally Deformed and Superdeformed Nuclei. *Annual Review of Nuclear and Particle Science*, 1995, v. 45 485–541.
44. Chen Y.J., et al. Theoretical simulation for identical bands. *European Physical Journal*, 2005, v. A24 185–191.
45. He X.T., et al. The  $i_{13/2}$  proton intruder orbital and the identical superdeformed bands in 193, 194,  $^{195}\text{Tl}$ . *European Physical Journal*, 2005, v. A23 217–222.
46. Nazarewicz W., et al. Natural-parity states in superdeformed bands and pseudo  $SU(3)$  symmetry at extreme conditions. *Physical Review Letters*, 1990, v. 64 1654–1657.
47. Rigollet C., Bonche P. and Flocard H. Microscopic study of the properties of identical bands in the  $A=150$  mass region C. Rigollet. *Physical Review*, 1999, v. C59 3120–3127.

# Emergence of Particle Masses in Fractal Scaling Models of Matter

Hartmut Müller

Advanced Natural Research Institute in memoriam Leonhard Euler, Munich, Germany. [www.anr-institute.com](http://www.anr-institute.com)

Based on a fractal scaling model of matter, that reproduces systematic features in the distribution of elementary particle rest masses, the paper presents natural oscillations in chain systems of harmonic quantum oscillators as mechanism of particle mass generation.

## 1 Introduction

The origin of particle masses is one of the most important topics in modern physics. In this paper we won't discuss the current situation in the standard theory and the Higgs mechanism. Based on a fractal scaling model [1] of natural oscillations in chain systems of harmonic oscillators we present an alternative mechanism of mass generation.

Possibly, natural oscillations of matter generate scaling distributions of physical properties in very different processes. Fractal scaling models [2] of oscillation processes are not based on any statements about the nature of the link or interaction between the elements of the oscillating chain system. Therefore the model statements are quite generally, what opens a wide field of possible applications.

Within the last 10 years many articles were published which show that scaling is a widely distributed natural phenomenon [3–7]. As well, scaling is a general property of inclusive distributions in high energy particle reactions [8] – the quantity of secondary particles increases in dependence on the logarithm of the collision energy.

Particularly, the observable mass distribution of celestial bodies is connected via scaling with the mass distribution of fundamental particles [9], that can be understood as contribution to the fundamental link between quantum – and astrophysics.

Based on observational data, Haremein, Hyson and Rauscher [10, 11] discuss a scaling law for all organized matter utilizing the Schwarzschild condition, describing cosmological to subatomic structures. From their point of view the universality of scaling suggests an underlying polarizable structured vacuum of mini white and black holes. They discuss the manner in which this structured vacuum can be described in terms of resolution of scale analogous to a fractal scaling as a means of renormalization at the Planck distance.

In the framework of our model [1], particles are resonance states in chain systems of harmonic quantum oscillators and the masses of fundamental particles are connected by the scaling exponent  $\frac{1}{2}$ . For example, the logarithm of the proton-to-electron mass ratio is  $7\frac{1}{2}$ , but the logarithm of the W-boson-to-proton mass ratio is  $4\frac{1}{2}$ . This means, they are connected by the equation:

$$\ln(m_w/m_{\text{proton}}) = \ln(m_{\text{proton}}/m_{\text{electron}}) - 3 \quad (1)$$

The logarithm of the W-boson-to-electron mass ratio is  $4\frac{1}{2} + 7\frac{1}{2} = 12$ :

$$\ln(m_w/m_{\text{electron}}) = 12. \quad (2)$$

Already within the eighties the scaling exponent  $\frac{3}{2}$  was found in the distribution of particle masses by V. A. Kolombet [12]. In addition, we have shown [9] that the masses of the most massive bodies in the Solar System are connected by the scaling exponent  $\frac{1}{2}$ . The scaling exponent  $3 \times \frac{1}{2}$  arises as consequence of natural oscillations in chain systems of similar harmonic oscillators [2]. If the natural frequency of one harmonic oscillator is known, one can calculate the complete fractal spectrum of natural frequencies of the chain system. Spectral nodes arise on the distance of  $\frac{1}{2}$  logarithmic units. Near spectral nodes the spectral density reaches local maximum and natural frequencies of the oscillating chain system are distributed maximum densely. We suspect, that stable particles correspond to main spectral nodes which represent rational number logarithms.

The colossal difference between the life times of stable and “normal” particles is amazing. The life-time of a proton is minimum  $10^{34}$  times larger than the life of a neutron, although the mass difference between them is only 0.13% of the proton rest mass. From this point of view seems that the stability of a particle is not connected with its mass.

In the framework of the standard theory, the electron is stable because it's the least massive particle with non-zero electric charge. Its decay would violate charge conservation. The proton is stable, because it's the lightest baryon and the baryon number is conserved. Therefore the proton is the most important baryon, while the electron is the most important lepton and the proton-to-electron mass ratio can be understood as a fundamental physical constant. Within the standard theory, the W- and Z-bosons are elementary particles which mediate the weak force. The rest masses of all these particles are measured with high precision. The precise rest masses of other elementary or stable particles (quarks, neutrinos) are nearly unknown and not measured directly.

The life-times of electron and proton seem not measurable. In addition, there is no comparison between the life of a proton ( $\tau_{\text{proton}} > 10^{30}$  years) and the age of the visible universe ( $\tau_{\text{universe}} > 10^{10}$  years). Though, there is an interesting scale similarity between the product of the proton life  $\tau_{\text{proton}} > 10^{30}$  years and the proton mass generating frequency  $\omega_{\text{proton}}$ , on

the one side, and the product of the age  $\tau_{\text{universe}} > 10^{10}$  years of the visible universe and the Planck frequency  $\omega_{\text{Planck}}$ , on the other side:

$$\omega_{\text{proton}} = E_{\text{proton}}/\hbar = 938 \text{ MeV}/\hbar = 1.425 \cdot 10^{24} \text{ Hz} \quad (3)$$

$$\omega_{\text{proton}} \tau_{\text{proton}} > 10^{60}$$

$$\omega_{\text{Planck}} = \sqrt{(c^5/\hbar G)} = 1.855 \cdot 10^{43} \text{ Hz} \quad (4)$$

$$\omega_{\text{Planck}} \tau_{\text{universe}} > 10^{60}.$$

If both products are of the same scale, we can write:

$$\omega_{\text{proton}} \tau_{\text{proton}} \cong \omega_{\text{Planck}} \tau_{\text{universe}}. \quad (5)$$

Because the frequencies  $\omega_{\text{proton}}$  and  $\omega_{\text{Planck}}$  are fundamental constants, the equation (5) means that possibly exists a fundamental connection between the age of the visible universe and the proton life-time.

## 2 Methods

Based on the continued fraction method [13] we will search the natural frequencies of a chain system of many similar harmonic oscillators in this form:

$$\omega_{jk} = \omega_{00} \exp(S_{jk}). \quad (6)$$

$\omega_{jk}$  is a set of natural frequencies of a chain system of similar harmonic oscillators,  $\omega_{00}$  is the natural angular oscillation frequency of one oscillator,  $S_{jk}$  is a set of finite continued fractions with integer elements:

$$S_{jk} = n_{j0} + \frac{1}{n_{j1} + \frac{1}{n_{j2} + \frac{1}{\dots + \frac{1}{n_{jk}}}}} = [n_{j0}; n_{j1}, n_{j2}, \dots, n_{jk}], \quad (7)$$

where  $n_{j0}, n_{j1}, n_{j2}, \dots, n_{jk} \in \mathbb{Z}$ ,  $j = 0, \infty$ . We investigate continued fractions (7) with a finite quantity of layers  $k$ , which generate discrete spectra, because in this case all  $S_{jk}$  represent rational numbers. Possibly, the free links  $n_{j0}$  and the partial denominators  $n_{j1}, n_{j2}, \dots, n_{jk}$  could be interpreted as some kind of "quantum numbers". The present paper follows the Terskich [13] definition of a chain system, where the interaction between the elements proceeds only in their movement direction. Model spectra (7) are not only logarithmic-invariant, but also fractal, because the discrete hyperbolic distribution of natural frequencies  $\omega_{jk}$  repeats itself on each spectral layer.

The partial denominators run through positive and negative integer values. Ranges of relative low spectral density (spectral gaps) and ranges of relative high spectral density (spectral nodes) arise on each spectral layer. In addition to the first spectral layer, fig. 1 shows the second spectral layer  $k = 2$  with  $|n_{j1}| = 2$  (logarithmic representation). Maximum spectral density areas (spectral nodes) arise automatically on the distance of integer and half logarithmic units.

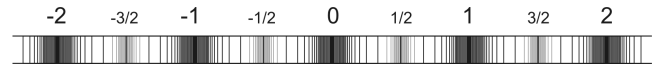


Fig. 1: The spectrum (7) on the first layer  $k = 1$ , for  $|n_{j0}| = 0, 1, 2, \dots$  and  $|n_{j1}| = 2, 3, 4, \dots$  and, in addition, the second spectral layer  $k = 2$ , with  $|n_{j1}| = 2$  and  $|n_{j2}| = 2, 3, 4, \dots$  (logarithmic representation).

Fractal scaling models of natural oscillations are not based on any statements about the nature of the link or interaction between the elements of the oscillating chain system. For this reason we assume that our model could be useful also for the analysis of natural oscillations in chain systems of harmonic quantum oscillators. We assume that in the case of natural oscillations the amplitudes are low, the oscillations are harmonic and the oscillation energy  $E$  depends only on the frequency ( $\hbar$  is the Planck constant):

$$E = \hbar\omega. \quad (8)$$

In the framework of our model (6) all particles are resonance states of an oscillating chain system, in which to the oscillation energy (8) corresponds the particle mass  $m$ :

$$m = \omega\hbar/c^2. \quad (9)$$

In this connection the equation (9) means that quantum oscillations generate mass. Under consideration of (6) now we can create a fractal scaling model of the mass spectrum of model particles. This mass spectrum is described by the same continued fraction 7, for  $m_{00} = \omega_{00} \hbar/c^2$ :

$$\ln(m_{jk}/m_{00}) = [n_{j0}; n_{j1}, n_{j2}, \dots, n_{jk}]. \quad (10)$$

The frequency spectrum (7) and the mass spectrum (10) are isomorphic. The mass spectrum (10) is fractal and consequently it has a clear hierarchical structure, in which continued fractions (7) of the form  $[n_{j0}; \infty]$  and  $[n_{j0}; 2, \infty]$  define main spectral nodes, as fig. 1 shows.

## 3 Results

Based on (10) in the present paper we will calculate a list of model particle masses which correspond to the main spectral nodes and compare this list with rest masses of well measured stable and fundamental particles – hadrons, leptons, gauge bosons and Higgs bosons.

The model mass spectrum (10) is logarithmically symmetric and the main spectral nodes arise on the distance of 1 and  $\frac{1}{2}$  logarithmic units, as fig. 1 shows. The mass  $m_{00}$  in (10) corresponds to the main spectral node  $S_{00} = [0; \infty]$ , because  $\ln(m_{00}/m_{00}) = 0$ . Let's assume that  $m_{00}$  is the electron rest mass  $0.510998910(13) \text{ MeV}/c^2$  [14]. In this case (10) describes the mass spectrum that corresponds to the natural frequency spectrum (7) of a chain system of vibrating electrons. Further stable or fundamental model particles correspond to further main spectral nodes of the form  $[n_{j0}; \infty]$  and  $[n_{j0}; 2]$ . Actually, near the node  $[12; \infty]$  we find the W- and Z-bosons,

S	calculated (10) mass-interval $m_{jk}c^2$ (MeV)	corresponding particle	particle mass $mc^2$ (MeV) [14, 15]	$\ln(m/m_{00})$	d
[0; $\infty$ ]	0.451 – 0.579	electron ( $m_{00}$ )	$0.510998910 \pm 0.000000013$	0.000	0.000
[7; 2, $\infty$ ]	815 – 1047	proton	$938.27203 \pm 0.00008$	7.515	0.015
[7; 2, $\infty$ ]	815 – 1047	neutron	$939.565346 \pm 0.000023$	7.517	0.017
[12; $\infty$ ]	73395 – 94241	W-boson	$80398 \pm 25$	11.966	-0.034
[12; $\infty$ ]	73395 – 94241	Z-boson	$91187.6 \pm 2.1$	12.092	0.092
[12; 2, $\infty$ ]	121008 – 155377	Higgs-boson?	$125500 \pm 540$	12.411	-0.089
[13; $\infty$ ]	199509 – 256174	EWSB?			
[51; 2, $\infty$ ]	$(1.048 - 1.345) \times 10^{22}$	Planck mass	$1.22089(6) \times 10^{22}$	51.528	0.028

Table 1: The calculated  $S$ -values (7) of  $\frac{1}{4}$  logarithmic units width and the corresponding calculated model mass-intervals of main spectral nodes for the electron calibrated model mass spectrum. The deviation  $d = \ln(m/m_{00}) - S$  is indicated.

but near the node [7; 2,  $\infty$ ] the proton and neutron masses, as table 1 shows.

Theoretically, a chain system of vibrating protons generates the same spectrum (10). Also in this case, stable or fundamental model particles correspond to main spectral nodes of the form  $[n_{j0}; \infty]$  and  $[n_{j0}; 2, \infty]$ , but relative to the electron calibrated spectrum, they are moved by  $-7\frac{1}{2}$  logarithmic units. Actually, if  $m_{00}$  is the proton rest mass  $938.27203(8)$  MeV/ $c^2$  [14], then the electron corresponds to the node  $[-7; -2, \infty]$ , but the W- and Z-bosons correspond to node  $[4; 2, \infty]$ .

Consequently, the core claims of our model don't depend on the selection of the calibration mass  $m_{00}$ , if it is the rest mass of a fundamental resonance state that corresponds to a main spectral node. As mentioned already, this is why the model spectrum (10) is logarithmically symmetric.

Because a chain system of any similar harmonic oscillators generates the spectrum (10),  $m_{00}$  can be much less than the electron mass. Only one condition has to be fulfilled:  $m_{00}$  has to correspond to a main spectral node of the model spectrum (10). On this background all particles can be interpreted as resonance states in a chain system of harmonic quantum oscillators, in which the rest mass of each single oscillator goes to zero. In the framework of our oscillation model this way can be understood the transition of massless to massive states.

Within our model particles arise as resonance states in chain systems of harmonic quantum oscillators and their mass distribution is logarithmically symmetric. In [1] we have investigated the distribution of hadrons (baryons and mesons) in dependence on their rest masses. We have shown that all known baryons are distributed over an interval of 2 logarithmic units, of [7; 2,  $\infty$ ] to [9; 2,  $\infty$ ]. Maximum of baryons occupy the logarithmic center [8; 2,  $\infty$ ] of this interval. Maximum of mesons occupy the spectral node [8;  $\infty$ ] that split up the interval of [0;  $\infty$ ] to [12;  $\infty$ ] between the electron and the W- and Z-bosons proportionally of  $\frac{2}{3}$ . In addition, we have shown that the mass distribution of leptons isn't different of the baryon and meson mass distributions, but follows them.

The rest mass of the most massive lepton (tauon) is near the maximum of the baryon and meson mass distributions.

In the framework of our model [1], the Planck frequency  $\omega_{\text{Planck}}$  corresponds to a main spectral node of the model mass spectrum (10). Actually, relative to the proton mass generating frequency  $\omega_{\text{proton}}$  the Planck frequency  $\omega_{\text{Planck}}$  corresponds to the main node [44;  $\infty$ ] of the frequency spectrum (6):

$$\ln \frac{\omega_{\text{Planck}}}{\omega_{\text{proton}}} = \ln \frac{1.855 \times 10^{43}}{1.425 \times 10^{24}} \cong 44. \quad (11)$$

Relative to the electron mass generating frequency  $\omega_e$  the Planck frequency  $\omega_{\text{Planck}}$  corresponds to the spectral node [51; 2,  $\infty$ ]:

$$\ln \frac{\omega_{\text{Planck}}}{\omega_e} = \ln \frac{1.855 \times 10^{43}}{7.884 \times 10^{20}} \cong 51.5 = 44 + 7.5. \quad (12)$$

The Planck frequency  $\omega_{\text{Planck}}$  is  $e^{44}$  times larger than the proton mass generating frequency  $\omega_{\text{proton}}$  and the same relationship is between the Planck mass  $m_{\text{Planck}}$  and the proton rest mass  $m_{\text{proton}}$ :

$$\ln \frac{m_{\text{Planck}}}{m_{\text{proton}}} = \ln \frac{2.177 \times 10^{-8}}{1.673 \times 10^{-27}} \cong 44 \quad (13)$$

$$m_{\text{Planck}} = \sqrt{(\hbar c/G)} = 2.177 \times 10^{-8} \text{ kg.}$$

The Planck mass  $m_{\text{Planck}} \cong 21.77 \mu\text{g}$  corresponds to the main node [44;  $\infty$ ] of the proton calibrated mass spectrum (10) and therefore, probably,  $m_{\text{Planck}}$  is the rest mass of a fundamental particle. In the framework of our model [1] the gravitational constant  $G$  is connected directly with the fundamental particles masses. Now we can calculate  $G$  based on the proton rest mass  $m_{\text{proton}}$ :

$$G = \frac{\hbar c}{(e^{44} m_{\text{proton}})^2} \quad (14)$$

## Resume

In the framework of the present model discrete scaling mass distributions arise as result of natural oscillations in chain systems of harmonic quantum oscillators. With high precision, the masses of known fundamental and stable particles are connected by the model scaling factor  $\frac{1}{2}$ . Presumably, the complete mass distribution of particles is logarithmically symmetric and, possibly, massive particles arise as resonance states in chain systems of quantum oscillators.

Within our model any chain system of harmonic quantum oscillators generates the same mass spectrum (10) and the corresponding to the spectral node  $[12; 2, \infty]$  observed particle mass of 125 GeV [15] can be interpreted as resonance state in a chain system of oscillating protons, for example.

## Acknowledgements

The author is deeply grateful to S. E. Shnoll, V. A. Panchevlyuga and V. A. Kolombet for valuable discussions and support.

Submitted on September 29, 2012 / Accepted on September 30, 2012

## References

1. Müller H. Fractal scaling models of natural oscillations in chain systems and the mass distribution of the celestial bodies in the Solar System. *Progress in Physics*, 2010.
2. Müller H. Fractal scaling models of resonant oscillations in chain systems of harmonic oscillators. *Progress in Physics*, 2009.
3. Ries A., Fook M. V. L. Fractal Structure of Nature's Preferred Masses: Application of the Model of Oscillations in a Chain System. *Progress in Physics*, 2010.
4. Ries A., Fook M. V. L. Application of the Model of Oscillations in a Chain System to the Solar System. *Progress in Physics*, 2011.
5. Kelvin K. S. Wu, Ofer Lahav, Martin J. Rees. The large-scale smoothness of the Universe. *Nature*, Vol. 397, 1999.
6. Barenblatt G. I. *Scaling*. Cambridge University Press, 2003.
7. Tatischeff B. Fractals and log-periodic corrections applied to masses and energy levels of several nuclei. arXiv:1107.1976v1, 2011.
8. Feynman R. P. Very High-Energy Collisions of Hadrons, *Phys. Rev. Lett.* 23, 1969, 1415.
9. Müller H. Fractal scaling models of natural oscillations in chain systems and the mass distribution of the celestial bodies in the Solar System. *Progress in Physics*, 2010.
10. Haramain N., Hyson M., Rauscher E. A. Proceedings of The Unified Theories Conference. 2008. Scale Unification: A Universal Scaling Law for Organized Matter, in Cs Varga, I. Dienes & R.L. Amoroso (eds.), The Noetic Press, ISBN 9780967868776.
11. Haramain N. Scaling Law for Organized Matter in the Universe. *Bull. Am. Phys. Soc.* AB006, Ft. Worth, October 2001.
12. Kolombet V. Macroscopic fluctuations, masses of particles and discrete space-time. *Biofizika*, 1992, v. 36, pp. 492–499 (in Russian)
13. Terskich V. P. The continued fraction method. Leningrad, 1955 (in Russian).
14. Particle listings. Astrophysical constants. Particle Data Group, www.pdg.lbl.gov.
15. Pier Paolo Giardino et al. Is the resonance at 125 GeV the Higgs boson? arXiv:1207.1347v1, 2012.

# Resonance and Fractals on the Real Numbers Set

Victor A. Panchelyuga, Maria S. Panchelyuga

Institute of Theoretical and Experimental Biophysics, Pushchino, Russia.

Research Institute of Hypercomplex Systems in Geometry and Physics, Friazino, Russia. E-mail: panvic333@yahoo.com

The paper shown that notions of resonance and roughness of real physical systems in applications to the real numbers set lead to existence of two complementary fractals on the sets of rational and irrational numbers accordingly. Also was shown that power of equivalence classes of rational numbers is connected with well known fact that resonance appear more easily for pairs of frequencies, which are small natural numbers.

## 1 Introduction

Well known that resonance is relation of two frequencies  $p$  and  $q$ , expressed by rational number  $r \in \mathbb{Q}$ :

$$r = \frac{p}{q}, \tag{1}$$

where  $p, q \in \mathbb{N}$  and  $\mathbb{N}$  is the set of natural numbers,  $\mathbb{Q}$  is set of rational numbers. If  $r$  is irrational number, i.e.  $r \in \mathbb{Q}^*$ , where  $\mathbb{Q}^*$  is set of irrational numbers, resonance is impossible.

Resonance definition as  $r \in \mathbb{Q}$  leads to the next question. For real physical system  $p, q$  and, consequently,  $r$  cannot be a fixed number due to immanent fluctuations of the system. Consequently, condition  $r \in \mathbb{Q}$  cannot be fulfilled all time because of irrational numbers, which fill densely neighborhood of any rational number. By these reasons, resonance condition  $r \in \mathbb{Q}$  cannot be fulfilled and resonance must be impossible. But it is known that in reality resonance exists. The question is: in which way existence of resonance corresponds with it's definition as  $r \in \mathbb{Q}$ ?

Also is known that resonance appear more easily for such  $r \in \mathbb{Q}$  for which  $p$  and  $q$  are small numbers. As will be shown this experimental fact is closely connected with the question stated above.

## 2 Rational numbers distribution

The question stated above for the first time was considered by Kyril Dombrowski [1]. He suppose that despite the fact that rational numbers distributed densely along the number axis this distribution may be in some way non-uniform. In cited work K. Dombrowski used proposed by Khinchin [2] procedure of constructing of rational numbers set, based on the following continued fraction:

$$\left\{ Q_i^{a_i} \right\} = \frac{1}{a_1 \pm \frac{1}{a_2 \pm \frac{1}{\dots \pm \frac{1}{a_i \pm \frac{1}{\dots}}}}} \tag{2}$$

where  $a_1, a_2, \dots, a_i = \overline{1, N}, i = \overline{1, N}$ . Continued fraction (2) gives rational numbers, which belongs to interval  $[0, 1]$ .

Is known that exists one-to-one correspondence between  $[0, 1]$  and  $[1, \infty)$  intervals. I.e., any regularities obtained from (2) on the interval  $[0, 1]$  will be also true and for interval  $[1, \infty)$ .

In case  $N \rightarrow \infty$  expression (2) leads to

$$\left\{ Q_i^{a_i} \mid N \rightarrow \infty \right\} \rightarrow \mathbb{Q}.$$

Apparently, in this case no distribution available, because rational numbers distributed along number axis densely.

For case of real physical system, condition  $N \rightarrow \infty$  means that any parameters of the system must be defined with infinite accuracy. But in reality parameters values of the systems cannot be defined with such accuracy even if we have an ideal, infinite-accuracy measuring device. Such exact values simply don't exist because of quantum character of physical reality.

All this means that for considered physical phenomenon – resonance – we need to limit parameter  $i$  in (2) by some finite number  $N$ . Fig. 1 presents numerical simulation of (2) for the first two cases of finite  $N$ :  $N = 1, N = 2$ , and  $N = 3$ . In the case  $N = 1$  (Fig. 1a) we have only one value  $i = 1$ , and from (2) we can obtain:

$$\left\{ Q_1^{a_1} \right\} = \frac{1}{a_1}, \quad i = 1, \quad a_1 = \overline{1, \infty}. \tag{3}$$

In the case of  $N = 2$ , analogously:

$$\left\{ Q_i^{a_i} \right\} = \frac{1}{a_1 \pm \frac{1}{a_2}} = \frac{a_2}{a_1 a_2 \pm 1}, \quad i = 1, 2, \quad a_1, a_2 = \overline{1, \infty}. \tag{4}$$

For the case  $N = 3$  we have

$$\left\{ Q_i^{a_i} \right\} = \frac{1}{a_1 \pm \frac{1}{a_2 \pm \frac{1}{a_3}}} = \frac{a_2 a_3 \pm 1}{a_1 (a_2 a_3 \pm 1) \pm a_3}, \tag{5}$$

$$i = 1, 2, 3; \quad a_1, a_2, a_3 = \overline{1, \infty}.$$

It's easy to see that final set presented in Fig. 1c has a fractal character. Vicinity of every line in Fig. 1b is isomorphic to

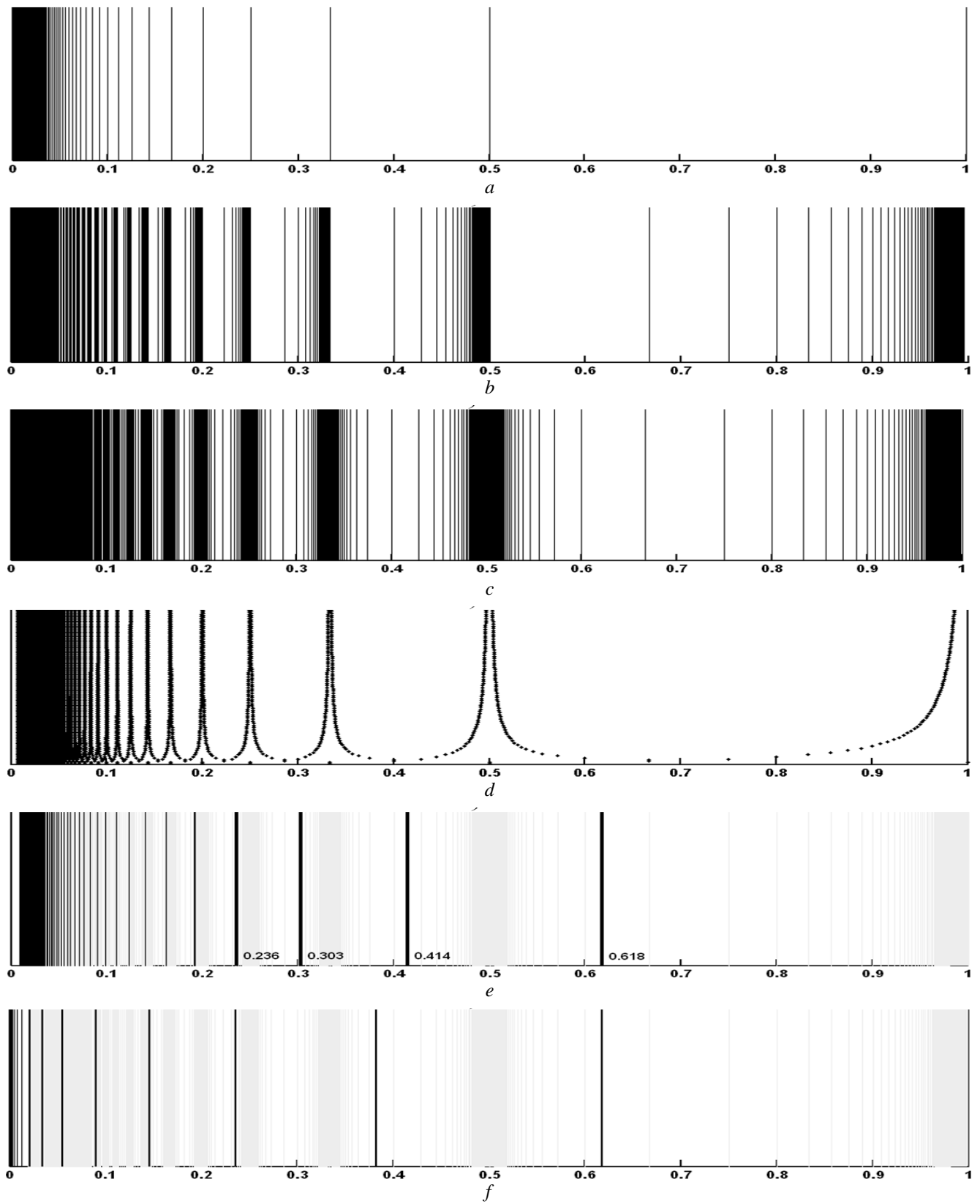


Fig. 1: Rational (a)–(d) and irrational (e)–(f) numbers distribution.

whole set in Fig. 1a. Consequently, vicinity of every line in Fig. 1c is isomorphic to whole set in Fig. 1b. Apparently that such regularity will be repeated on every next step of the algorithm and we can conclude that (2), in the case of  $N \rightarrow \infty$ , gives an example of mathematical fractal, which in the case of finite  $N$  gives an pre-fractal, which can be considered as physical fractal.

From Fig. 1c we can conclude that rational numbers for the case of finite  $N$  distributed along number axis inhomogeneously. This conclusion proves density distribution of rational numbers, constructed on the base of set presented in Fig. 1c, and given in Fig. 1d.

Summarizing, we can state that roughness of parameters of real physical system modeled by finite  $N$  in (2) leads to inhomogeneous fractal distribution of rational numbers along number axis. As follows from Fig. 1d major maxima in the distribution defined by first steps of algorithm given in (3).

### 3 Equivalence classes of rational numbers and resonance

Expression (1) can be rewrite in terms of wavelength  $\lambda_p$  and  $\lambda_q$ , which corresponds to frequencies  $p$  and  $q$ :

$$r = \frac{p}{q} = \frac{\lambda_q}{\lambda_p}. \tag{6}$$

Suppose, that  $\lambda_q > \lambda_p$ . Then (6) means that wavelength  $\lambda_q$  is an integer part of  $\lambda_p$ . In this case resonance condition can be write in the form  $\lambda_q \bmod \lambda_p = 0$ , or in more general form:

$$n \bmod i = 0, \tag{7}$$

where  $i, n \in \mathbb{N}, i, n = \overline{1, \infty}$ . All  $i$ , which satisfy (7) gives integer divisors of natural number  $n$ . Fig. 2 gives graphical representation of numbers of integer divisors of  $n$ , obtained from (7).

Analogously to previous, roughness of physical system in the case of (7) can be modeled if instead of  $n \rightarrow \infty$  will be used condition  $n \rightarrow N$ , where  $N$  is quite large, but finite natural number. In this case we can directly calculate power of equivalence classes of  $n$ , which belong to segment  $[1, N]$ . Result of the calculation for  $N = 5000$  is given in Fig. 3.

As follows from Fig. 3a–b the power of equivalence classes is maximal only for first members of natural numbers axis.

From our point of view this result can explain the fact that resonance appears easier when  $p$  and  $q$  are small numbers. Really, for the larger power of equivalence classes exist the greater number of pairs  $p$  and  $q$  (different physical situations), which gives the same value of  $r$ , which finally make this resonance relation more easy to appear.

An interesting result, related to the power of equivalence classes, is presented in Fig. 4. This result for the first time was described, but not explained in [3]. In Fig. 4 are presented diagrams, obtained by means of the next procedure.

Number sequence, presented in Fig. 2, was divided onto

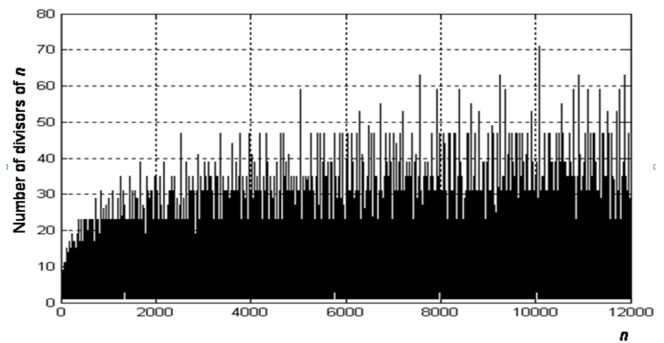
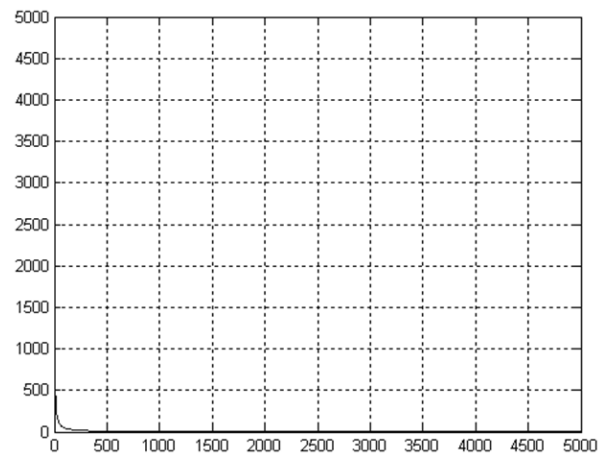
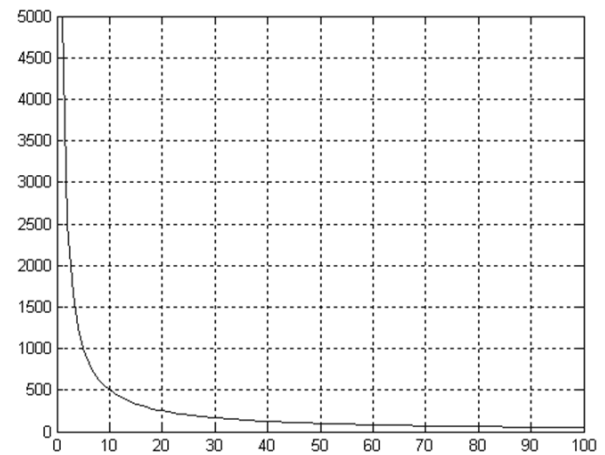


Fig. 2: Numbers of integer divisors of  $n$ .



(a)



(b)

Fig. 3: Power of equivalence classes for  $N = 5000$ , (a); magnified part of (a) for  $N = 100$ , (b). X-axis: value of  $N$ , Y-axis: power of equivalence classes.

equal  $\Delta n$ -points segments. In this way we obtain  $\frac{N}{\Delta n}$  segments. The points in the segments was numerated from 1 to  $\Delta n$ . Finally all points with the same number in  $\frac{N}{\Delta n}$  segments were summarized.

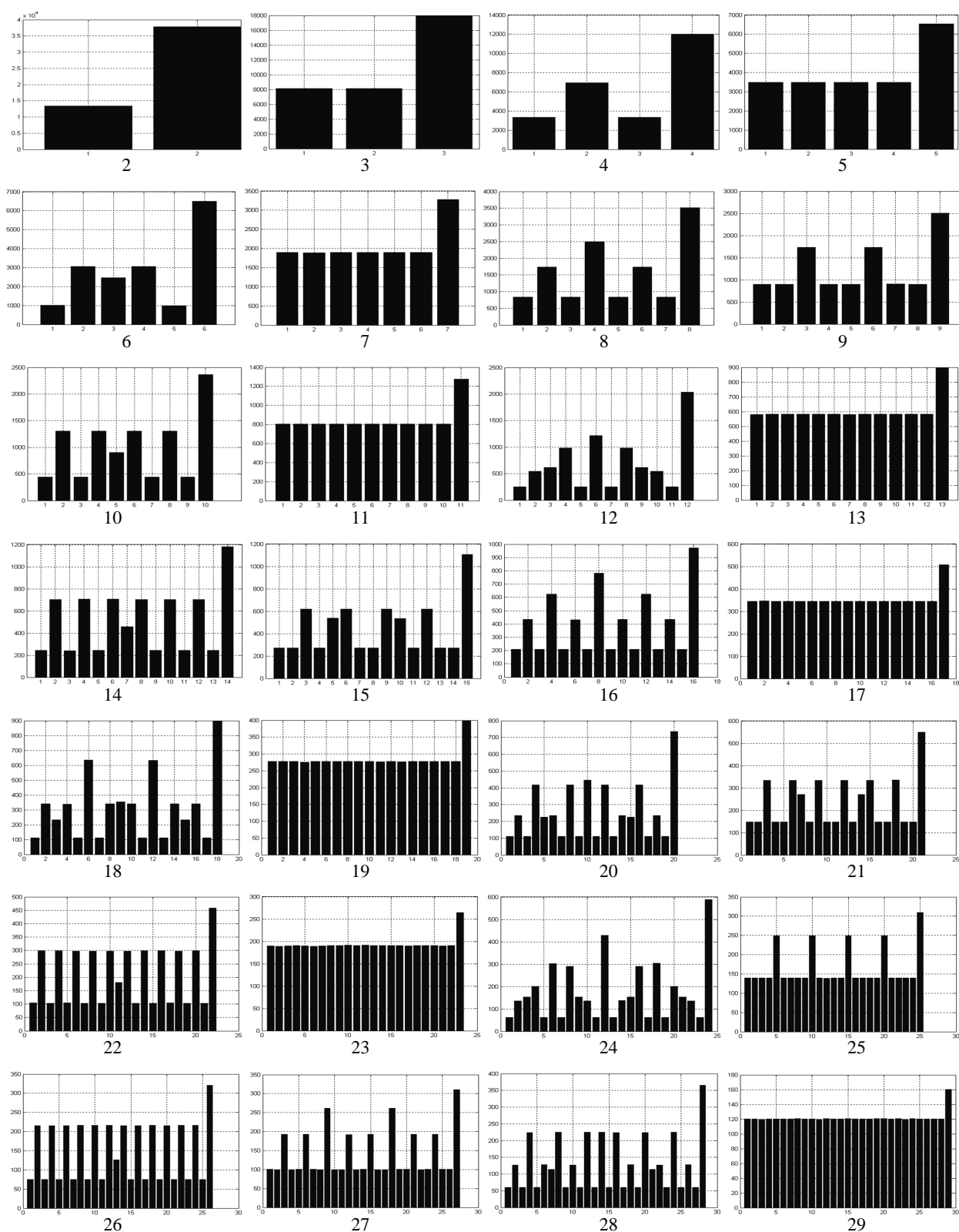


Fig. 4: Diagrams constructed on the base of sequence, presented in Fig. 2. The length of  $\Delta n$ -points segments pointed by number below the diagrams.

It can be seen from Fig. 4 that form of straight case when  $\Delta n$  is a prime number diagram always have a line. Otherwise presents some unique pattern. If we examine patterns, displayed in Fig. 4, we can find that in the role of buildings blocks, which define structure of the patterns with relatively big  $\Delta n$ , serve the patterns obtained for relatively small  $\Delta n$ . The patterns with small  $\Delta n$  based on numbers with greater power of equivalence classes and therefore manifests itself through summarizing process in contradiction from relatively big values of  $\Delta n$ .

**4 On irrational numbers distribution**

Presented in Fig. 1c–d rational numbers distribution displays some rational maxima. Existence of such maxima means that in the case of rational relations, which correspond to the maxima, resonance will appear more easy and interaction between different parts of considered physical system will be more strong. If parameters of the system correspond to the maxima, such system becomes unstable, because of interaction, which is maximal for this case.

Analogously to rational maxima is interesting to consider existence of irrational maxima, which in opposition to rational one, must correspond to minimal interaction between parts of the system and to its maximal stability. Work [1] suppose that irrational maxima correspond to minima in rational numbers distribution. In the role of “the most irrational numbers” was proposed algebraic numbers, which are roots of equation

$$\alpha^2 + ab + c = 0. \tag{8}$$

Assume that  $c = -1$ . Then

$$\alpha = \frac{1}{\alpha + b} = \frac{1}{b + \frac{1}{b + \frac{1}{b + \dots}}} = \frac{\sqrt{b^2 + 4} - b}{2}. \tag{9}$$

Infinite continued fraction gives the worst approximation for irrational number  $\alpha$  the smaller is its  $k + 1$  component. So, the worst approximation will be in the case  $b = 1$ :

$$\alpha_1 = \frac{1}{1 + \frac{1}{1 + \frac{1}{1 + \dots}}} = \frac{\sqrt{5} - 1}{2} = 0.6180339. \tag{10}$$

The case  $b = 1$  corresponds to co-called golden section. Further calculations on the base of (9) give:

$$\alpha_2 = \frac{1}{2 + \frac{1}{2 + \frac{1}{2 + \dots}}} = \frac{\sqrt{8} - 2}{2} = 0.4142135,$$

$$\alpha_3 = 0.3027756,$$

$$\alpha_4 = 0.2360679,$$

.....

Results of calculations are presented in Fig. 1e. Grey lines in Fig. 1e give rational numbers distribution, which is identical to Fig. 1c. Black lines give results of numerical calculation, based on (9) for  $b = \overline{1, 100}$ . Bold black lines point cases  $\alpha_1, \dots, \alpha_4$ .

As possible to see from Fig. 1e algebraic numbers with grows of  $b$  have tendency became closer to rational maxima. This result, indicate that such numbers, possibly, are not the best candidate for “the most irrational ones” [1].

In present work we don’t state the task to find explicit form of irrational numbers fractal. It is clear, that first irrational maxima must be connected with golden section. The question is about the rest of the maxima. Fig. 1f gives another attempt to construct such maxima on the base of set, given by generalized golden proportion [4]. It is obvious from Fig. 1f that this case also is far away from desired result.

**5 Summary**

All results described in the paper are based on the notions of resonance and roughness of real physical system. This notions in applications to set of real numbers leads to existence of rational numbers distribution, which has fractal character. Maxima of the distribution (Fig. 1d) correspond to maximal sensitivity of the system to external influences, maximal interaction between parts of the system. Resonance phenomena are more stable and appear more easy if  $r(1)$  belong to rational maxima (Fig. 1d).

Obtained rational numbers distribution (Fig. 1c–d) contains also areas where density of rational numbers are minimal. It’s logically to suppose that such minima correspond to maxima in irrational numbers distribution. We suppose that such distribution exists and is complementary to distribution of rational numbers. Maxima in such distribution correspond to high stability of the system, minimal interaction between parts of the system, minimal interaction with surrounding.

Both irrational and rational numbers distribution are related to the same physical system and must be consider together.

Question about explicit form of irrational numbers distribution remains open. At the moment we can only state that main maxima in this distribution must corresponds to co-called golden section (10).

Ideas about connection between resonance and rational numbers distribution can be useful in [4–8] where used the same mathematical apparatus, but initial postulates are based on the model of chain system.

### Acknowledgements

The authors is grateful to S.E. Shnoll, V.A. Kolombet, H. Müller and D. Rabounski for valuable discussions and support.

Submitted on September 29, 2012 / Accepted on September 30, 2012

### References

1. Dombrowski K. Rational Numbers Distribution and Resonance. *Progress in Physics*, 2005, v. 1, 65–67.
2. Khinchin A. Ya. Continued fractions. M., 1978. (in Russian)
3. Shnoll S.E. et al. About regularities in discrete distributions of measuring results (cosmophysical aspects). *Biophysics*, 1992, v. 37, No. 3, 467–488. (in Russian)
4. Stakhov A. P. Codes of golden proportion. M., 1984. (in Russian)
5. Müller H. Fractal Scaling Models of Resonant Oscillations in Chain Systems of Harmonic Oscillators. *Progress in Physics*, 2009, v. 2, 72–76.
6. Müller H. Fractal scaling models of natural oscillations in chain systems and the mass distribution of the celestial bodies in the Solar system. *Progress in Physics*, 2010, v. 1, 62–66.
7. Müller H. Fractal scaling models of natural oscillations in chain systems and the mass distribution of particles. *Progress in Physics*, 2010, v. 3, 61–66.
8. Ries A., Vinicius M. Lia Fook Application of the model of oscillations in a chain system to the Solar System. *Progress in physics*, 2011, v. 1, 103–111.

LETTERS TO  
PROGRESS IN PHYSICS

**LETTERS TO PROGRESS IN PHYSICS****Atomic Masses of the Synthesed Elements (No.104–118)  
being Compared to Albert Khazan's Data**

Albert Khazan

E-mail: albkhazan@gmail.com

Herein, the Hyperbolic Law of the Periodic System of Elements is verified by new data provided by theory and experiments.

A well-known dependence exist in the Periodic Table of Elements. This dependence links atomic masses of chemical elements with their numbers in the Table. Our research studies [1, 2] produced in the recent years showed that this dependence continues onto also the region of the synthetic elements located, in the Table, from Period 7 upto the end of Period 8. As is seen in Fig. 1, our calculations can be described by an equation whose coefficient of truth approximation is  $R^2 = 0.99995$ . However the experimental data obtained by the nuclear physicists, who synthesed the super-heavy elements, manifest a large scattering which gives no chance to get a clear dependence in this region. This is because their experiments were produced in the hard conditions, and only single atoms were synthesed that makes no possibilities for any statistics. Despite this drawback, the nuclear physicists continue attempts to synthese more and more super-heavy elements, still giving their characteristics to be unclear exposed. At the present day, 15 super-heavy elements (No.104–118) were synthesed. Obtained portions of them are as microscopic as the single atoms [3]. Therefore, masses of the products of the reactions are estimated on the basis of calculations. Analysis of the calculated data being compared to the data obtained on the basis of our theory is given in Fig. 2. The upper arc shows the difference between the atomic masses obtained on the basis of the experimental data (which are unclear due to the large scattering) and our exact calculations. All given in the Atomic Units of Mass (A.U.M.).

In the upper arc of Fig. 2, these numerical values are converted into percents. As is seen, this arc has a more smooth shape, while there is absolutely not deviations for elements No. 105 and No. 106. Most of the deviations is less than 2%. Only 5 points reach 2.5–3.6%. Proceeding from these results, we arrive at the following conclusion. Because our calculation was true on the previous numerical values, it should be true in the present case as well. Hence, the problem rises due to the complicate techniques of the experiments, not doubts in our theory which was checked to be true along all elements of the Periodic Table. It is important to note that our theoretical prediction of element No.155 [1, 2], heavier of whom no other elements can be formed, arrived after this.

Concerning the experimental checking of our theory. There are super-heavy elements which were synthesed already

later as my first research conclusions were published in 2007 [1]. These new elements — their characteristics obtained experimentally (even if with large scattering of the numerical values) — can be considered as the experimental verification of the theory I suggested [1, 2], including the Hyperbolic Law in the Periodic Table of Elements, and the upper limit of the Table in element No.155.

Submitted on September 01, 2012 / Accepted on September 13, 2012

**References**

1. Khazan A. Upper Limit in the Periodic Table of Elements. Progress in Physics, 2007, v. 1, 38–41.
2. Khazan A. Upper Limit in Mendeleev's Periodic Table — Element No. 155. American Research press, Rehoboth (NM), 2012.
3. Web Elements: the Periodic Table on <http://webelements.com>

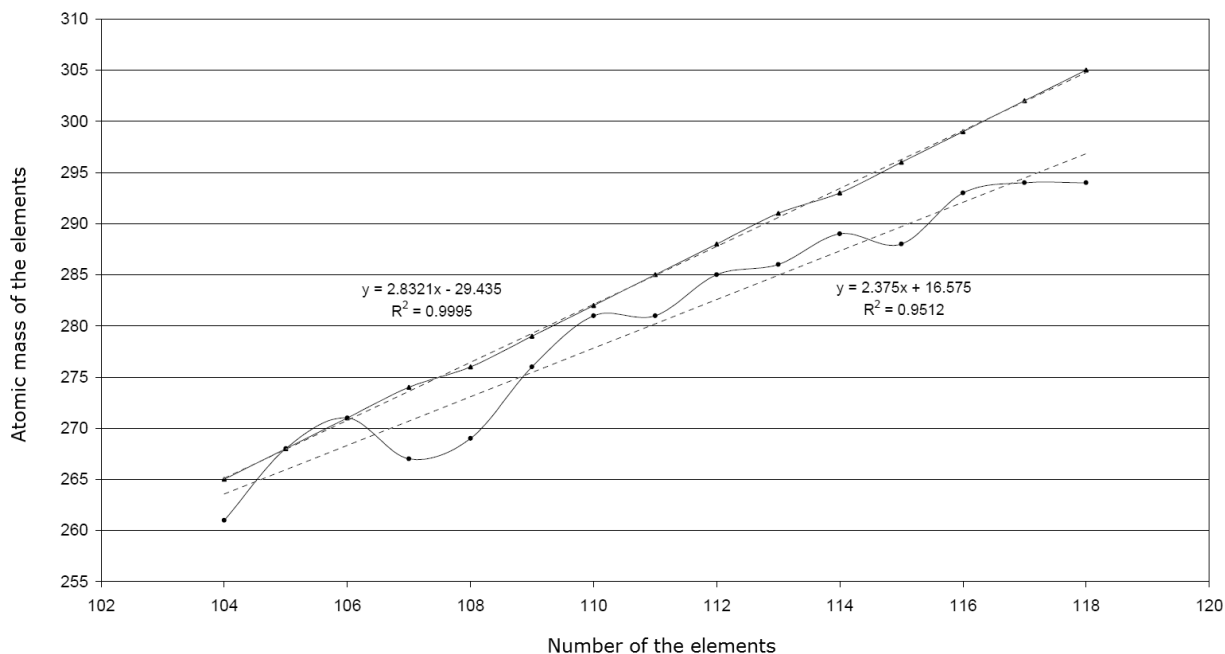


Fig. 1: Dependence of the atomic masses of the elements on their number in the Periodic Table. The experimental data (obtained with large scattering of the numerical values) are shown as the curved arc. Our calculations are presented with the straight line.

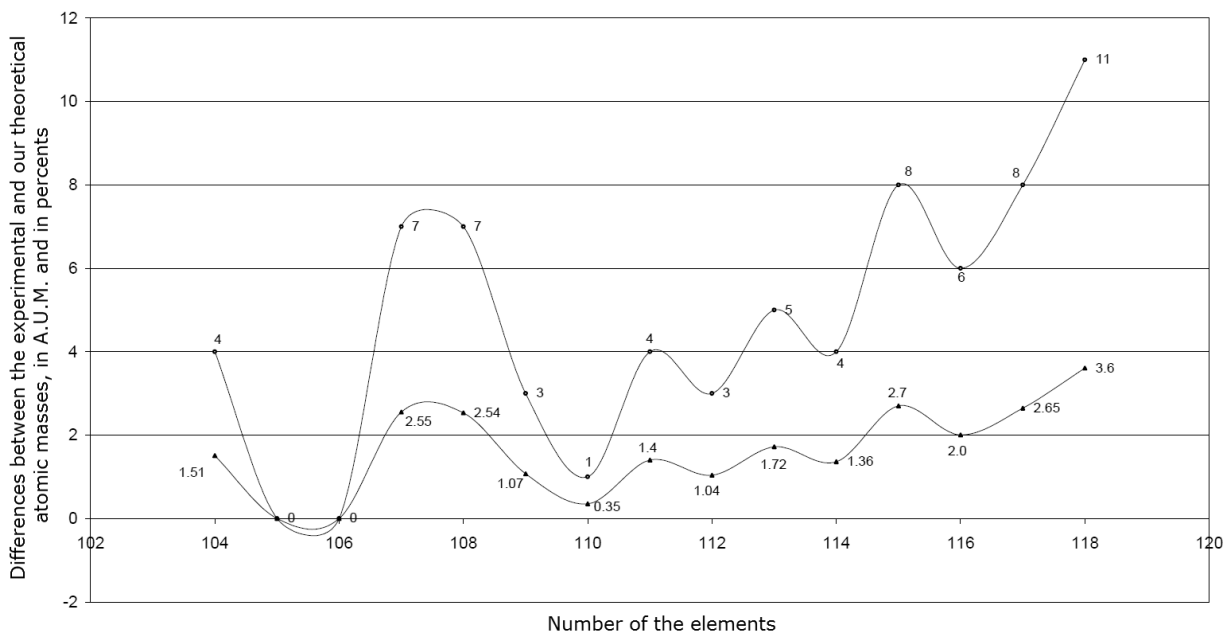


Fig. 2: Differences between the atomic masses (experimental and our theoretical), obtained in the region of the super-heavy (synthetic) elements No.104–No.188. The upper arc manifests the differences in A.U.M. (g/mole). The lower arc — the same presented in percents.

**Progress in Physics is an American scientific journal on advanced studies in physics, registered with the Library of Congress (DC, USA): ISSN 1555-5534 (print version) and ISSN 1555-5615 (online version). The journal is peer reviewed and listed in the abstracting and indexing coverage of: Mathematical Reviews of the AMS (USA), DOAJ of Lund University (Sweden), Zentralblatt MATH (Germany), Scientific Commons of the University of St.Gallen (Switzerland), Open-J-Gate (India), Referential Journal of VINITI (Russia), etc. Progress in Physics is an open-access journal published and distributed in accordance with the Budapest Open Initiative: this means that the electronic copies of both full-size version of the journal and the individual papers published therein will always be accessed for reading, download, and copying for any user free of charge. The journal is issued quarterly (four volumes per year).**

**Electronic version of this journal: <http://www.ptep-online.com>**

**Editorial board:**

**Dmitri Rabounski (Editor-in-Chief), Florentin Smarandache, Larissa Borissova**

**Editorial team:**

**Gunn Quznetsov, Andreas Ries, Chifu E. Ndikilar, Felix Scholkmann**

**Postal address:**

**Department of Mathematics and Science,  
University of New Mexico, 705 Gurley Avenue, Gallup, NM 87301, USA**

**Printed in the United States of America**